UNIVERSIDAD DE MURCIA

Escuela de Doctorado

TESIS DOCTORAL

# *Estudio de la refracción periférica y el comportamiento visual en la prevención de la miopía*

*Study of Peripheral Refraction and Visual Behavior in Myopia Prevention*


AUTOR/A Zhenghua Lin

DIRECTOR/ES Pablo Artal Soriano


2025

UNIVERSIDAD DE MURCIA Escuela de Doctorado

TESIS DOCTORAL

# *Estudio de la refracción periférica y el comportamiento visual en la prevención de la miopía*

*Study of Peripheral Refraction and Visual Behavior in Myopia Prevention*

AUTOR/A Zhenghua Lin

DIRECTOR/ES Pablo Artal Soriano

2025

UNIVERSIDAD DE MURCIA

# DECLARACIÓN DE AUTORÍA Y ORIGINALIDAD DE LA TESIS PRESENTADA PARA OBTENER EL TITULO DE DOCTOR/A

*Aprobado por la Comisión General de Doctorado el 19 de octubre de 2022.*

Yo, D. Zhenghua Lin, habiendo cursado el Programa de Doctorado en Ciencias de la VISIÓN (PLAN 2020) de la Escuela Internacional de Doctorado de la Universidad de Murcia (EIDUM), como autor/a de la tesis presentada para la obtención del título de Doctor/a titulada:

Estudio de la refracción periférica y el comportamiento visual en la prevención de la miopía

y dirigida por:

D.: Pablo Artal Soriano
D.:
D.:

**DECLARO QUE:**

La tesis es una obra original que no infringe los derechos de propiedad intelectual ni los derechos de propiedad industrial u otros, de acuerdo con el ordenamiento jurídico vigente, en particular, la Ley de Propiedad Intelectual (R.D. legislativo 1/1996, de 12 de abril, por el que se aprueba el texto refundido de la Ley de Propiedad Intelectual, modificado por la Ley 2/2019, de 1 de marzo, regularizando, aclarando y armonizando las disposiciones legales vigentes sobre la materia), en particular, las disposiciones referidas al derecho de cita, cuando se han utilizado sus resultados o publicaciones.

Del mismo modo, asumo ante la Universidad cualquier responsabilidad que pudiera derivarse de la autoría o falta de originalidad del contenido de la tesis presentada, en caso de plagio, de conformidad con el ordenamiento jurídico vigente.

Murcia, a (30/5/2025)

*(firma)*

| Información básica sobre protección de sus datos personales aportados: | |
|---|---|
| Responsable | Universidad de Murcia.<br>Avenida teniente Flomesta, 5. Edificio de la Convalecencia. 30003; Murcia.<br>Delegado de Protección de Datos: dpd@um.es |
| Legitimación | La Universidad de Murcia se encuentra legitimada para el tratamiento de sus datos por ser necesario para el cumplimiento de una obligación legal aplicable al responsable del tratamiento. art. 6.1.c) del Reglamento General de Protección de Datos |
| Finalidad | Gestionar su declaración de autoría y originalidad |
| Destinatarios | No se prevén comunicaciones de datos |
| Derechos | Los interesados pueden ejercer sus derechos de acceso, rectificación, cancelación, oposición, limitación del tratamiento, olvido y portabilidad a través del procedimiento establecido a tal efecto en el Registro Electrónico o mediante la presentación de la correspondiente solicitud en las Oficinas de Asistencia en Materia de Registro de la Universidad de Murcia |

*Esta DECLARACIÓN DE AUTORÍA Y ORIGINALIDAD debe ser insertada en la quinta hoja, después de la portada de la tesis presentada para la obtención del título de Doctor/a.*

# Index

# Resumen

En la última década se ha registrado un aumento significativo en la prevalencia de la miopía a nivel mundial, especialmente en Asia Oriental. Según el Libro Blanco sobre la Prevención y Control de la Miopía en Niños y Adolescentes del Instituto Oftalmológico Aier (China), la tasa de miopía entre los niños y adolescentes chinos alcanzó el 52.7% en 2021. Resulta alarmante que más del 70% de los estudiantes universitarios chinos ya presenten miopía. Este incremento representa un creciente problema de salud pública, ya que la miopía alta no controlada no solo reduce la calidad visual del individuo sino que también aumenta el riesgo de enfermedades oculares graves como desprendimiento de retina, degeneración macular, glaucoma y cataratas. Por lo tanto, existe una necesidad urgente de comprender integralmente cómo se desarrolla la miopía y explorar estrategias innovadoras basadas en evidencia para prevenir o ralentizar su progresión.

Entre diversos factores contribuyentes, se ha sugerido que el desenfoque retiniano periférico juega un papel importante en el desarrollo de la miopía. Por ejemplo, estudios en animales, particularmente en monos bebés, han demostrado que inducir hipermetropía periférica puede acelerar la progresión miópica (Smith et al, IOVS, 2007). Estos resultados sobre modificación de refracción periférica fueron corroborados al eliminar la visión foveal. Estudios clínicos también han encontrado que anteojos diseñados para crear desenfoque miópico mediante microlentes periféricas pueden retardar la progresión de la miopía. Sin embargo, algunos estudios clínicos han concluido resultados controvertidos indicando que la refracción periférica no se correlaciona con el desarrollo de la miopía. Esto probablemente se debe a la limitada resolución espacial de los datos de refracción periférica en estudios tempranos. Por ejemplo, el instrumento más comúnmente utilizado en clínicas (autorrefractor de visión abierta WAM-5500, GrandSeiko, Japón) generalmente mide la refracción periférica a -

30°, -20°, -10°, 0°, +10°, +20° y +30° en dirección horizontal. Esta medición requiere rotación ocular del sujeto, siendo relativamente lenta y con datos de baja repetibilidad.

Para abordar estas limitaciones, desarrollamos un nuevo instrumento para medir mapas de refracción periférica bidimensionales (2D) utilizando un sensor de frente de onda Hartmann-Shack. Los mapas 2D se reconstruyeron combinando escaneo horizontal automático con secuencias de fijaciones oculares en dirección vertical, cubriendo un campo visual rectangular de 60° × 36° (horizontal × vertical). Posteriormente, realizamos un estudio longitudinal para observar la evolución de la refracción periférica con la progresión miópica en más de 200 niños durante más de dos años.

Los mapas de refracción periférica en hipermétropes, emétropes y miopes generalmente coincidieron con estudios previos en dirección horizontal, mostrando miopía/hipermetropía relativa periférica en hipermétropes/miopes y refracción relativamente plana en emétropes. Nuestro estudio publicó por primera vez detalles más completos del patrón refractivo periférico 2D entre diferentes grupos, mostrando significativa variabilidad individual. Los resultados principales indicaron que el desenfoque periférico en toda la región vertical central puede predecir el inicio o desarrollo de miopía en emétropes pero no en hipermétropes o miopes. La correlación fue más fuerte en la retina superior que en la inferior. El análisis de la evolución refractiva periférica durante dos años consecutivos reveló que el desenfoque periférico relativo es más probablemente una consecuencia que un factor causal al inicio de la miopización. Esto podría explicarse por el retraso acomodativo en el campo superior durante trabajos cercanos prolongados o factores genéticos humanos inherentes. Este fenómeno podría iniciar o reforzar el estiramiento retinal superior y el remodelado escleral. Por tanto, la refracción periférica intrínseca se relaciona de alguna manera con la respuesta acomodativa durante actividades de visión cercana. Además, los resultados sugirieron que el inicio de la miopía probablemente ocurre primero en la retina superior antes de extenderse a la inferior, proporcionando un bioindicador temprano para

prevención.

Otro factor importante en la progresión miópica es el retraso acomodativo, definido como la demora o insuficiencia de acomodación ante estímulos cercanos. Este retraso puede causar desenfoque retinal hipermetrópico, particularmente en campos visuales centrales y periféricos durante tareas cercanas, proporcionando así un estímulo para elongación axial. Aunque los mecanismos precisos siguen debatiéndose, muchos clínicos atribuyen al menos parte de la naturaleza progresiva de la miopía a la exposición sostenida a imágenes retinianas borrosas por retraso acomodativo. Por ello, comprender la relación entre respuestas acomodativas y modificación refractiva periférica resulta crucial para investigadores.

Para investigar este aspecto, evaluamos lentes basadas en desenfoque periférico: DIMS (Segmentos Múltiples con Desenfoque Incorporado, Hoya Co., Japón), Stellest (EssilorLuxottica, Francia) y MyoCare (Zeiss, Alemania). Estas lentes se colocaron frente al ojo para evaluar la respuesta acomodativa dinámica tras modificar la refracción periférica. La evaluación se realizó con un innovador instrumento de doble paso para garantizar fiabilidad. Durante el experimento, el estímulo acomodativo se estableció en aproximadamente 5D para objetivo cercano y 0.33D para lejano. Sorprendentemente, no se encontraron diferencias significativas en la amplitud de respuesta acomodativa entre los distintos lentes de tratamiento miópico, validándose tanto en niños como adultos. Como estas lentes usan microlentes periféricas, repetimos el experimento con lentes regulares pero eliminando material en el campo central. Las lentes incluían plano, +3D de desenfoque periférico, -3D de desenfoque y -3D de astigmatismo. No obstante, los resultados fueron idénticos a los de lentes de tratamiento, sugiriendo que la modificación refractiva periférica no altera la respuesta acomodativa, al menos en adaptaciones cortas. Es plausible que futuras lentes de control miópico mejoren su eficacia aumentando la potencia óptica de microlentes periféricas.

Además de técnicas basadas en desenfoque (DIMS, MyoCare, Stellest), la lente DOT (SightGlass Vision, EE.UU.), que reduce el contraste retinal, ha ganado popularidad reciente. Esta técnica no añade desenfoque óptico periférico sino que utiliza óptica difusa para reducir contraste. Cabe destacar que las lentes basadas en desenfoque también pueden reducir contraste periférico, siendo este efecto proporcional al desenfoque inducido. Por tanto, es posible que estas técnicas retarden la miopía modificando el contraste retinal. Para investigar esto, necesitábamos un instrumento que registrara imágenes retinianas objetivamente, sin verse afectado por imágenes proyectadas del entorno visual. La técnica de doble paso resultó ideal para este fin.

Brevemente, esta técnica crea una fuente puntual en la retina, cuyo reflejo llega al sensor del dispositivo a través de una lente sintonizable, permitiendo registrar la función de dispersión de punto (PSF) ocular. El contraste se calculó en una región específica de la imagen PSF con mejor enfoque, utilizando una métrica que superó en sensibilidad y repetibilidad al contraste tradicional de Michelson. El análisis mostró que las lentes Stellest produjeron mayor reducción de contraste, seguidas por MyoCare y DIMS. Esta capacidad para reducir contraste periférico podría reflejar su eficacia en control miópico si la teoría principal de la lente DOT es correcta, aunque se requieren más estudios para confirmarlo.

El comportamiento visual se relaciona con la refracción periférica. Nuestro estudio de dos años sobre su evolución mostró que el desenfoque miópico en retina superior de niños emétropes es un factor de riesgo para miopización, posiblemente por exposición prolongada a tareas cercanas como deberes escolares. En estos casos, el sujeto gira los ojos hacia abajo, produciendo desenfoque hipermetrópico en retina superior que iniciaría la expansión ocular desde esa zona. Desde la perspectiva fisiológica, la retina periférica muestra mayor densidad de bastones con la excentricidad, encargados de detectar movimiento, contornos y visión escotópica. Por tanto, podrían esperarse cambios en comportamiento visual tras modificar refracción periférica. Sin embargo,

han faltado métodos confiables para evaluar este comportamiento, utilizando frecuentemente cuestionarios (con riesgo de sesgo de memoria) o dispositivos basados en orientación cefálica (como Clouclip, RangeLife y Vivor) que introducen errores sistemáticos por inconsistencia entre línea de mirada y orientación cefálica.

Para abordar esta brecha metodológica, desarrollamos un algoritmo que estima distancia de mirada basado en la relación geométrica entre imágenes pupilares y distancia de fijación, incorporado luego a un marco de gafas impreso en 3D con microprocesadores y cámaras pupilares, funcionando como rastreador ocular portátil. Esta herramienta calcula distancia robustamente mediante convergencia ocular. El marco personalizado permite insertar lentes de prueba, proporcionando visión nítida al usuario para obtener respuestas precisas durante experimentos. Configuramos un sistema experimental para probar el rendimiento del rastreador, proporcionando distancias de fijación precisas (equivalentes dióptricos de 0.5D a 6.7D) a 25° bilaterales y dirección central, permitiendo comparar valores estimados con estándares de oro.

El objetivo principal fue evaluar repetibilidad y precisión del dispositivo en estimar distancia de mirada, mientras que el secundario fue investigar factores de confusión potenciales y su relación con amplitud acomodativa. Los resultados mostraron buena concordancia para objetos en eje visual central, mejorable con calibración simple. El rendimiento fue menor para objetivos periféricos a 25°, mostrando tendencias de sesgo diferentes entre objetivos izquierdos, derechos y centrales, sugiriendo posibles mecanismos de fijación distintos para campos centrales y periféricos. El coeficiente de correlación intraclase demostró excelente repetibilidad. No encontramos correlaciones significativas entre mayoría de las métricas visuales investigadas (equivalente esférico, desviación cercana/lejana, amplitud acomodativa) y distancia de mirada, aunque el punto cercano de convergencia sí se relacionó significativamente con la precisión del dispositivo. Aunque requiere mejoras en rendimiento periférico, nuestro rastreador representa un avance significativo sobre sistemas comerciales existentes.

En resumen, esta tesis proporciona nuevas perspectivas sobre la compleja interacción entre óptica periférica, acomodación y comportamiento visual en desarrollo y control de la miopía: (A) Desarrollamos exitosamente un método de alta resolución para medir refracción periférica 2D, revelando que el desenfoque retinal superior podría servir como biomarcador temprano de miopía en emétropes; (B) La exposición a corto plazo al desenfoque periférico inducido por diversas lentes de control no influye significativamente en la respuesta acomodativa; (C) Todas las lentes estudiadas redujeron significativamente el contraste retinal periférico, siendo Stellest la más efectiva, sugiriendo un posible mecanismo común de eficacia; (D) Un rastreador ocular personalizado montado en gafas demostró alta repetibilidad y precisión razonable en estimación de distancia de mirada, superando alternativas comerciales y ofreciendo aplicaciones prometedoras para futuros estudios de comportamiento visual.

Colectivamente, estos hallazgos contribuyen a una comprensión más profunda de la etiología de la miopía y proporcionan bases para optimizar enfoques diagnósticos y terapéuticos en su manejo. La evidencia sugiere que tanto factores ópticos periféricos como mecanismos de contraste retinal juegan roles importantes en la progresión miópica, mientras que el desarrollo de tecnologías de seguimiento ocular preciso abre nuevas vías para investigar la relación entre comportamiento visual y desarrollo de errores refractivos. Futuras investigaciones deberán explorar estos mecanismos con mayor profundidad para desarrollar intervenciones aún más efectivas que puedan abordar este creciente problema de salud pública a escala global.

# Summary

There has been a significant increase in myopia prevalence in the world during the last decade, especially in East Asia. According to *China White Paper on Myopia Prevention and Control in Children and Adolescents* by Aier Eye Institute (China), the myopia rate among Chinese children and adolescents reached 52.7% in 2021. Alarmingly, more than 70% of Chines undergraduate students are already myope. This surge represents a growing public health concern, as uncontrolled high myopia not only reduces the visual quality of the individual but also increases the risk of serious ocular diseases such as retinal detachment, macular degeneration, glaucoma, and cataracts. Therefore, there is an urgent need for a comprehensive understanding of how myopia develops and to explore innovative, evidence-based strategies to prevent or slow its progression.

Among various contributing factors, peripheral retinal defocus has been suggested to play an important role in the development of myopia. For instance, animal studies, particularly in infant monkeys, has shown that imposing peripheral hyperopia in infant monkeys can accelerate myopia progression (Smith et al, IOVS, 2007). These results for peripheral refraction modification were corroborated by removing foveal vision. Clinical studies have also found that spectacles designed to create myopic defocus by using micro lenslets in the periphery can slow myopia progression. However, some clinical studies also concluded controversial results that peripheral refraction is not correlated to myopia development. This is probably caused by the limited spatial resolution of peripheral refraction data from early studies. For example, the most commonly used instrument in clinics (open view autorefractor WAM-5500, GrandSeiko, Japan) is usually for measuring peripheral refraction at -30°, -20°, -10°, 0°, +10°, +20° and +30° in horizontal direction. The measurement needs the rotation of the eye of the subject, and therefore a kind of time consuming and the data shows relatively low repeatability.

To address these limitations, we developed a new instrument for measuring two-dimensional (2D) peripheral refraction maps using a Hartmann-Shack wavefront sensor. 2D peripheral refraction maps were reconstructed by combining automatic horizontal scanning with sequences of eye fixations in the vertical direction. The map covering a rectangular visual field of 60° × 36° (horizontal × vertical). Then, a longitudinal study was conducted to observe the evolution of peripheral refraction with myopia progression in more than 200 children for over two years.

The peripheral refraction maps in hyperopes, emmetropes, and myopes generally aligned with previous studies in horizontal direction, showing relative peripheral myopia/hyperopia in hyperopes/myopes and relatively flat refraction in emmetropes. More details in the whole 2D peripheral refractive pattern across different refraction groups were first published from current study and showed significant variability of individuals. The primary results indicated that peripheral defocus in the whole central vertical region can predict myopia onset or development in emmetropes but not in hyperopes or myopes. The correlation is stronger in the superior retina than inferior retina. The analysis of peripheral refraction evolution over two consecutive years revealed that relative peripheral defocus is more likely a consequence of myopia progression rather than a causative factor at the beginning of myopization. This could be explained by the accommodative lag in the superior field for near work overtime or inherent genetic factors of human beings. This phenomenon may initiate or reinforce superior retinal stretching and scleral remodeling. Therefore, the intrinsic peripheral refraction is somehow related to the accommodation response of the near work activity. In addition, the results also revealed that the myopia onset probably happened first in the superior retina, then it gradually goes to the inferior retina, which provides an early bio-indicator for myopia prevention.

Another important factor contributing to myopia progression is accommodative lag,

which is defined as the delay or insufficiency of accommodation in response to near stimuli. Accommodative lag may result in hyperopic retinal defocus, particularly in the central and peripheral visual fields during near tasks, thereby providing a stimulus for axial elongation. While the precise mechanisms remain debated, many clinicians attribute at least part of the progressive nature of myopia to sustained exposure to blurred retinal images caused by accommodative lag. Therefore, understanding the relationship between accommodation responses and peripheral refraction modification appears important to myopia researchers.

To further investigate this issue, we employed a set of prominent examples of peripheral defocus-based lenses: DIMS (Defocus Incorporated Multiple Segments, Hoya Co., Ltd, Japan), Stellest (EssilorLuxottica, Franch), and MyoCare (Zeiss, Germany). The lenses were fitted in the front of the eye to evaluate the dynamic accommodation response after peripheral refraction was modified by those lenses. The evaluation of accommodation response was performed with a novel double-pass instrument to ensure the reliability of the results. During the experiment, the accommodation stimulation was set as approximately 5D for near target and 0.33D for distant target. To observe a stable refraction status, the dynamic accommodation response in 11 seconds (17 anchor points) was segmented to 3 seconds, 5 seconds, and 3 seconds for far, near, and far fixation targets. Surprisingly, no significant difference was found in the amplitude of accommodation response across various myopia treatment glasses. This result was validated in both children and adults. Since both of the myopia treatment glasses use micro lenslets in the peripheral field, we repeated the experiment with regular glasses but removed the material in the central field. The refraction of the regular glasses includes plano, +3D peripheral defocus, -3D peripheral defocus, and -3D astigmatism. Nevertheless, the same results appeared again in those regular glasses as we found in myopia treatment glasses. Those results suggested that peripheral refraction modification does not alter accommodation response, at least for short adaptation. It is plausible that future myopia control lenes might improve the myopia control efficacy

by increasing the amount of optical power of micro lenslets in the periphery.

In addition to the defocus-based techniques (DIMS, MyoCare, Stellest, et al.), the reducing retinal image contrast technique, DOT lens (SightGlass Vision, USA), has been recently popular for myopia control in practice. This novel technique does not add optical defocus in the periphery but uses diffusion optics to reduce the contrast of images. A common knowledge is defocus-based myopia control lenses can also reduce image contrast through the peripheral defocus region. Furthermore, the amount of the reduced image contrast is related to the amount of the induced optical defocus. Therefore, it is possible that defocus-based techniques slow myopia development by changing the retina image contrast. To investigate this issue, we need an instrument to record retinal image in an objective manner, which means the contrast calculation should not be affected by the projected retinal image from the visual environment. For this reason, double-pass technique becomes an idea instrument to record retinal images (retinal reflex).

In brief, the double-pass technique used in current study can create a point source on the retina, then the retinal reflex goes to the sensor of the device through a tunable lens. Based on the tunable lens, the through-focus point spread function (PSF) of the eye can be recorded by the instrument. Then, a specific region of the best focus PSF image was used for calculating the contrast. The formula for calculating this value is the same as the one used in statistics for calculating the coefficient of variation, which shows the variability of the data. A comparison between this new metric and the traditional metric (Michelson contrast) was conducted in the thesis. In brief, the new metric is outperforming the traditional metric in both sensitivity and repeatability. The contrast analysis shows that Stellest lenses demonstrated the highest contrast reduction, then it was followed by MyoCare and DIMS. The capability for reducing the retinal contrast in the periphery can somehow reflect the performance of myopia control efficacy of those lenses if the principal theory of DOT lens comes into existence. However, more

studies are needed to verify this hypothesis in the future.

Visual behavior is somehow related to peripheral refraction. Our two-year study regarding the evolution of peripheral refraction shows that myopic defocus in superior retina in emmetropic children is a risk factor for myopization. This could be a consequence of long-time exposure to near work activities, typically like doing the homework for kids. In such circumstances, the subject will rotate his eyes downwards. If the light from the visual center perfectly focuses on the retina, then the light from the inferior field will produce hyperopic defocus on the superior retina, and therefore the eyeball starts expanding from the superior side. This could explain why in emmetropic children more myopic defocus is related to more myopia progression in the next one or two years. From the perspective of eye physiology, peripheral retina shows increasing density of rod cells with eccentricity, with the primary function of identifying moving objects, contour shapes, and scotopic vision. Therefore, it could be expected some changes in visual behavior after modifying peripheral refraction. However, reliable methods to evaluate visual behavior have been lacking, and relevant research is often conducted using indirect methods, such as questionnaires, which might cause re-call bias, or head-orientation-based devices (like Clouclip, RangeLife, and Vivor), which introduce systematic errors due to the inconsistency between line of sight and head orientation.

To address this methodological gap, we developed an algorism to estimate gaze distance based on the geometric relationship between pupil images and fixation distance. The algorism was then incorporated into a 3D printed spectacle frame with microprocessors and pupil cameras. Thus, the device can is also a kind of portable eye tracker. This tool robustly supports distance calculation based on eye convergence. The customized spectacle frame can also insert trial lens, providing sharp vision for the wearer, so it helps to get an accurate response during the experiment. An experimental setup for testing the fixation distance was built for testing the performance of the eye tracker. The

setup provides accurate fixation distance (dioptric distance equal to 0.5D, 1D, 2D, 3D, 4D, 5D, 6.7D) for the subject at bilateral 25 degrees and central direction. Thus, the estimated distance from the eye tracker and the gold standard value can be compared.

The main goal of the experiment for the eye tracker was to evaluate the repeatability and accuracy of the device in estimating gaze distance. The secondary goal was to investigate potential confounding factors affecting gaze distance estimation and its relationship with accommodation amplitude. As a result, we successfully created a testing environment for the eye tracker to evaluate its performance. The results showed relatively good agreement for objects located along the central visual axis, the results can be further improved with simple calibration with the distance testing setup. A less well performance for the targets at peripheral field at 25 degrees was observed. The trend of the measure bias for left and right targets are different compared to each other, and as well for the central targets, which potential reminds a different fixation mechanism for the near targets for central field and peripheral field. The intraclass correlation coefficient demonstrated excellent repeatability for two measurements. We did not find significant correlations between most of the investigated visual function metrics: spherical equivalent refraction of (OD, OS, the mean of OD/OS), near deviation, distance deviation, accommodation amplitude (OD, OS, the mean of OD/OS) and gaze distance. However, the near point of convergence is significantly relative to the accuracy of the device. While peripheral performance needs improvement, our eye tracker represents a significant advancement over existing commercial systems.

In summary, this thesis provides several novel insights into the complex interplay between peripheral optics, accommodation, and visual behavior in the context of myopia development and control:

A. We successfully developed a high-resolution method to measure two-dimensional peripheral refraction using a Hartmann-Shack wavefront sensor. Longitudinal

application of this method revealed that superior retinal defocus may serve as an early biomarker for myopia onset in emmetropes.

B. Short-term exposure to peripheral defocus induced by various myopia control lenses does not significantly influence the accommodative response in children or adults.

C. All myopia control lenses studied significantly reduced peripheral retinal image contrast, with Stellest lenses producing the greatest effect. This may represent a common underlying mechanism for efficacy across different designs.

D. A custom-built, spectacle-mounted eye tracker demonstrated high repeatability and reasonable accuracy in gaze distance estimation, outperforming head-orientation-based alternatives. The technology offers promising applications in future visual behavior studies.

Collectively, these findings contribute to a deeper understanding of myopia etiology and provide a foundation for optimizing both diagnostic and therapeutic approaches in myopia management.

# List of abbreviations

| | |
|---|---|
| 2D | Two-dimensional |
| SER | Spherical equivalent refraction |
| AL | Axial length |
| BC | Base curve zone |
| RC | Reverse curve zone |
| AC | Alignment curve zone |
| PC | Peripheral curve zone |
| LASIK | Laser-Assisted In Situ Keratomileusis |
| LASEK | Laser Epithelial Keratomileusis |
| SMILE | Small Incision Lenticule Extraction |
| ICL | Implantable Collamer Lens |
| PEK | Photorefractive Keratectomy |
| PSRS | Posterior scleral reinforcement surgery |
| RPE | Retinal pigment epithelium |
| MMD | Myopic macular degeneration |
| IMI | International Myopia Institute |
| DIMS | Defocus Incorporated Multiple Segment Lens |
| VPR | Voptica Peripheral Refraction |
| MRT | Multispectral refractive topography |
| RPR | Relatively peripheral refraction |
| PR | Peripheral refraction |
| DOT | Diffusion optics technology |

| | |
|---|---|
| PSF | Point spread function |
| GD | Gaze distance |
| IOP | Intraocular pressure |
| HY | Hyperopes |
| EM | Emmetropes |
| MY/MYO | Myopes |
| RM-ANOVA | Repeated measures ANOVA |
| S1/S2/S3<br>M1/M2/M3<br>L1/L2/L3 | The specific region of 2D-PR map<br>S-superior side, M-middle side, L-lower side;<br>1- temporal side, 2-middle, 3-nasal side |
| VA | Visual acuity |
| SV/SVG | Single vision glasses |
| AA | Amplitude of accommodation |
| RMS | Root mean square |
| $C_{RMS}$ | RMS contrast |
| $C_{Michelson}$ | Michelson contrast |
| $C_{Sobel}$ | Sobel contrast |
| CV | Coefficient of variation |
| $C_{CV}$ | CV contrast |
| BCVA | Best-corrected visual acuity |
| VF | Visual field |
| cen- | Well centered lens |
| de- | Decentered lens |
| ICC | Intraclass correlation coefficient |
| 95CI | 95% confidence interval |
| NPC | Near point of convergence |
| ACC | Accommodation response |

| | |
|---|---|
| OD | Right eye |
| OS | Left eye |
| OU | Binoculars |

# Chapter 1. Introduction

# 1.1 Myopia

## 1.1.1 What is myopia

Theoretically, myopia is identified if the parallel rays of light from a distant object cannot focus properly on the fovea when the accommodation of the eye is relaxed. The distance between the optical focus and the retinal plane is called the refractive error. However, if the refractive error (spherical equivalent refraction, SER) is less than a certain value (usually 0.5 diopters [D]), the subject will still be recognized as emmetrope rather than myope due to the depth of focus. The threshold value for the depth of focus may vary depending on the standards of the region.

The most well-known symptom of myopia is the blurry vision when looking at distant objects but somehow keeping relatively clear vision for near objects. The distance for keeping clear vision depends on the degree of refractive error. If the severity of myopia is extremely high, some other symptoms may also occur as the consequence of fundus damage.

The symptoms of myopia include deterioration of distant vision, visual fatigue, dry eye, exotropia, and exophthalmos [1]. If the fundus is damaged due to the stretching of eyeball in high myopia, which is the so-called pathological myopia, the associated symptoms could be observed like visual obstructions, double vision, color vision abnormalities, light perception abnormalities, decreased contrast sensitivity and floaters.

The subject should go to the eye care doctors if the aforementioned symptoms were observed. The key to diagnosing myopia is to measure the refraction of the eye under distant vision, which needs the SER $\leq$ -0.5D [2]. The measure can be done with autorefractor for objective refraction or phoropter for subjective refraction. Cycloplegia is recommended for young subjects to acquire accurate results, especially for children

less than 12 years old [3]. Adults can also be administered with mydriasis depending on the accommodation status or the requirement of the ophthalmic exam.

Usually, myopia can be categorized by the degree of refractive error, contribution of optical power (axial myopia or refractive myopia), and pathological changes of ocular fundus.

Slight myopia: SER ≤ -3.00 D
Moderate myopia: -3.00 D ≤ SER ≤ -5.00 D / -6.00 D
High myopia: SER ≤ -5.00 D / -6.00 D

It should be noted that the choice of threshold for high myopia is varied across different studies [4]. But the most frequently used threshold value is -6.00 D [5-8]. Another frequently used threshold value is -5.00 D [9]. This was suggested by World Health Organization as the uncorrected myopia of -5.00 D correspondence to the visual acuity of 6/172, which meet the criteria for blindness (<3/60) [2].

Pre-myopia is a special status prior to the onset of myopia. The range of refraction is equal to emmetropia (-0.50 D ≤ SER ≤ [+0.50 D ~ +0.75 D]). This concept is important as there is no solution to really shorten the eye length after the development of axial myopia. Thus, a pre-myopia stage provides caution for children who are under the high risk of myopization. There are multiple ways to achieve the goal of myopia prevention in this period. Clinicians are used to evaluate the risk by comparing the SER and the age of the subject. For emmetropic children, age-specific threshold values are as follows: <+0.75 D (6 years), ≤+0.50 D (7–8 years), ≤+0.25 D (9–10 years), and ≤0 D (11 years) [10]. A 5-years study by Mutti et al. indicates that emmetropic children who developed myopia in the next year exhibit accelerated pattern of axial elongation [11]. There are other factors that might be used as predictors during the stage of pre-myopia, like peripheral refraction, viewing distance, ambient light intensity, visual acuity,

refraction, gender, lens thickness, corneal curvature and the interaction between varies ocular components.

Axial myopia is the most common type of myopia in clinics. This is usually because of the over extension of eyeball, whereas the refractive power of other optical components (cornea, crystalline lens, vitreous body) maintains its normality.

In refractive myopia, the curvature, or the refractive index of the optical components of the eye are extremely high, resulting in extra myopic power, but meanwhile maintaining the normal axial length. In the so-called simple myopia, the fundus of the subject is in general health, with SER ≥ -6.00 D. The progression of myopia is within normal speed. Visual acuity can be improved by simple optical correction with spectacles. General ophthalmic exams do not manifest any abnormalities in visual functions.

In pathological myopia the SER of the eye is usually ≤ -6.00 D, with various kinds of pathological change can be observed in the posterior segment of the eye that leads to irreversible loss in best corrected visual acuity (BCVA). The excessive acceleration of axial length can be found in adults.

### 1.1.2 The solutions for myopia

The optimal solution to control myopia is to block the progression of myopia during the pre-myopia stage. As mentioned, myopia progression can be predicted by combination of different metrics in baseline and hence raise cautions from clinicians to take care of myopization. There are some strategies to control myopia which have been validated in myopes but also potentially applied to prevention, like low dose atropine, ambient light intensity, outdoor activities, peripheral retinal refraction modification (multi-focus soft contact lens, orthokeratology, defocus incorporated multiple segment spectacles). It is strongly recommended to establish a myopia management strategy for

individuals until at least 16 years old, which is usually the age cease myopia progression [12, 13].

Single vision glasses (SVG) have been widely used in myopia correction for hundreds of years. It is safe, cost effective, convenient to carry on and easy to be accepted by subjects. However, it should be noticed that if the degree of myopia is extremally high (<-10D, depending on the material of the lens) or if the anisometropia (interocular difference of foveal refraction) is larger than 2.00 D, it is recommended to use rigid contact lens to avoid headaches, eye fatigue or visual distortion due to the difference of image magnification on the retina.

Contact lens is directly applied to the subject's cornea for myopia correction. This minimizes the change of magnification on the retina and provides a better visual field for wearers. The optical power of the lens is less than frame glasses. Thus, the contact lens is a better option for high myope. However, there is higher demand for contact lenses users to keep proper cleaning to avoid potential risk like keratitis. The cost of contact lenses is also higher than frame glasses.

Orthokeratology (ortho-k), or overnight corneal reshaping lenses, is a type of specially designed gas-permeable rigid contact lens for correct myopia by overnight wearing. The subject does not need any extra optical correction in the daytime for maintaining clear vision. Ortho-K is popular in clinics, not just for its convenience for correction, but also as a myopia treatment. It is well documented that Ortho-K can retard axial elongation in teenagers from 30% to 70% comparing to single vision glasses [14-17].The lens is usually constructed by four zones: The Base Curve Zone (BC), Reverse Curve Zone (RC), Alignment Curve Zone (AC) and Peripheral Curve Zone (PC). Each zone has its unique function such as correct refractive error (BC), assisting central corneal reshaping and stabilizing (RC), positioning lens (AC), and maintaining tear flow for oxygen transmission (PC). In some specially designed Ortho-K, the RC zone

is removed for simplified the lens fitting protocol for subjects with relatively regular corneal shape [18].

There are various types of refractive surgery for improve unaided visual acuity by modifying corneal tissue. It is becoming more and more popular around the world as it could help subjects to acquire good vision rapidly after surgery and significantly improve their sports experience. The most common types of refractive surgery include Laser-Assisted In Situ Keratomileusis (LASIK) [19], Photorefractive Keratectomy (PRK) [20], Laser Epithelial Keratomileusis (LASEK) [21], Small Incision Lenticule Extraction (SMILE) [21], and Implantable Collamer Lens (ICL) [8].

Posterior scleral reinforcement surgery (PSRS) is usually applied to the subjects with pathological change in fundus such as retinal detachment, myopic maculopathy, and abnormal acceleration of axial length [22]. It helps reinforce the posterior portion of the eye to avoid over stretch or thinning of sclera and thereby stop myopia progression. The surgery is not common in clinics for general myopia prevention as it has rigorous surgical indicator for patients and potential risks like infection and surgical complications.

The structural complications of myopia usually happened in high degree myopes, but not absolutely related to fovea refraction or axial length. The pathological changes can be found in the retina, the retinal pigment epithelium (RPE), Bruch's membrane, choroid, optic nerve, optic nerve head, and sclera. In brief, the structural changes include retinal detachment, myopic traction maculopathy, myopia-associated glaucoma-like optic neuropathy, retinal tears, myopic macular degeneration (MMD), posterior staphyloma, choroidal neovascularization and myopic choroidal atrophy [2].

## 1.1.3 The prevalence of myopia

The prevalence of myopia has been increasing dramatically across the continents in the last decades. It was estimated that the myopic population will increase from 1500 millions in 2000 to 4800 million in 2050, which corresponds to half of the human population (figure 1-1) [23]. The prevalence raises cautions for eye care doctors as it is the primary cause of irreversible visual impairment and blind eye disease in the world [23-25]. The potential loss of global economic productivity caused by refractive error is another threat to our society. It was found that 268,800 million [26] dollars losses of purchasing power parity-adjusted gross domestic product due to visual impairment by WHO subregion. Thus, the problem of great myopia prevalence is not just related to personal health but also should be taken care by policy makers for economic burden.

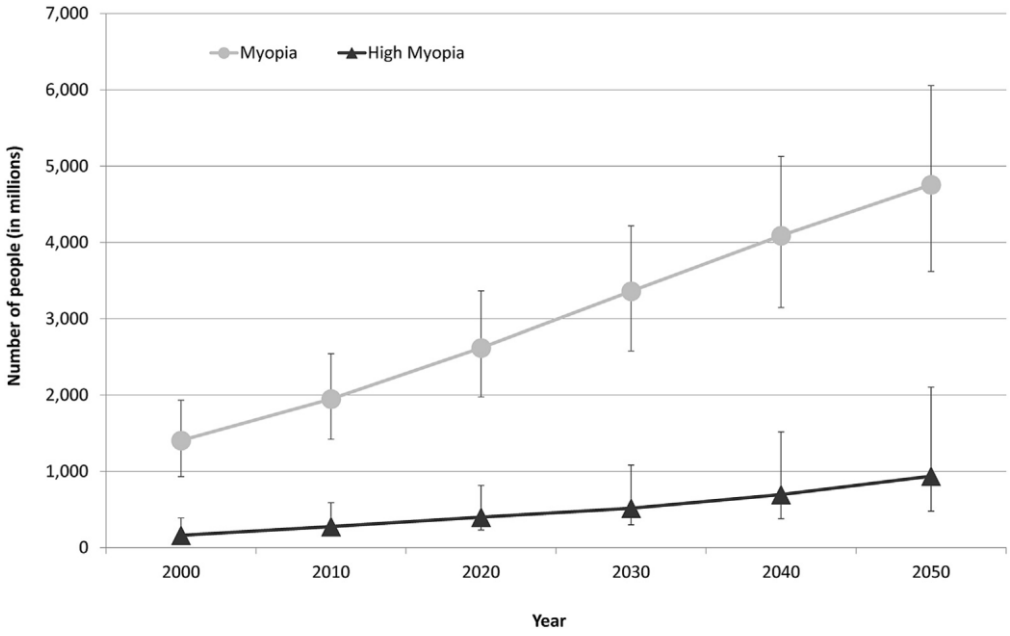


Figure 1-1. The figure illustrates the projected global prevalence of myopia and high myopia at ten-year intervals from 2000 to 2050, with error bars representing 95% CI [23].

The concern of myopia prevention or using various myopia control strategies was well developed in recent years [27]. This is reported by IMI (International Myopia Institute)

regarding updated information of concern/activity about myopia. In general, the online survey received 3195 respondents from various continents, and the concern for myopia control is significantly higher in Asia than other continents. Single vision glasses are the most popular solution for myopia correction, but the situation seems to be changed in recent years, after which shows more diversity on myopia control solutions comparing to the report in 2019 [28]. Orthokeratology used to be perceived as the most efficacious intervention for myopia control according to the previous surveys [28, 29], but combination therapy is now considered as the most effective method. This is because of the fast development of myopia research in recent years. Other myopia control solutions like myopia control spectacles, contact lenses and pharmaceutical approaches are becoming more and more popular with eye care practitioners.

The concern and activity on myopia is different among continents. Asia showed the highest concern [27]. From the report, it is kind of interesting to see that both Australasia and Asia are more open to use various kinds of new developed techniques for myopia control, and although the concern from Australasia is lower than Asia, clinical activity has no difference between two continents. South America and Europe showed less concern about myopia. This could be explained by less serious myopia prevalence in those two continents [8.61% childhood myopia in south Africa [30], 4.7 childhood myopia in Africa [31]]. Such low prevalence could be related to the combination of genetic and visual behavior influence. For example, the peripheral refraction in emmetropic children is different among Chinese, Spanish, and British [32]. It is also well known that outdoor activities and sunshine exposure are higher in Europeans and Africans than Chinese due to the academic pressure that keeps Chinese children to stay at home. The difference on visual environment could lower the risk to become myope for Europeans and Africans. However, even though the myopia prevalence is kind of low in Africa, the trajectory from meta-analysis predicted 3-fold increase from 2001 to 2050 [31]. This indicated a serious public health burden in future due to the poor access to eye care service in Africa.

Although the general myopia prevalence in Asia is relatively high compared to other continents, the difference among countries is significant. It is well documented that Chinese [33-36], Singaporeans [9, 37, 38], Korean [39] own the highest myopia prevalence over the world, followed by Bangladeshi (more than 55%) [40], Indian (around 18%) [41, 42] and Laotian (around 2%) [43]. Except for genetics, education background [35], urbanization [41, 44], green space [45, 46] and outdoor activities [47-50] are the important factors for the difference among those countries. For example, a study in Beijing revealed that populations younger than 65 years old who live in urban areas exhibited more macular myopia compared to people from rural areas, and more people with better education background were found in urban group as expected. The more area of green space [45], or higher space frequence [51] in the visual environment could be a potential approach for myopia control, as it does not give students any economic burden for their families. The myopia prevalence from Laos is kind of low comparing to other more developed countries like China and South Korea. The less urbanization and more green space are suspected for the discrepancy. A research team from Aier Eye Hospital Group is conducting clinical trial with wall paper in class room in southwest China to valid the theory [52].

In summary, the trend of myopia prevalence is increasing worldwide, which raises the concern and activities for myopia control across the continents. The activity for myopia prevention should be carried out prior to the development of myopia otherwise there is no way to get back to emmetropia. This requires a well-managed database for closely following the development of ocular refraction, and an evidence-based systematic approach for evaluating the risk of developing myopia. It is recommended that a combination of pharmaceutical and optical methods for robust myopia control, but the economic status of the local population should also be considered. For low-income countries, the access of eye care services is prioritized to other myopia treatment approaches for the population. The rapid growth of the health burden by myopia needs

full collaboration of police makers, research institutes and eye care clinics to address this cross-century problem for the whole of humankind.

# 1.2 The theories of myopia

## 1.2.1 Peripheral optics

Ocular optics are important for the development of myopia progression. The ocular optics include three primary factors to be studied, which are lower order aberrations (defocus and astigmatism), higher order aberrations (primarily coma and spherical aberration) and retinal contrast that is related to the eye's aberrations and scatter. To study ocular optics, there are two basic factors that needed to be considered: pupil size and field of view. Pupil size is closely linked to higher-order aberrations, while the field of view significantly impacts overall visual quality. Traditionally, clinicians have focused primarily on the optical quality of the central visual field, as it provides high-acuity vision. However, recent research has increasingly emphasized the importance of the peripheral visual field in myopia control.

Optical defocus is the most important theory for studying childhood myopia in the past decades. Experimentally, there are two primary theories for developing myopia in animal studies, which are form-deprivation [53-56] and optical defocus [55]. The theory of form-deprivation suggests that a lack of visual stimulation or poor visual quality can lead to abnormal growth of the eye and finally results in myopia [57]. The theory of optical defocus was first observed by Schaeffel et al. in 1988 [58]. They found that chickens raised with positive lenses exhibited more hyperopia in central retina, whereas those with negative lenses developed more myopia in central field (figure 1-2). Hence, they propose the hypothesis that eyes have the characteristics to adjust the eyeball by following the focus of light. The hypothesis was validated in numerous animal studies like chick [58-60], rhesus monkeys [61], guinea pig [62], and marmosets [63].

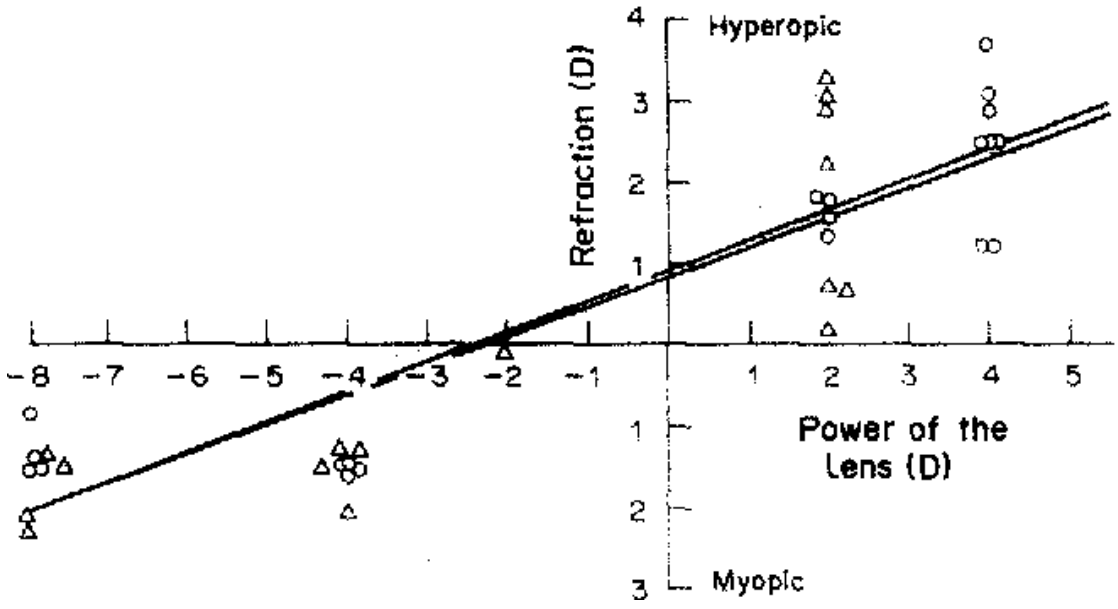


Figure 1-2. Refraction of chicken eyes against the power of experimental lenses after three weeks [58].

The theory of defocus could also be explained by the lag of accommodation. The lag of accommodation is a special situation in the human eye. It happens when the eye (ciliary muscle) does not provide enough accommodation response while the subject is looking at a near object. The difference between real accommodation and the required accommodation caused hyperopic defocus, what can result in myopia progression. The amount of lag is dependent on the fixate distance, age, and the degree of myopia. Researchers speculate that such amount of mild hyperopic defocus (around 1D) is a kind of special hyperopic defocus status in retina. It will finally lead to myopia progression and axial elongation [64-68].

Traditionally, clinicians are more interested in central field, as cone cells are the main contributor of sharp vision that mostly distributed in the fovea of macular. However, it also retarded the application of defocus theory on myopia prevention for some decades. The issue was later proved can be resolved by erase the optical effect in central retina [53, 54, 69, 70]. In brief, those studies tested the myopia progression with various lenses (positive defocus or negative defocus) in rhesus monkeys. They found that central

vision is not necessarily needed for lens induced myopia by ablating fovea by argon laser. After this study, the theory of peripheral defocus is becoming more and more popular in the field of myopia prevention.

There are multiple myopia control products that are related to defocus theory. For example, multi-focus spectacles [Defocus Incorporated Multiple Segment Lens (DIMS) [71-73], MyoCare [74], Stellest [75, 76]], soft contact lens [77], and orthokeratology [1, 75]. The results from those studies indicate that myopia progression can be slowed down by adding myopic defocus in the peripheral retina. However, a study from Japen found that peripheral defocus spectacles MyoVision do not support the therapeutic effect for slowing down myopia progression [78]. The treatment efficacy among individuals is also varied in different myopia control products. The conflicts between those studies can be explained by unawareness of intrinsic peripheral retinal refraction, ethnics, optical design of the products, wearing time of the products and so on.

Peripheral refraction is a crucial factor in understanding how peripheral optics influence myopia progression. Peripheral optics can be divided into two categories. The first category is the intrinsic peripheral retinal refraction of the subjects, which needs to be measured by refractometer. The second category is the additional refraction induced by myopia control products, determined by the optical design of these products. The treatment effect on myopia progression must be brought by a combination of both intrinsic peripheral refraction and additional peripheral refraction. To better understand how peripheral refraction works on myopia progression, it is important to have a proper device that provides peripheral retinal refraction in a reliable way.

The research about peripheral retinal refraction and myopia can be traced from two studies published in 1971 [79, 80]. The authors measured peripheral refraction in around 500 pilots by using retinoscope. The method was simple, time consuming, just available for a few eccentricities, but admitted by optometrist (figure 1-3). They

measured peripheral refraction across central 120 degrees of visual field and found that the pattern of peripheral refraction can be categorized into 5 types, each type corresponding to a specific refractive statue (myopia, emmetropia, and hyperopia). The study kicks off the study of peripheral refraction in human eye.

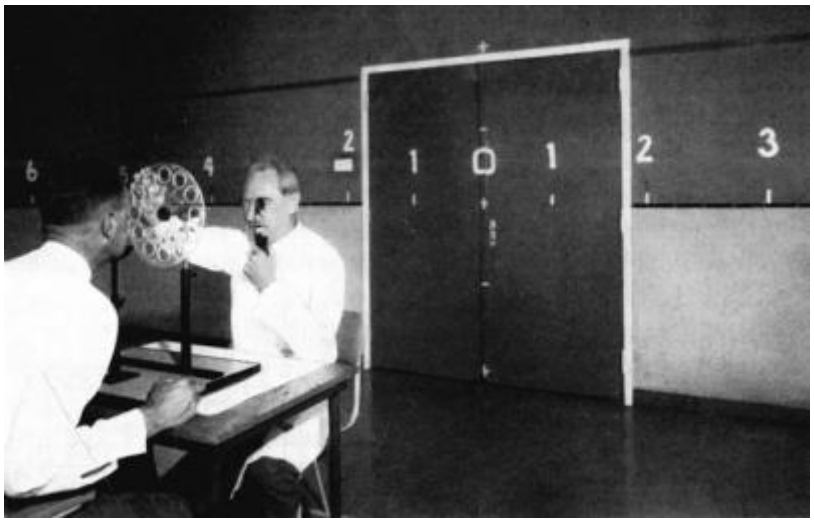


Figure 1-3. Retinoscope for peripheral refraction [79].

There are numerous studies that investigated peripheral refraction in the human eye. However, limited by the efficiency of the device for peripheral field, most of the studies just reported peripheral refraction in horizontal meridian or added few other eccentricities [37, 81-94]. A few studies investigated two-dimensional peripheral refractive maps, but the limited sampling points cannot provide satisfied resolution for deep understanding of peripheral refraction [95-97].

The devices for measuring peripheral refraction are listed below:

**Retinoscopy:** The traditional method for peripheral refraction, reliable, but the efficiency for peripheral measurement is quite dependent on the experience of the optometrist. The measurement for 5 eccentricities would take approximately 10 minutes to complete the exam [79, 80].

**Open-view autorefractor:** The commercialized representative devices include WAM-5500 and NVision-K 5001. The subject can have open view during the test. The measurement of peripheral refraction is achieved by rotating the eyeball to preset angles. Voptica Peripheral Refraction (VPR) is a prototype used in the thesis, and it also belongs to the scope of this category [98, 99]. Eccentric photorefractor is another prototype developed by Schaeffel et al. for measuring peripheral refraction [99, 100]. But the device poses a blind zone for a specifical range of refraction, and it cannot provide information about higher order aberrations.

**Closed view autorefractor:** This category includes BHVI-EyeMapper [101] and MRT (multispectral refractive topography) [102]. BHVI-EyeMapper is a prototype developed at the Brien Holden Vision Institute. The device has multiple fixed beam splitters, one scanning mirror, and one wavefront sensor. The device can provide fast exam and reliable data for peripheral refraction. The major problem for the device is the limited eccentricity for peripheral measurement, and the close view design restricted itself from further application on peripheral refraction in vertical direction. The principle of MRT is based on the relationship between blurring estimation and theoretical peripheral refraction. The problem with the device is it only provides rough estimation on spherical equivalent refraction, and no available information about calibration for peripheral eccentricity can be found or proved online.

Although the device for measuring peripheral refraction varies across different studies, the findings are basically the same for horizontal direction. In general, hyperopes present relative peripheral myopia in the peripheral field, and myopes demonstrate relative peripheral hyperopia. The relatively peripheral refraction (RPR) in emmetropes can be hyperopia or myopia, but relatively flat (close to zero diopter) compared to the other groups. RPR can be calculated by subtracting central retinal refraction from peripheral refraction across the field. It seems that the consequences of eye development with RPR modification in human trials and animal studies are the same as

we observed from intrinsic RPR from human eye. However, there are few studies with conflicting results [68, 103-105] suggesting that peripheral defocus cannot predict the development of myopia progression. The discrepancy between intrinsic RPR and additional RPR can be attributed to the incomprehensive understanding of characteristics of peripheral refraction of human eye, which is seriously limited by the clinical available device for peripheral refraction. To address this gap, we previously conducted some clinical studies based on the prototype (VPR) that we developed some years ago. The technique provides insights into the distribution pattern of different populations [8, 32, 106-109].

Defocus is important in the field of peripheral refraction, but it is not the only optical metric that can be linked to myopia. Astigmatism, higher order aberrations and retinal contrast are the other metrics that may show significant connection. For example, peripheral spherical equivalent refraction (SER) is the most frequently used metric to describe RPR. The relative value is increasing with eccentricity and the degree of refractive error. However, we notice that the component of astigmatism takes most of the SER value in the periphery [32, 107, 110], which means that astigmatism may be also a contributor to myopia progression. Higher order aberrations, like coma and spherical aberration, are the other metrics that showed connection with myopia progression [15, 64, 92, 111, 112].

DOT (diffusion optics technology) is a newly designed lens to slow myopia progression by reducing contrast signaling in the retina [113]. The clinical trial reported 74% reduction and 59% reduction in refraction for two types of design. The results were surprising to the field as this lens did not change peripheral defocus to control myopia.

In summary, peripheral refraction is a primary theory for the development and prevention of childhood myopia. The relevant research has been conducted over the last 40 years. However, due to the lack of peripheral refractor that can be applied to large

scale longitudinal studies, the critical question about the relationship between peripheral refraction from various retinal regions and myopia progression is still unable to be answered.

## 1.2.2 Lag of accommodation

Accommodation refers to the ability to adjust the focal length of the eye for sharp vision by adjusting the shape of crystalline lens for objects at various distances. The process involves several ocular components: crystalline lens, ciliary muscles and zonular fibers (figure 1-4). When the subject is looking at a distant object, the ciliary muscles relax and the zonular fiber tighten, the lens reduces its curvature by thinning the body, and then the focal length of the eye increases. While the subject is looking at the near object, those ocular components work in an opposite way, and then the power of the ocular optics increases. Both actions are for a clear image to be located on retina.

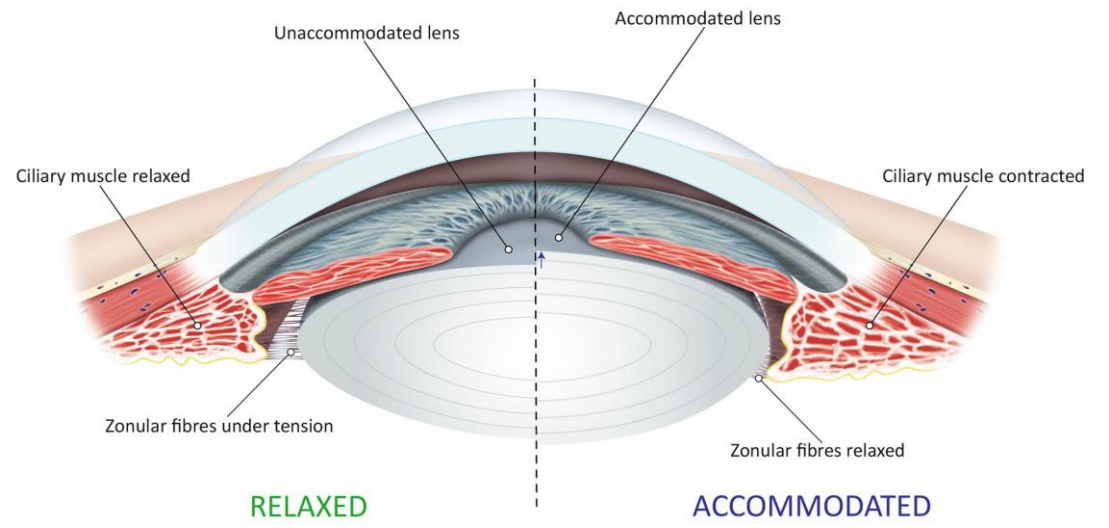


Figure 1-4. Anatomy in anterior eye structure in the relaxed (left) and accommodated (right) status [114].

Nevertheless, the accommodation is not always accurate because of the existence of the depth of focus of the eye. This is influenced by visual function, ocular refraction,

chromatic aberrations, pupil size and neural factors [114-116]. The inaccurate behavior of accommodation response includes two categories: over accommodation and accommodative lag. If the accommodation response is more than the need of the subject, then it belongs to over accommodation. If the accommodation response is less than the need of the subject, it is the so-called accommodative lag.

The influence of accommodation on myopia's progression has been debated for decades. Some researchers indicated that the lag of accommodation is the trigger of myopia progression [64-67], and other studies gives the opposite conclusion [117-120]. It seems that the increase of the accommodative lag is more like a consequence of myopia progression rather than a cause. Interestingly, an orthokeratology study found that more accurate accommodation response (less accommodation lag) is linked with lower axial progression [64].

The influence of accommodative lag in myopia progression can be explained by defocus theory. According to the previous study, even though the accommodative lag is less than 0.5D, still it would be sufficient to promote myopia progression [121]. Theoretically, when the lag of accommodation happened, the lens cannot provide enough power for the light to focus accurately on the retina. This can cause blurring and hyperopia in the whole visual field. According to the defocus theory, the eye will gradually elongate the axial length to neutralize defocus or blurred images, resulting in extra myopia progression.

In summary, the influence of accommodation lag is a long debate question. Further studies need to be carried to validate the effect of accommodation response, especially dynamic transient response [122], on myopia progression.

### 1.2.3 Near work activities

Prolonged near work (e.g., reading, writing, and smartphone use) have long been studied as potential contributors to myopia development [47, 123-125]. A recently published meta-analysis that included 254,037 patients revealed that the odds ratio of developing myopia increased 26% in children or 21% in adults when exposed to near work [126]. Academic pressure from higher education also increased the time for near work, resulting in more myopia progression in children [127]. Nevertheless, some of the longitudinal studies indicated that near work activities are not significantly related to myopia progression [128-131].

The mechanisms through which near work contributes to myopia are complex and multifaceted. It can be explained by over-accommodation or accommodative spasm, and both situations will induce malfunction of accommodation response for near distance visual tasks, resulting in blur image or hyperopic defocus in periphery. Except for the optics effect in human eye, the decreased blood supply in choroid may be another reason for the over extension of the eye [132].

The quantification of near work is critical when conducting relevant studies. It is very likely that traditional quantitative methods like questionnaire would lead to recall bias after certain event happened for hours or even more [47]. For this concern, there are several wearable devices were developed for recording near work activity: Clouclip [47, 124, 125], RangeLife [133], Vivior [134] and ultrasonic sensor [135]. Although those devices have fixated distance detectors along with the head of wearer, this feature also limited the accuracy for estimate visual distance while subject is looking at peripheral targets, or when the object to be looked at is kind of small like hand-held electronic devices. Based on the rule of near triad response (or accommodation-convergence reflex), convergence, accommodation and pupil miosis are the three elements of ‘near triad’ for looking at near object [136]. This feature provides the possibility of estimate

gaze distance by tracking pupil position without concern of the line of the sight of wearer.

There is also a presbyopia correction wearable device, Mompean et al. [137, 138]. It consists of two cameras for recording pupil position that drive optoelectronic lenses for near vision for presbyopes. The device can be simplified with only pupil cameras for estimate binocular gaze distance for near work activities. The device has the potential to provide accurate data for myopia research. Chapter six of the thesis provides detailed information about the validation of this device for evaluating gaze distance.

## 1.3 The motivation of the thesis

We will explore the following problems.

**1. How does the eye's inherent peripheral refraction influence myopia development?**

Spectacles with peripheral refraction modification have been shown to affect myopia progression. However, the inherent/intrinsic peripheral refraction shows certain variability in population. Thus, the peripheral refraction profile should be considered when providing prescribed myopia control lenses. Some questions are worth exploring. For instance, should different diopters be added to various parts of the lens? Does the optical effect differ between emmetropes and myopes? Is peripheral relative refraction the cause or consequence of myopia progression?

To address these questions, a device capable of measuring inherent two-dimensional peripheral refraction with high resolution should be developed. Additionally, a longitudinal study involving children is necessary to validate these points.

**2. Does a modified peripheral refraction slow myopia progression by adjusting accommodation response?**

Peripheral refraction modification for myopia control is a widely discussed topic. Improvements in accommodative lag are often considered a key factor in myopia control, although this remains a topic of debate. To explore this, a methodology should be developed that can modify peripheral optics while simultaneously recording the accommodation response. Furthermore, recent interest has grown around retinal contrast. A device capable of quantifying retinal contrast would provide valuable insights into how peripheral refraction aids in controlling myopia.

**3. Can we develop a wearable device that can estimate binocular gaze distance associated with accommodation?**

Gaze distance is closely tied to near-work activities, but currently, no device is available to estimate it accurately. Developing such a wearable device would help bridge the gap in precisely evaluating near-work activities and visual behavior, allowing for more accurate assessments of their impact on myopia progression.

## 1.4 Objectives of the thesis

- To illustrate the functionality of inherent/intrinsic peripheral refraction in myopia progression
- To investigate the role of accommodation response in myopia control for multifocal spectacles, and how dose the lenses influence retinal image quality.
- To develop a lightweight wearable device for estimating binocular gaze distance

# Chapter 2. Instrumentation and methods

# 2.1 Voptica Peripheral Refraction (VPR)

## 2.1.1 Introduction

The Voptica peripheral refraction (VPR) is a Hartmann-Shack wavefront sensor for measuring aberrations in horizon meridian of human eye. The device could be used to measure two-dimensional peripheral refraction by adding fixation targets at vertical direction, which requires compliant rotation of the eye.

## 2.1.2 The principle of the device

The Hartmann-Shack wavefront sensor precisely measures optical aberrations (both low- and high-order) using a lenslet array to split the wavefront and a camera to record the focal spots for wavefront reconstruction. The lenslet array is a specially designed optical component that is composed of a matrix of microlenses. The camera is placed at the focal length of the microlenses. If the system under testing has no aberrations, then a matrix of light spots will be observed on the detector with geometric center of the spots corresponding to the center of the micro lenses. If the system is affected by aberrations, the center of the light spots will shift accordingly. Based on the shifted distance, the aberrations can be described typically as an expansion of Zernike polynomials [139].

The instrument was first described in 2011 by Jaeken et al [98] (figure 2-1 & figure 2-2). In brief, the device has a Hartmann-Shack wavefront sensor conjugated with the center of the subject's pupil by two lenses. The sensor, light source and lenses were mounted on an optical arm that was capable of rotating 80 degrees (from temporal side to nasal side). One long regular mirror and one hot mirror were fixed on the main body of the device. The wavelength of the laser was 780 nm. When the subject is ready for the measurement, the optical arm will move from one side to the other side to perform the scan in horizontal direction. The system acquires 61 Hartmann-Shack images in

~1.3 seconds. The camera and motor were synchronized at 50 fps and 50°/s, respectively, though their maximum capabilities are 60 fps and 80°/s. Inter-subject variability showed an average standard deviation of 0.13D across the visual field.

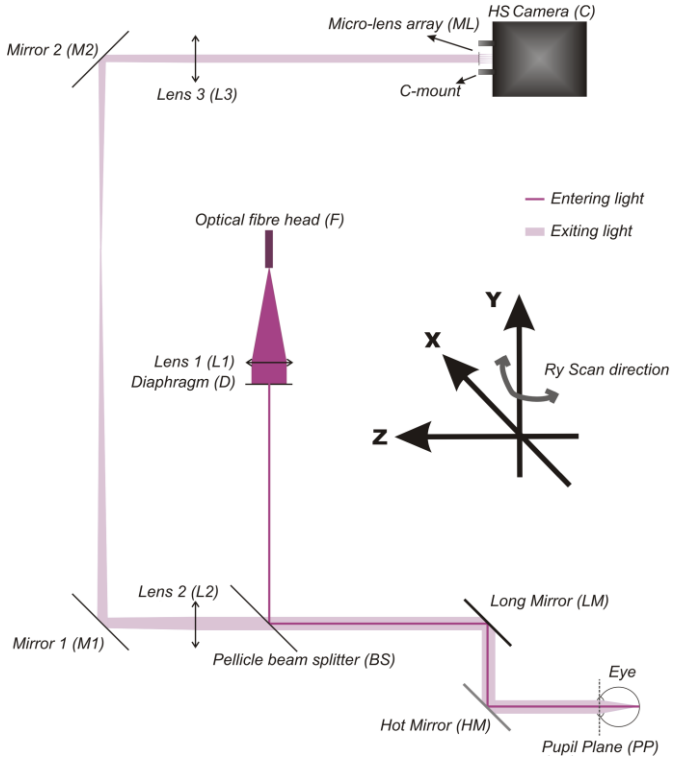


Figure 2-1. Schematic side view of the optical design of the HS wavefront sensor scanner [98].

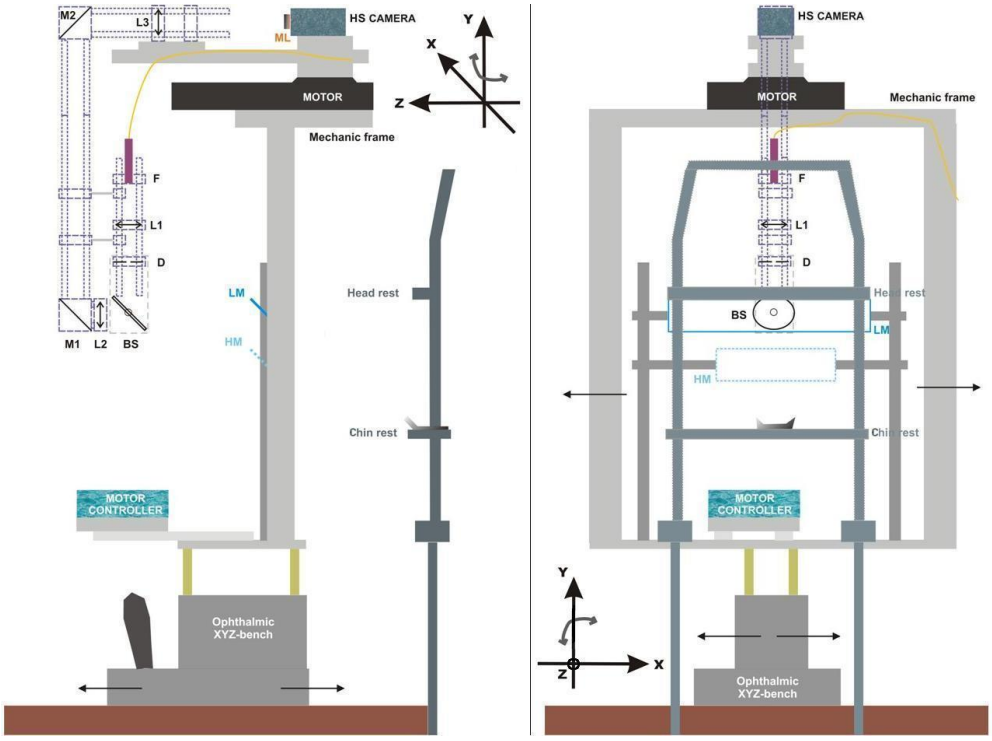


Figure 2-2. Schematic side (left) and front (right) view of the HS-scanner showing the layout of the instrument. The arrows show the direction of possible movement of the ophthalmic bench [98].

The accuracy and calibration of the device was also been published [99]. The repeatability of the device was tested with 12 adults (see results in figure 2-3. Unpublished data), while the evaluation was performed by 5 consecutive measurements in and without cycloplegia. The average standard deviation of the measures across all the eccentricities was used to express the repeatability of the device. The mean of standard deviation for all subjects prior to cycloplegia was 0.18D, which is smaller than the general requirement for clinical test (0.25 D). After cycloplegia, the mean of SD decreased to 0.13D. These results indicate a good inter-subject variability of the device.

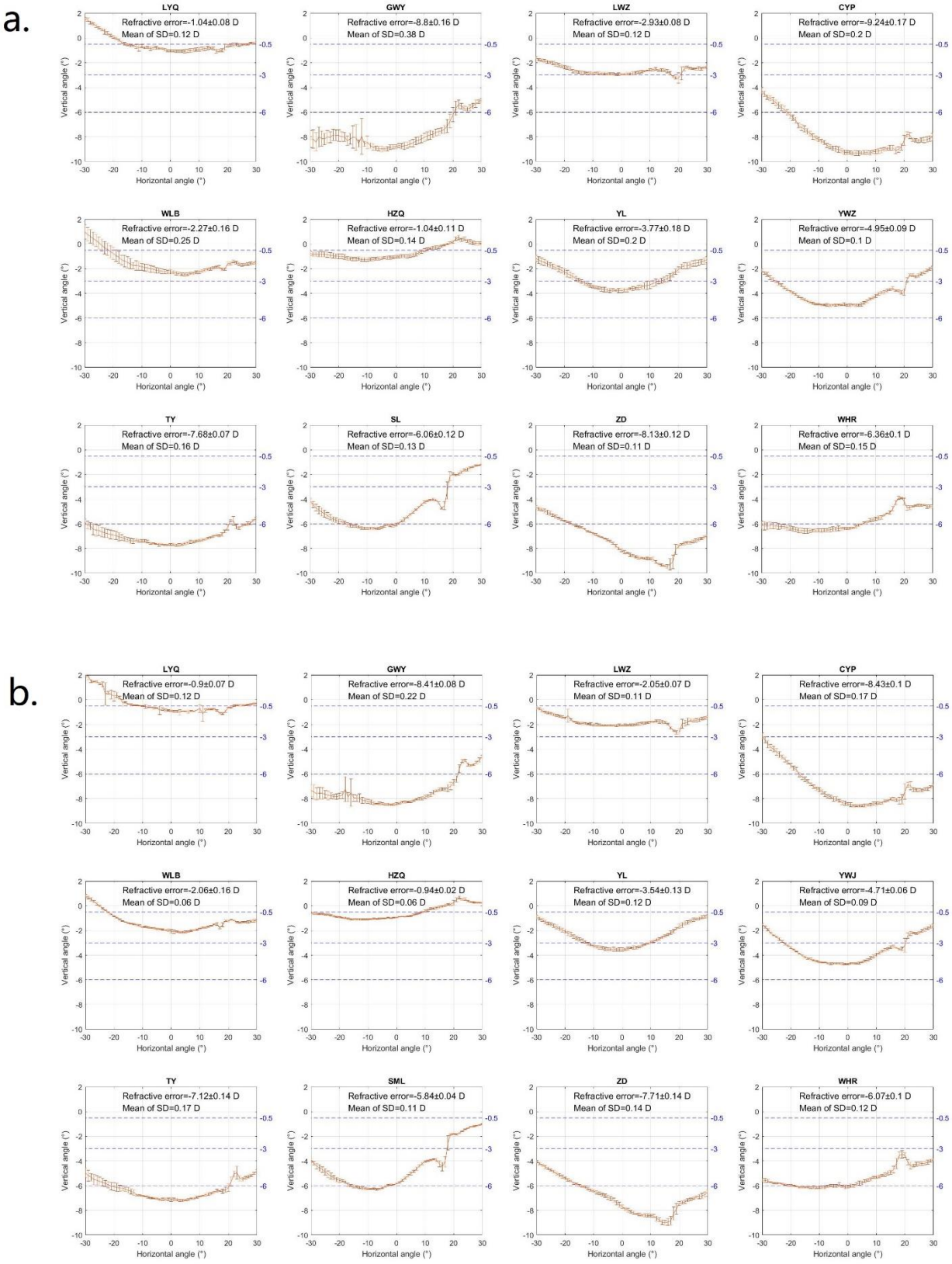


Figure 2-3. Peripheral refraction across horizontal meridians for 12 subjects. a.)

Peripheral refraction prior to cycloplegia. b.) Peripheral refraction after cycloplegia. The error bar means standard deviation of 5 measures. The mean of SD in the figure 2-3 represents the average standard deviation for all eccentricities for the 5 measures.

### 2.1.3 Adaptation of the system

We added one extra target system for the measurements at different vertical directions (See the testing environment in figure 2-4). The vertical target system includes 10 regular bulbs, one remote controller, one tripods, and some papers for wrapping the bulbs. The bulbs are controlled by the practitioner through remote controller. All bulbs are wrapped by black paper to avoid leaking of light. Then, the front side of the black cover was cut out to make a cross-shape like target (height = 4.7 cm, line width = 0.5 cm) with a few layers of regular white paper attached to control the intensity of light. Considering the regular height of the indoor room, the distance from the target to the eye was controlled at 2.5 meters. The upper limit (corresponding to inferior retina) and the lower limit (corresponding to superior retina) for the visual field in vertical direction was set as 20 degrees and 16 degrees. The range was defined to reduce the interference of eye lashes on peripheral refraction measurement. The interval of the targets was set as 4 degrees, thus, there were 10 targets fixed with the tripod by metal clips. Ideally, the fifth target corresponds to the central horizontal peripheral refraction passes through macular. See a schematic about the principle of 2-D measurement in figure 2-5.

Figure 2-4. The testing environment and the physical appearance of the device.

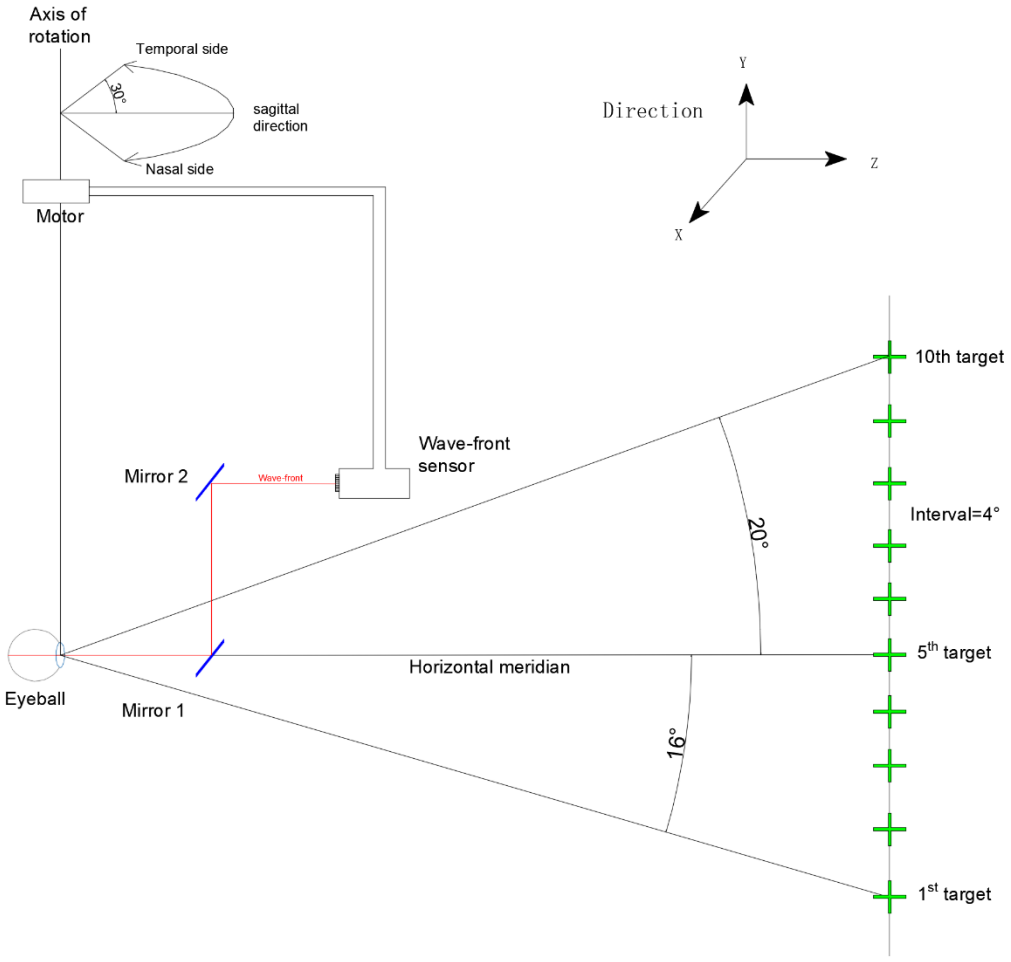


Figure 2-5. The schematics of the device for measuring 2-D peripheral refraction map.

## 2.1.4 Measurement's protocol

The position of the light bulbs on the tripod should be determined and well-fixed before experiment.

First time calibration

i) Initialize the VPR program (figure 2-6)

ii) Turn on the central bulb (the 5$^{th}$ bulb, which corresponding to the coordinate origin of the 2-D map) of the target system.

iii) Place subject in position. Adjust the height of the chin-test until the lateral canthus align with the marker in the side of the holder.

iv) Move the optical arm to the position Zero degrees. The subject should be able to see the laser right in front. If not, adjust the position of the tripods until the bulb aligns with the instrument's laser.

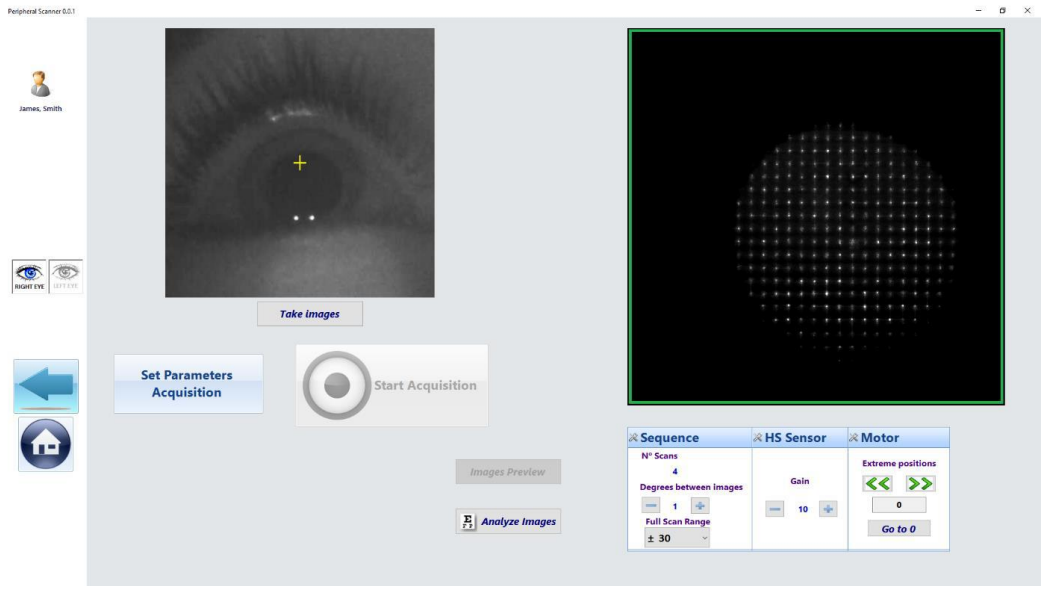


Figure 2-6. The measurement window of VPR program.

The relative position between VPR and the target system are not fixed completely. Thus, there might be slight movement of the system due to unintentional contact by the subject or the practitioner. At least one regular check should be performed prior to the

test at the beginning of the day to ensure the right position.

Measurement protocol

i) Initialize the VPR program.

ii) Turn on the fifth bulb of the target system.

iii) Subject in position. Adjust the height of the chin-test until the lateral canthus aligns with the marker in the side of the holder.

iv) Move the optical arm to the position Zero degrees. The subject should be able to see the laser right in front.

v) Move the optical arm to the position at nasal 30 degrees and temporal 30 degrees to check if the projected laser on iris is always tilt equally to the nasal side and temporal side. When the angle is zero degrees, the projected laser should always stay in the center of the pupil. This step needs repeat adjustment of the position of the optical arm in three dimensions.

vi) When the subject is ready, ask the subject to blink the eye and then click 'Start Acquisition' to measure peripheral refraction.

vii) When one measure was done, repeat step iv to step vi for the rest of the targets. The sequence of the measurement angle is:

0° → -16° → -12° → -8° → -4° → +4° → +8° → +12° → +16° → +20°.

## 2.1.5 Metrics

The metrics exported from VPR include Zernike coefficients Z3 to Z20. Lower order abbreviations Z3, Z4, Z5 were transformed into astigmatism components J0, J45, cylinder power, axis, SER, and spherical power. The details about this transformation are described elsewhere [139].

## 2.1.6 Two-dimensional peripheral refraction maps

The two-dimensional peripheral refraction map was retrieved by 10 horizontal scans by

using customized Matlab scripts. The process for generating 2D maps can be briefly described as follows:

i) Export the original csv files from VPR program.

ii) Extract different metrics.

iii) Recognize the measurements by identifying comments in column 'D' in the exported csv file. The numbers in column 'D' indicate the sequence of the bulbs. For example, number 1 corresponds to the lowest bulb, and number 10 corresponds to the highest bulb.

iv) Make average for the measurements if there were multiple measures for one bulb.

v) Identify the outliners: divide the curve to six sections for each horizontal measurement [the six sections are within the range x=: (1-10), (11-20), (21-30), (31-40), (41-51), (52-61)]. Calculate quartiles Q1 and Q3. If the value within the specific range is larger than [Q3+1.5*(Q3-Q1)] or smaller than [Q1-1.5*(Q3-Q1)], then the value can be defined as outliners. An example for removing outliers is presented as figure 2-7.

vi) Remove the outliers. Using one-dimensional data interpolation for missing data within the peripheral curve or predicting the missing data which is located at the edge of the curve.

vii) Using two-dimensional data interpolation to generate the final 2D map with resolution as 1 degree in vertical meridian (Figure 2-8).

In the 2D refraction maps, the x-axis denotes nasal (positive) and temporal (negative) retina, while the y-axis indicates superior (positive) and inferior (negative) retina. The color-code is in diopters or microns depending on the metrics displayed. For example, figure 2-8b shows an example of peripheral defocus map from an emmetropic subject. The figure shows a spiral distribution of peripheral refraction across the whole retina, with more hyperopic defocus in temporal-superior retina and more myopic defocus in inferior-nasal retina. A small region with significant myopic defocus in nasal 18 degrees

shows the effect of optical nerve to optical defocus. This feature can also be treated as a biomarker for identifying the nasal or temporal side of the eye.

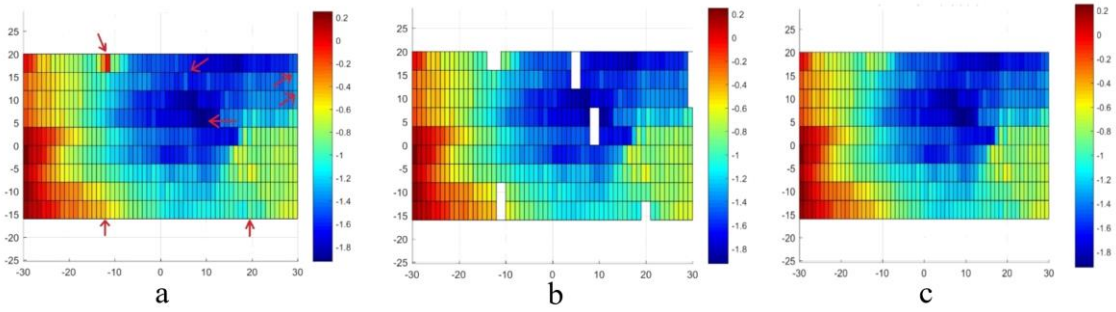


Figure 2-7. The original 2D maps and data cleaning. a). The original 2D map with outline data (indicated by red arrow). b). The original 2D map after removing outline data. c). Data interpolation for outline data in figure b.

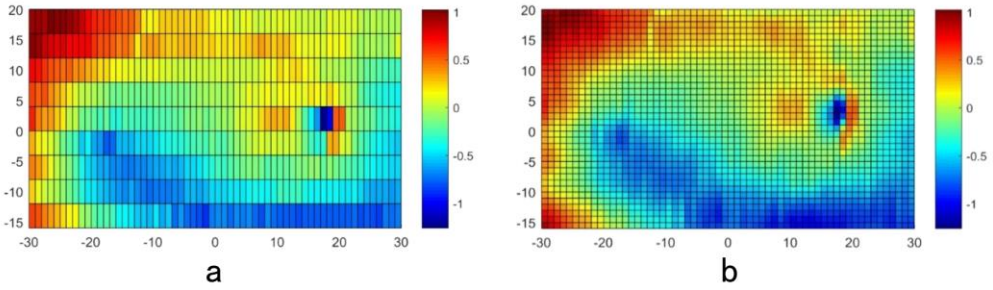


Figure 2-8. The refraction maps before and after 2D interpolation. a). The 2D map after data cleaning. b). The refractive map after 2-D interpolation for smooth map details.

# 2.2 Double-pass device

## 2.2.1 Introduction

Double-pass device determines the refraction of the eye via through-focus images of point spread function. The details about this method have been published extensively [140, 141]. The device consists of a 780 nm infrared laser that can produce a point-like spot (point spread function image, PSF) on retina. The device can induce defocus by a tunable lens from -10D to +10D. The step of diopter can be varied depending on the requirement for the speed of measurement.

## 2.2.2 The principle of the device

The device can determine the best focus image by simply selecting the image with maximum pixel value from a set of through-focus images. However, this method may not work if the subject has high astigmatism (figure 2-9). As the picture indicated below, the selected image with maximum pixel value just represents the front focus of an optical system. The calculation of astigmatism can be performed with another custom Matlab script (figure 2-10). Another approach to determine the best focus image is to find the valley of the ellipse ratio curve [140] (figure 2-11).

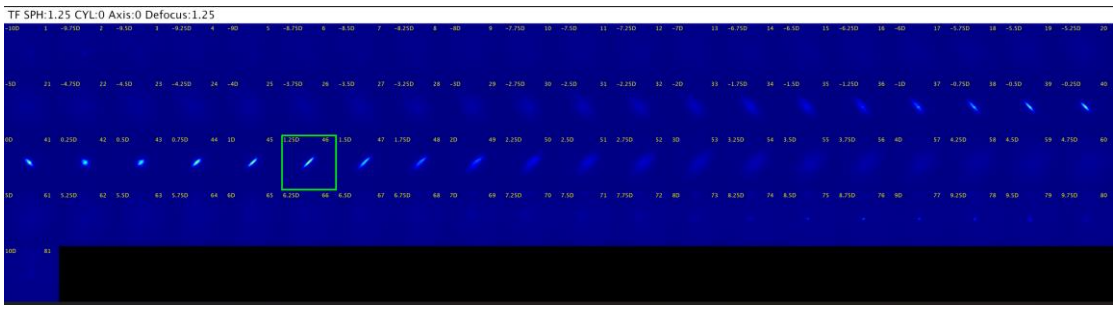


Figure 2-9. An example of through-focus image with high astigmatism. The selected image was found to possess maximum pixel value amount the group of PSF images, but it does not correspond to the best focus image. The labels of the PSF image indicate

the defocus of the optical system.

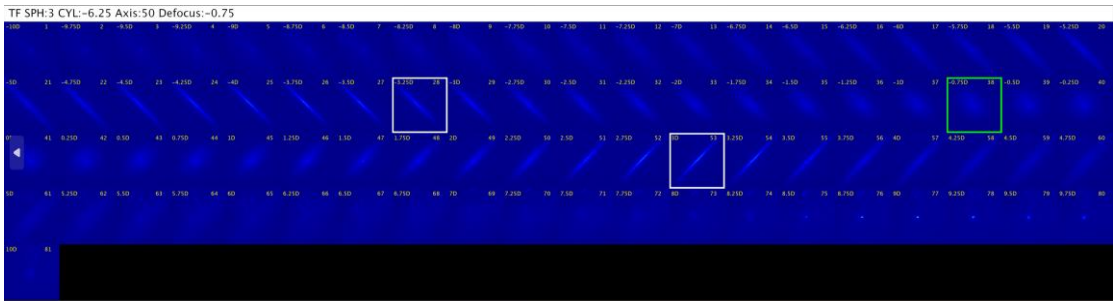


Figure 2-10. An example of through-focus image with correct selection for defocus. The green box indicates the best focus image (spherical equivalent refraction). The white boxes indicate the front focus and the back focus of the system. The white box with bigger value corresponds to the spherical refraction. The interval between the white boxes indicates the amount of cylinder power.

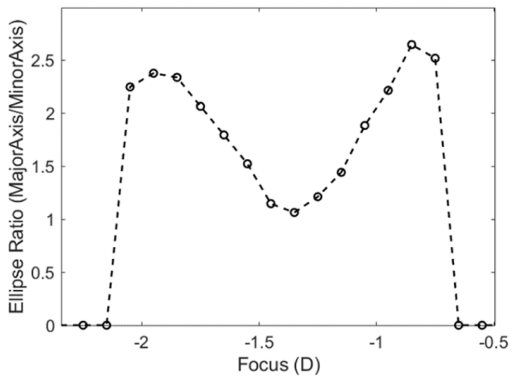


Figure 2-11. The ellipse ratio of through-focus image in an optical system with astigmatism.

The algorithm may fail the calculations due to lens reflection. Thus, a customized Matlab App was established to double check the results manually (figure 2-12). The operator can select the best focus image manually and then determine the right choice by clicking the panel of the PSF image matrix. The user can zoom in the image to check more details about the PSF image. As an example, figure 2-12 shows the red plot is the original results from the device. The yellow plot is the corrected results from the

practitioner.

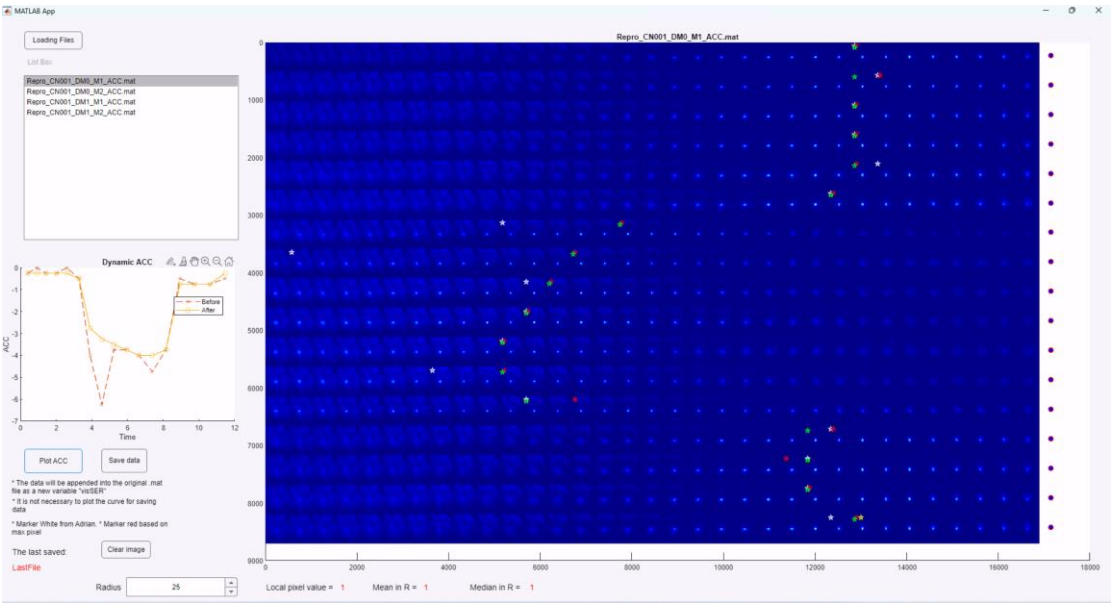


Figure 2-12. The Matlab App for checking best focus images manually with eyes.

## 2.2.3 Instrument setting

In addition to the double pass device, we prepared accessories for holding the myopia control lenses and for shifting targets. The modelling of the device was established in SolidWorks to better design and manufacture the components (see figure 2-13 and 2-14 for the modellings of the instrument; see figure 2-15 for the physical appearance of the instrument). The components are labeled, and the functionalities are explained below:

C1: The board for attach near target. It can rotate to display or hide the near target.

C2: The motor to control up and down of the near target.

C3: An Arduino Uno control board for the motor.

C4: The tracker to control the position of near target.

C5: The pulley for fixing the control board and the near target holder.

C6: The retainer for holding the frame of myopia control lenses.

C7: The myopia control lens.

C8: A model represents the subject.

C9: The handle for controlling the horizontal displacement of the myopia control lenses.

C10: The hot mirror. The pupil image can be reflected in the CMOS camera by the mirror. Subjects can see the targets through this transparent mirror.

The distance of the distant target was set as 3 meters.

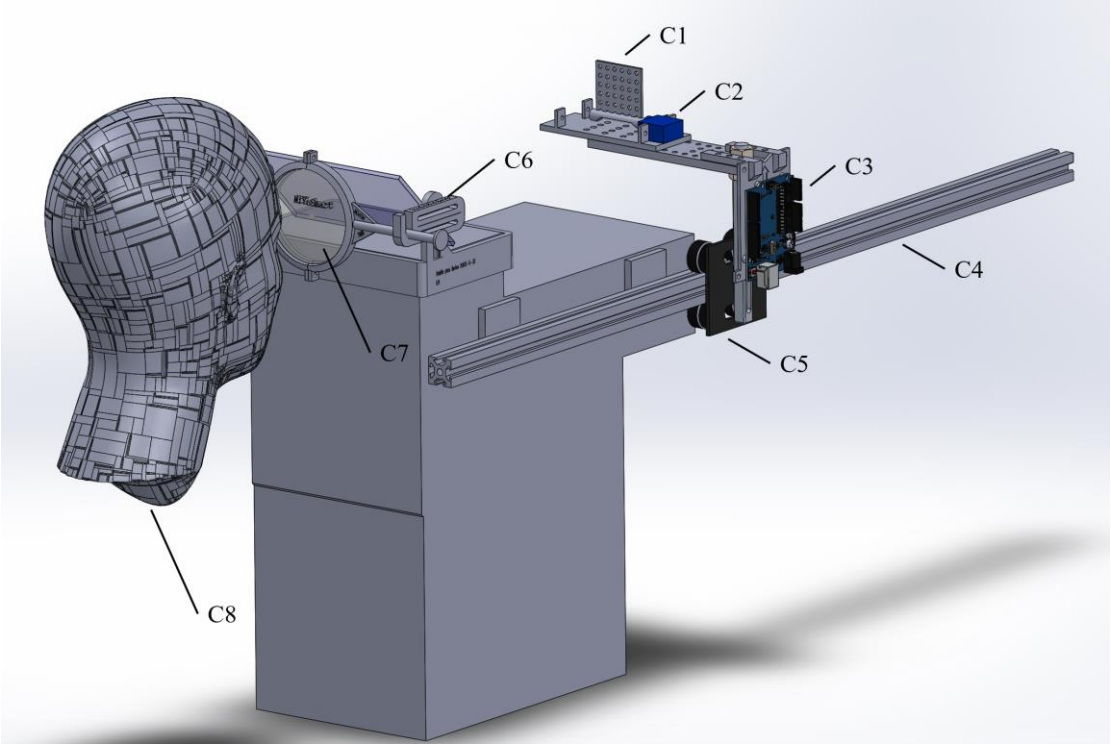


Figure 2-13. The modelling of the double-pass device from the perspective of subject.

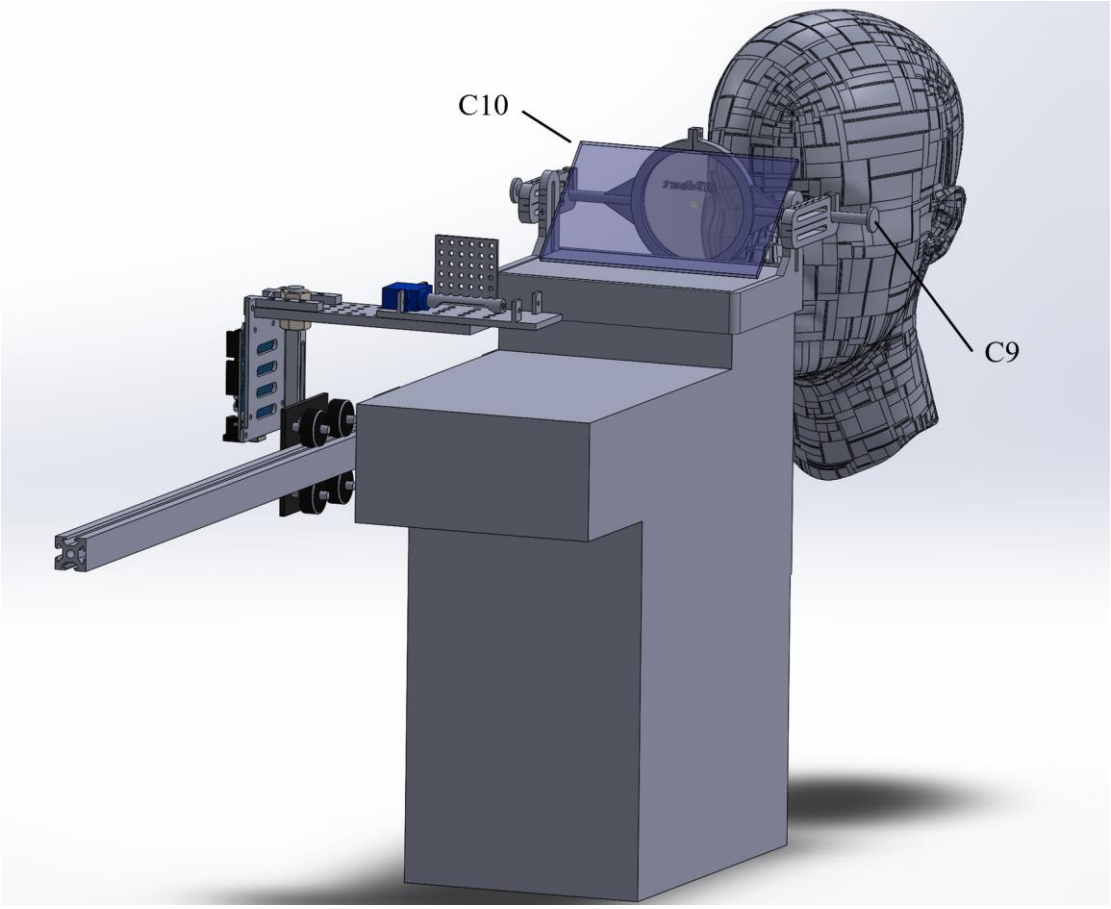


Figure 2-14. The modelling of the double-pass device from the perspective of operator.

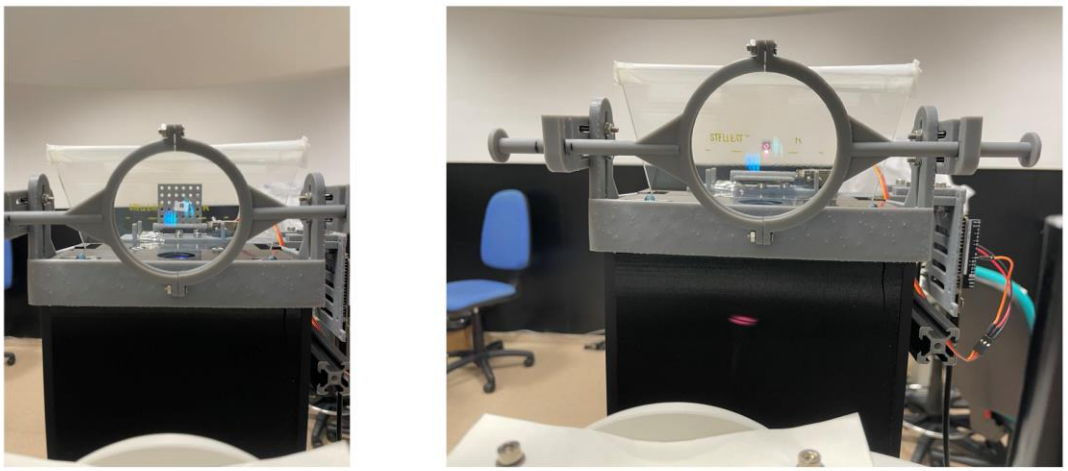

a b

Figure 2-15. The physical appearance of the double pass device from the perspective of subject. a). Demonstrate near target for stimulating accommodation. b). Demonstrate distant target for relaxing accommodation.

## 2.2.4 Protocol for measurements of the dynamic accommodation response

The device needs a starting point for dynamic accommodation test determined by the SER of the subject under the best corrected visual acuity. For acquiring dynamic accommodation response in high frequency, we set a range of through focus based on the SER of the subject [(-6D: 0.25D: +1D) for adults, (-7D: 0.25D: +1D) for children]. The through-focus range was finally determined by the standard range plus the SER of the subject. For example, if the refraction of the adult subject is -1.5D, then the through-focus range for the dynamic accommodation test would be -7.5D to -0.5D. In real, the SER of the subject always >-1.0D as the refraction was determined with prescribed glasses.

The camera's exposure time was established at 0.01 seconds, allowing the instrument to capture a full cycle of through-focus images in 0.65 seconds (33 images), resulting in 17/16 measurements for adults/children in the dynamic accommodation test. The moment for shifting targets from far to near was determined after the first 3 seconds after a complete set of through-focus images. When the time extended beyond 8 seconds, the target would shift from near to far again.

The experimental protocol is as follows:

i) Chose the type of lens based on the preset sequence.

ii) Fit the lens into the customized 3D printed frame and then attach the frame to the device for central vision or peripheral vision test.

iii) Place subject in position. Open the customized Matlab App.

iv) Turn on the pupil camera and LED lights for illuminating the subject. Move the device until the position is ready for measurement.

v) Measure the best focus of the eye. The device will record the through focus images

of the eye from -10D to +10D with step of 0.25D.

vi) Measure the dynamic accommodation response. The last time for distant, near, and again distant target is 3s, 5s, and 3s. The stimulation of accommodation was 0.33D for distant target and 4.5D (22 cm)/5.5D (18 cm) for adults/children.

Only the right eyes were recorded. The left eye covered during the experiment.

# 2.3 The wearable Eye-tracker

## 2.3.1 Introduction

The Eye-tracker is a customized wearable pupil tracker for estimating gaze distance. It was manufactured in the form of spectacles with the capability of visual correction. When the subject was wearing the spectacles, an Android based application was applied to receive pupil images by WIFI connection, and the distance estimation was performed on a smartphone. The device is a useful tool for the study of visual behavior. See figure 2-16 for the image of testing room and a screenshot of the app.

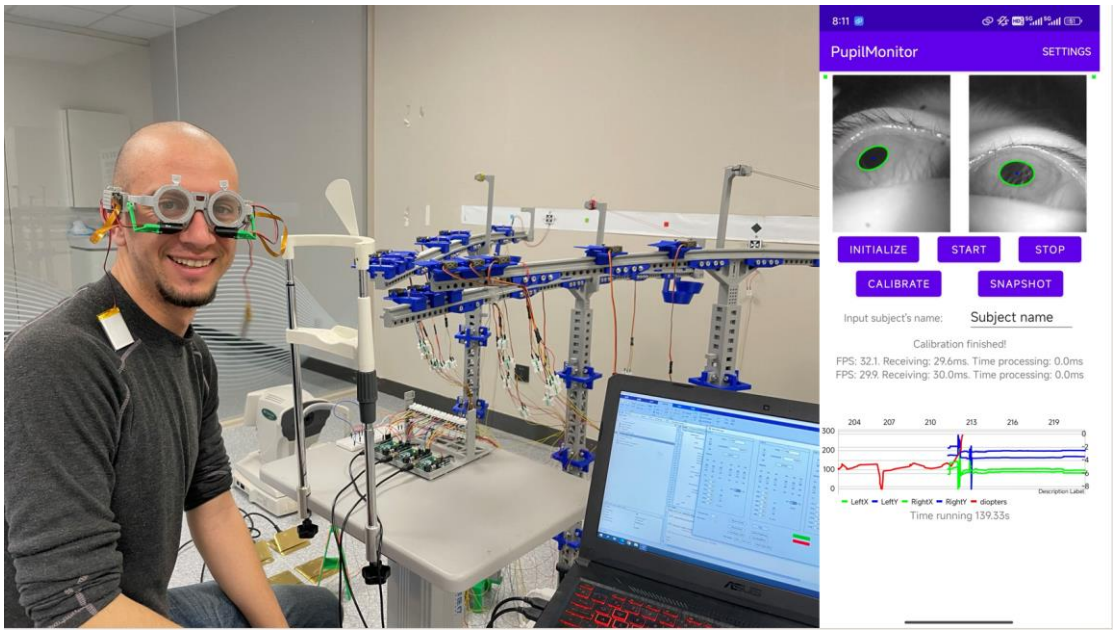


Figure 2-16. The subject wearing the eye-tracker and the testing environment.

## 2.3.2 The preparation of the device

The Eye-tracker has a 3D-printed spectacles frame, two micro-cameras for capturing pupil images and infrared LEDs for illuminating, two ESP32 processors with antennas for wireless transmission, and two batteries for power supply. The pupil images can be sent from ESP32 to smartphone via WIFI connection and then performing the geometric calculation for gaze distance. The Android based application can display real

time plots for gaze distance and pupil images. The application can export dioptric distance data with time label in csv files for further analysis.

See figure 2-17 for the details of the Eye-tracker together with the label of critical components. The modelling is also attached as figure 2-18.

C1: The trial lens for refractive error correction.

C2: ESP32 processor.

C3: The 3D-printed arm for control inter-camera distance for subject's pupil distance.

C4: The pupil camera holder.

C5: The buckle for fitting the nose supporter.

C6: The antenna for WIFI connection.

C7: The pupil camera.

C8: The battery.

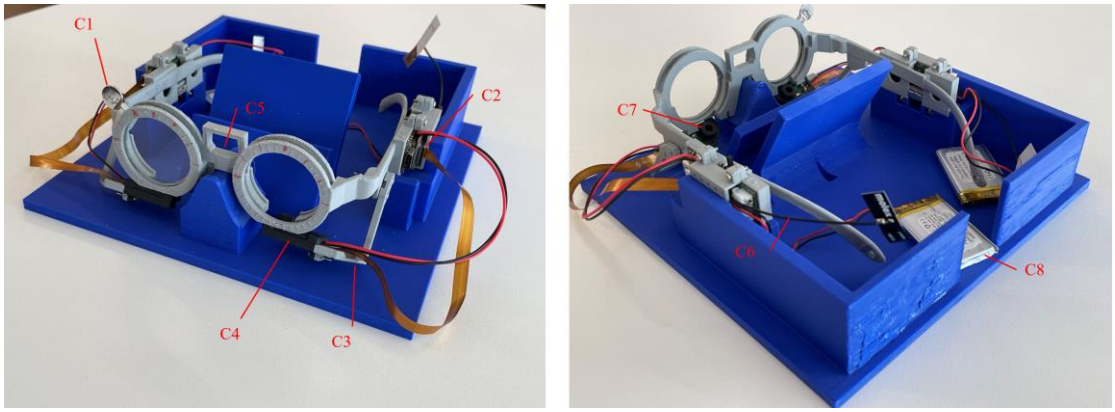


Figure 2-17. The 3D-printed Eye-tracker.

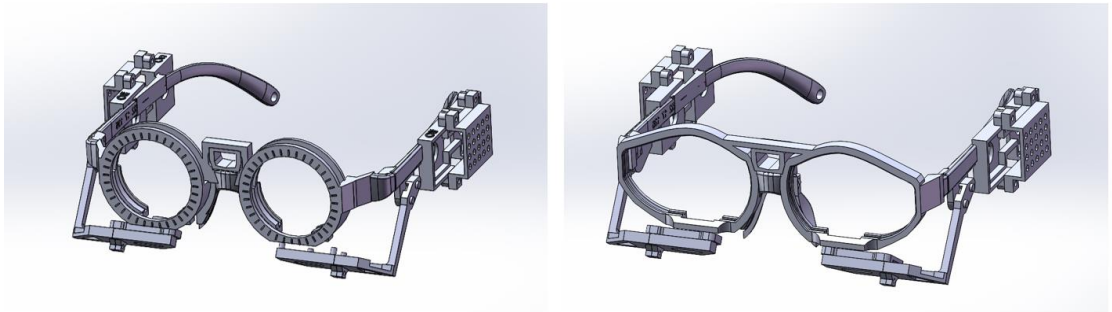

Figure 2-18. The modelling of the Eye-tracker. Left: the design for fitting with trial lens.

Right: the design for fitting prescribed spectacles.

As Figure 2-19 indicated, the device has a toolbox for subjects with different nose height and interpupillary distance. The practitioner can replace the nose supporter or the arm of the camera holder depending on the subject, so the projected image of the eyes can be located properly in pupil camera. This step is extremely important for the experiment. If the selected nose supporter or the arm of the camera holder is inappropriate for the subject, then the pupil image will be easy to move out of the boundary of the camera, so it fails the distance calculation.

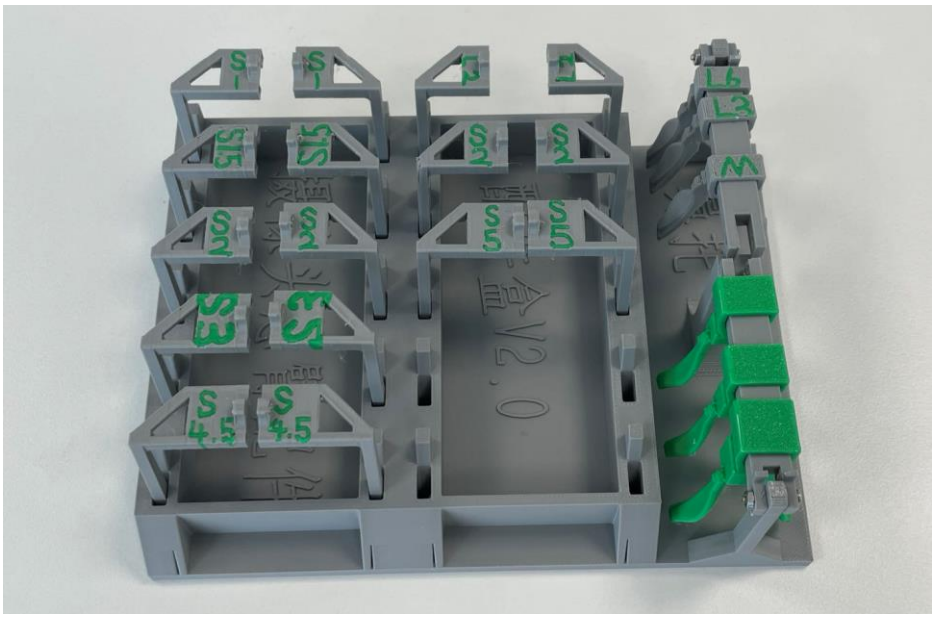


Figure 2-19. The toolbox for different sizes of nose supporter and the arm of the camera holder.

## 2.3.3 Estimation of the gaze distance

A schematic of mathematics of gaze distance evaluation is provided to understand how we convert pupil images to gaze distance (figure 2-20). The figure assumes that the subject is looking at a near object. Before the calculation, we need a starting point for each eye, which refers to the position of pupil center when looking far (the red points

in figure 2-20) for calculating the angle of binocular vergence of near fixation. The eyeball was assumed to be a sphere with radius equal to 12 mm, so we can estimate the angle of eye's rotation.

The testing room (on the 18th floor) has a transparent glass wall on one side; thus, the subject can look at infinity, which provides a nice experimental condition for the calibration of pupil location. In schematic, the Euclidean distance between F and N was estimated by the displacement of pupil center from the video. The pixel size was pre-defined based on the design distance from the eye to the camera.

The eye's rotation was calculated based on the law of cosines over the small green triangles in the figure 2-20.

$$\alpha' = \arccos\left(\frac{2r^2 - a^2}{2r^2}\right) \text{ or } \beta' = \arccos\left(\frac{2r^2 - a'^2}{2r^2}\right) \text{ (equation 2-1)}$$

$$\alpha = \frac{\pi}{2} - \alpha' \text{ or } \beta = \frac{\pi}{2} - \beta' \text{ (equation 2-2)}$$

When the subject is looking at peripheral target, $\beta = \frac{\pi}{2} + \beta'$.

Then, based on the measured interpupillary distance from autorefractor (C in figure 2-20), we can easily calculate GD based on Cosine Rule and Heron's formula. GD1 is for estimating GD with small angle of field, while GD2 is for object in peripheral field.

$$\gamma = \pi - (\alpha + \beta) \text{ (equation 2-3)}$$

$$A = \frac{C \cdot \sin(\alpha)}{\sin(\gamma)} \text{ (equation 2-4)}$$

$$B = \frac{C \cdot \sin(\beta)}{\sin(\gamma)} \text{ (equation 2-5)}$$

$$s = \frac{A+B+C}{2} \text{ (equation 2-6)}$$

$$area = \sqrt{s(s-A)(s-B)(s-C)} \text{ (equation 2-7)}$$

$$GD1 = \frac{2 \times area}{C} \quad \text{(equation 2-8)}$$

$$GD2 = \frac{1}{2}\sqrt{2A^2 + 2B^2 - C^2} \quad \text{(equation 2-9)}$$

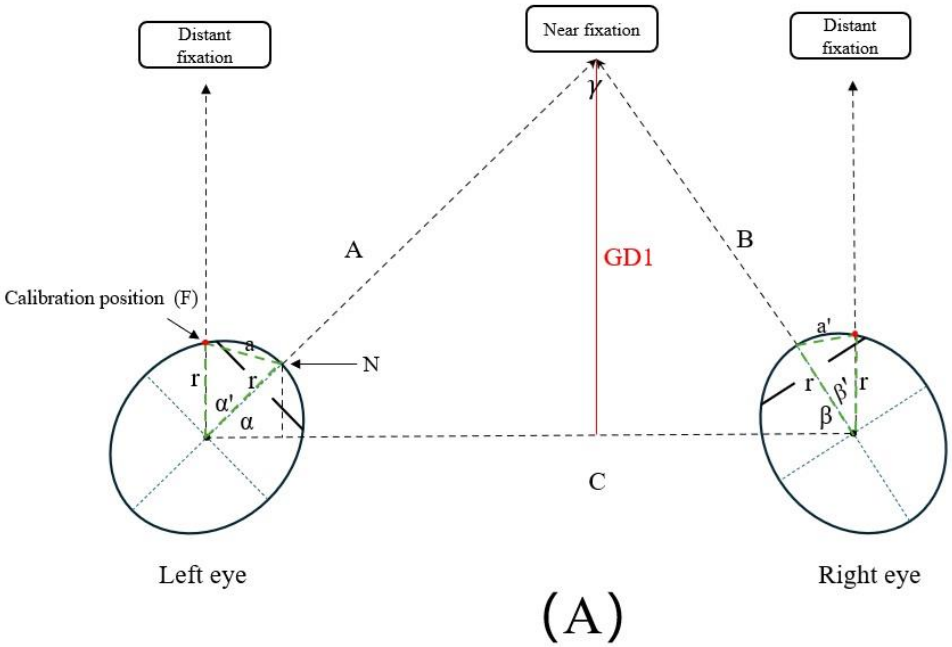


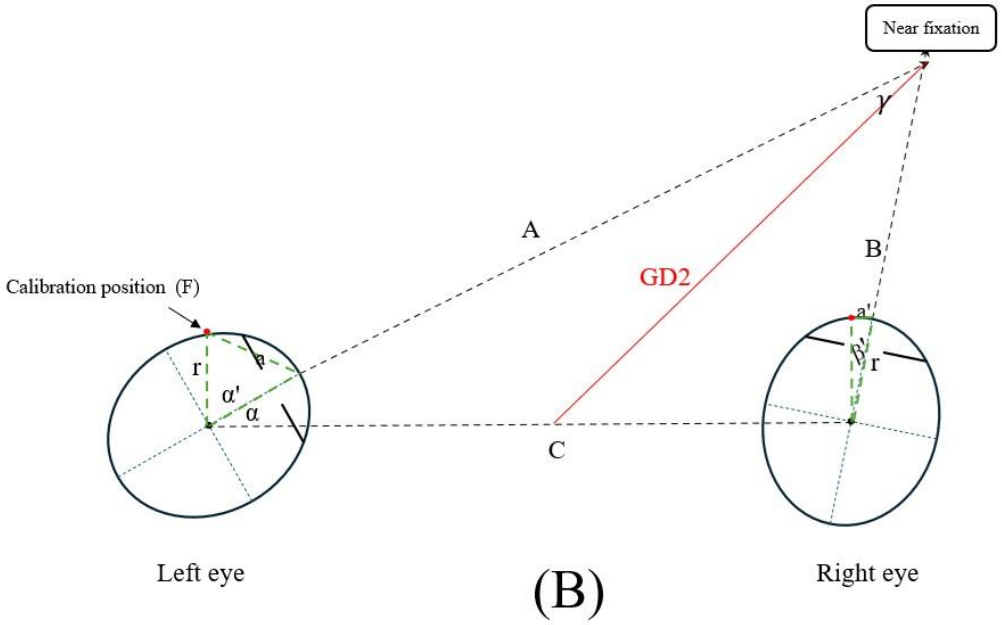


Figure 2-20. The geometry of gaze distance and binocular fixation. α' and β' are the angle of eye rotation. C is interpupillary distance. GD is gaze distance (from the fixation point to the middle of binoculars). Eyeball was assumed to be a sphere. r represents

radius. A, B, and C are the side lengths of the triangle. The small green dashed lines represent an isosceles triangle for calculating α' and β'. (A) and (B) are schematics for targets with small fixation angle (central target) or large fixation angle (peripheral target), respectively.

## 2.3.4 The preparation of the testing environment

We prepared a testing environment for the validation of accuracy and repeatability of the device. The experiment was conducted in a room with a transparent wall, which is the best choice for the calibration of the device in far distance. The accessories for the testing system are listed below (figure 2-21):

C1: LED light. The lights are 2 meters away from the subject.

C2: The target units. Each unit includes one servo motor, one target holder and one target clip.

C3: The connector for tripods. Each stainless-steel tube was connected with two connectors for the stability of the system.

C4: The stainless-steel tube.

C5: The tripods for holding accessories.

C6: Arduino Uno controller. Three controllers were used in the system.

C7: The laptop for controlling the LEDs and targets.

C8: The calibrator (see figure 2-22 for the physical appearance and figure 2-23 for the modelling). It can calibrate the distance from the nearest targets to the subject in three directions. Two calibrators were made to control the distance at 15 cm. One calibrator was made for peripheral targets at 25 degrees.

C9: The wearable Eye-tracker for recording pupil images.

C10: The toolbox with varies size of nose supporter and camera holder for different interpupil distance.

C11: The chinrest for place subjects.

There are seven targets for each direction (0 degree, ±25 degrees). The dioptric distance from the targets to the midpoint of the eyes are 6.7D (15cm), 5.0D (20cm), 4.0D (25cm), 3.0D (33cm), 2.0D (50cm), 1.0D (1m), and 0.5D (2m), respectively, from near target to distant target. The distance was controlled by the customized calibrator. The first six targets were attached to the servo motor. The farthest targets were attached to the wall and illuminated by LED light when needed. All the targets are Maltese cross corresponding to 1-degree visual field.

Figure 2-21. The front view (left) and side view (right) of the testing environment for the Eye-tracker.

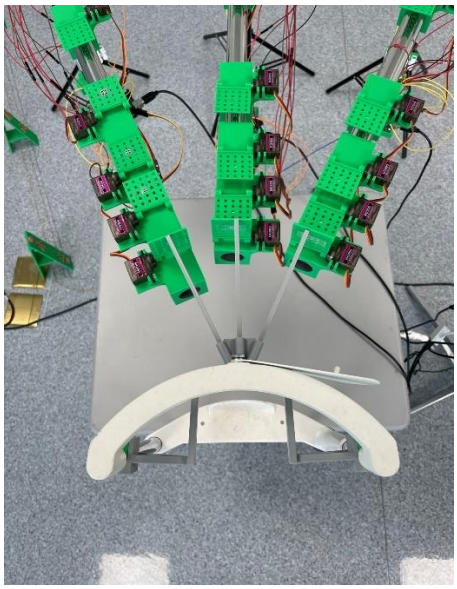

Figure 2-22. The vertical view of the testing system with the calibrator.

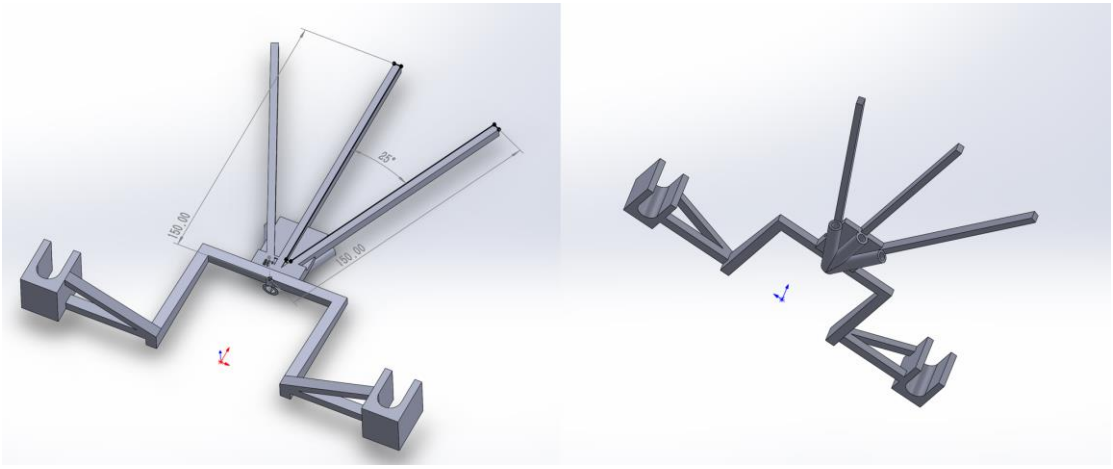


Figure 2-23. The modelling of the calibrator in SolidWorks. The calibrator was designed for the targets at central and peripheral 25 degrees for the dioptric distance 6.7D (15 cm).

## 2.3.5 The protocol of the evaluation

The experiment setup was used for evaluating the accuracy and repeatability of the device for estimate gaze distance. The targets were presented from far distance to near distance. The whole process was performed twice for repeatability.

Pre-experiment protocol:

S1: Subject fitted with the spectacles.

S2: Turn on the Android application and the device.

S3: Subject looking at distant target through transparent wall for a few seconds for the calibration of initial eye position in digital image. The distant target refers to the mansion that is thousands of meters away from the experiment room.

S4: After calibration, the subject was instructed to be in position for the experiment. The subject needs to put her head carefully within the chinrest.

S5: When the subject is ready, start the experiment protocol.

Experiment protocol:

S1: Flashing the three LED lights (10 HZ) at the same time to remind the subject to be ready for the test. This process will last 1.5 seconds.

S2: Lighting the farthest target (dioptric distance = 0.5D) for the central target for 4 seconds, then extinguish the light for 0.5 seconds.

S3: Lift the second farthest target (dioptric distance = 1.0D) for the central target for 4 seconds, then lay down the target for 0.5 seconds.

S4: Repeat step 3 until the nearest target.

S5: Repeat step 2 to step 4 for targets on the left/right side of the subject.

S6: Stop the Android application of the Eye-tracker and the Matlab application of the experiment setup. Check if the data was saved properly.

# Chapter 3. The role of peripheral refraction in myopia progression

# 3.1 Introduction

We developed a methodology to investigate 2-D peripheral refraction. The experiment was conducted in a group of Chinese children over a two-year observation period to explore its relationship with myopia progression. Upon completion of the experiment, the data were classified into three distinct datasets. Dataset 1 describes the evolution of peripheral refraction from baseline to the first follow-up visit, dataset 2 covers the period from baseline to the second follow-up visit, and Dataset 3 details the changes in peripheral refraction over the entire observation period.

# 3.2 Methods

## 3.2.1 Subjects

This study was carried out at Tangfeifan middle school, located in a rural region of Zhuzhou city, Hunan province, China. The subjects were recruited in two cohorts. The first cohort was started in October 2018, while the second cohort was started in March 2019. The separation of the cohort helped to recruit more volunteers during the study. The follow-up visits for 2-D peripheral refraction test were conducted twice with an interval of 12 months. The data from the two cohorts were merged for further analysis after the observational period completed. To keep the consistency of peripheral refraction during the study, prescribed single vision glasses were provided for all participants. If the central refraction of the subject changes in the next visit (6 months), new prescribed glasses were provided. See flow chat regarding details of subject recruitment in figure 3-1.

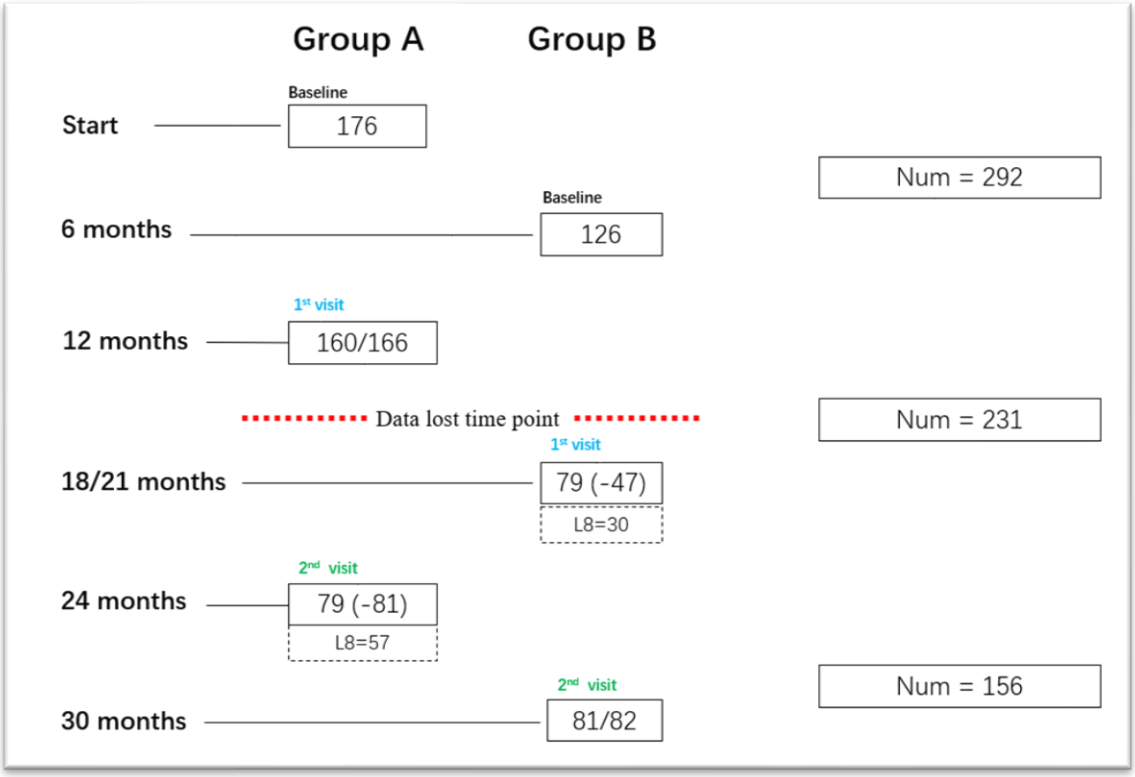


Figure 3-1. The flow chart illustrates the recruited subjects at each time point. The numbers in parentheses indicate the number of subjects lost compared to the previous visit. 'L8' represents the number of subjects in grade 8 (second-year middle school students). The number on the left side of the slash shows the subjects remaining after excluding unqualified 2-D maps. It is important to note that second-year middle school students were only available for follow-up for one year from the start of the study, with their last visit occurring at the 12-month mark. This limitation is due to school policies requiring students to focus on preparing for the high school entrance exam, leading to a significant loss of subjects after the 12-month time point.

The inclusion criteria included:

1. Participants had astigmatism under -1.5 diopters.
2. Achieved best-corrected visual acuity of at least 20/20.
3. No history of ocular pathology or systemic conditions affecting vision.
4. No prior myopia control interventions (orthokeratology, specialized contact

lenses, multifocal glasses, or pharmaceutical treatments).

The exclusion criteria include:

1. Elevated intraocular pressure (>21 mmHg).
2. Poor-quality Hartmann-Shack images due to excessive corneal reflections.
3. Inability to maintain stable monocular fixation during peripheral assessments.

The flow chart below illustrates the number of subjects at each visit. It is important to note that these numbers are solely based on the recorded VPR measurements for each visit. Some subjects may have missed some data from other tests. Additionally, a few subjects may have undergone repeated tests or had incorrect ID registrations during the visits, resulting in a reduced number after data cleaning and database integration. See figure 3-2 for more details on the data integration process. It is also worth mentioning that subjects who completed the second follow-up visit did not necessarily complete the first follow-up visit. The final number of available subjects, representing those who underwent a full examination, is presented in figure 3-3.

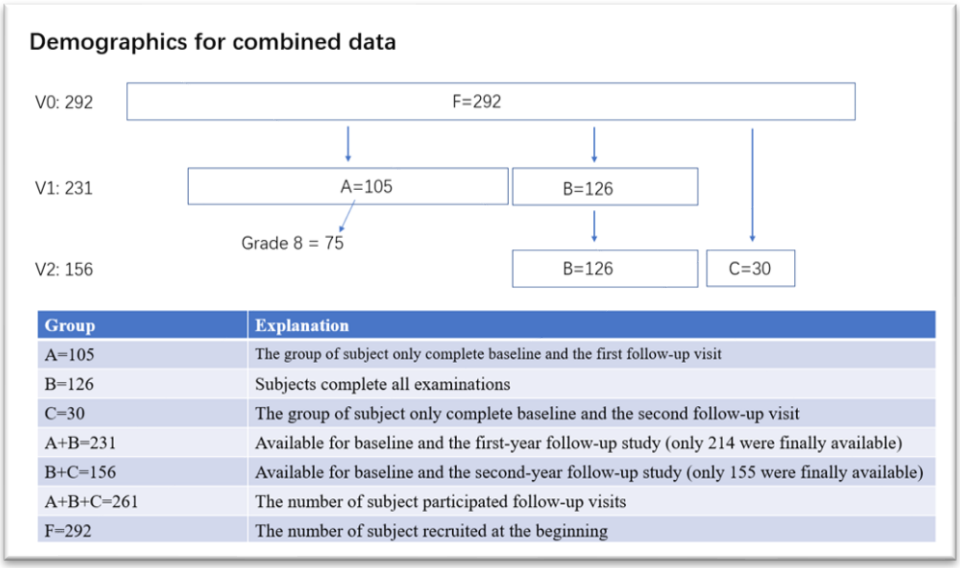


| Group | Explanation |
|---|---|
| A=105 | The group of subject only complete baseline and the first follow-up visit |
| B=126 | Subjects complete all examinations |
| C=30 | The group of subject only complete baseline and the second follow-up visit |
| A+B=231 | Available for baseline and the first-year follow-up study (only 214 were finally available) |
| B+C=156 | Available for baseline and the second-year follow-up study (only 155 were finally available) |
| A+B+C=261 | The number of subject participated follow-up visits |
| F=292 | The number of subject recruited at the beginning |

Figure 3-2. The demographics for the integrated database. 'V0,' 'V1,' and 'V2' represent the baseline, the first follow-up visit, and the second follow-up visit, respectively.

Please note that the numbers are based solely on the recorded VPR measurements. Some subjects may have missed other ophthalmic tests, rendering their data unusable for further analysis.

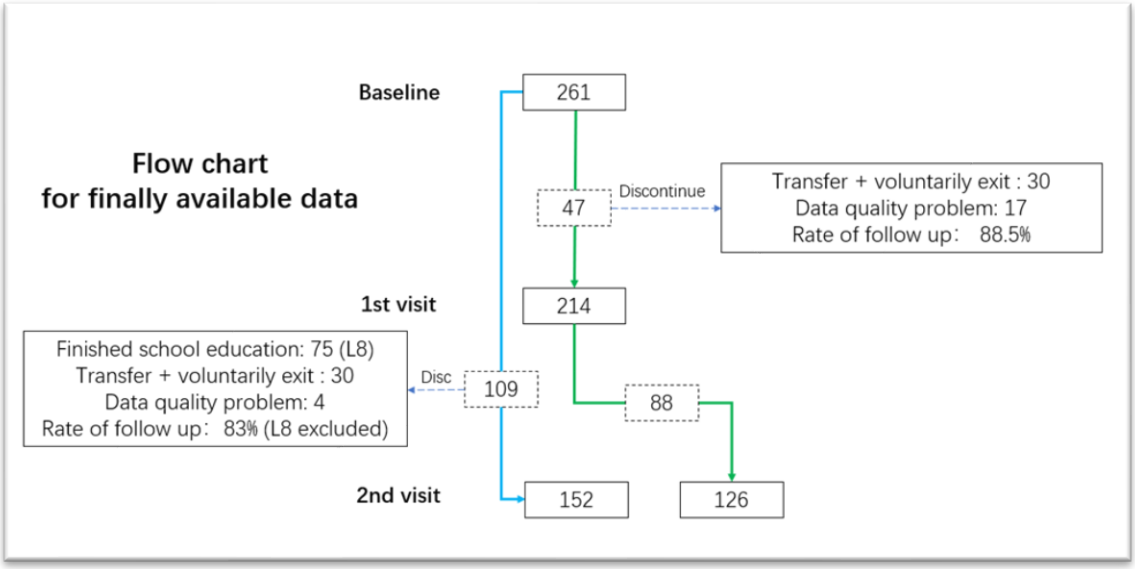


Figure 3-3. The flow-chart shows the available subjects for study the evolution of peripheral refraction throughout the years. Please note that the numbers are based solely on the recorded VPR measurements. A few subjects may lose the data regarding axial length. The finally available number for 1-year study, 2-year study, two-years sequential study is 214, 152, and 114, separately.

Study participation and follow-up

The study initially enrolled 260 children. During the one-year follow-up, 231 participants attended the first visit, while 155 completed the second-year visit. Notably, 29 children missed the first visit but participated in the second one. After excluding 16 subjects (first-year visit) and 3 subjects (second-year visit) due to poor-quality peripheral measurements, the final analytical datasets comprised:

- Dataset 1 (baseline to 1st follow-up): 214 children
- Dataset 2 (baseline to 2nd follow-up): 152 children

Demographics and refractive changes

- Age at baseline:
    - 1st follow-up group (214 subjects): 12.2 ± 1.4 years (range: 8–15)
    - 2nd follow-up group (152 subjects): 11.5 ± 1.2 years (range: 8–14)
- Central refraction (spherical equivalent):
    - 1st follow-up group: Baseline: −0.66 ± 1.40 D → 1-year: −1.03 ± 1.63 D
    - 2nd follow-up group: Baseline: −0.42 ± 1.18 D → 2-year: −1.26 ± 1.60 D

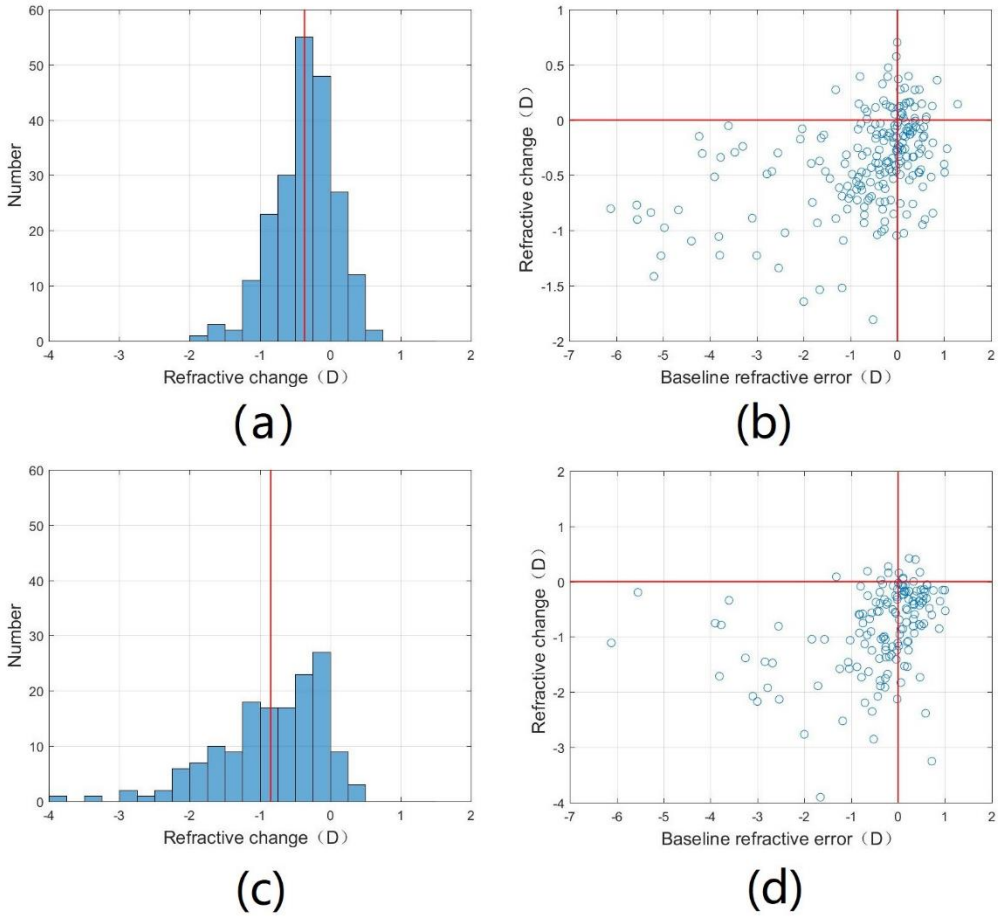


Figure 3-4. Demographics. Panels (a) and (c) display histograms of refractive error changes over 1-year and 2-year periods respectively, with red lines marking median

progression values. Panels (b) and (d) show scatter plots comparing baseline refractive error against subsequent 1-year and 2-year progression.

A total of 114 participants completed all study assessments (Dataset 3). At baseline, the cohort comprised 14 hyperopes (SER: +0.67 ± 0.16 D), 63 emmetropes (SER: 0.00 ± 0.28 D), and 37 myopes (SER: −1.80 ± 1.44 D). By the first-year follow-up, the distribution shifted to 9 hyperopes (SER: +0.61 ± 0.06 D), 44 emmetropes (SER: −0.04 ± 0.28 D), and 61 myopes (SER: −1.86 ± 1.46 D). At the second-year visit, the group further transitioned to 7 hyperopes (SER: +0.66 ± 0.11 D), 31 emmetropes (SER: −0.02 ± 0.27 D) and 76 myopes (SER: −2.23 ± 1.49 D). These subjects were analyzed separately to track longitudinal progression. Refer to figure 3-5 for the participant flow diagram.

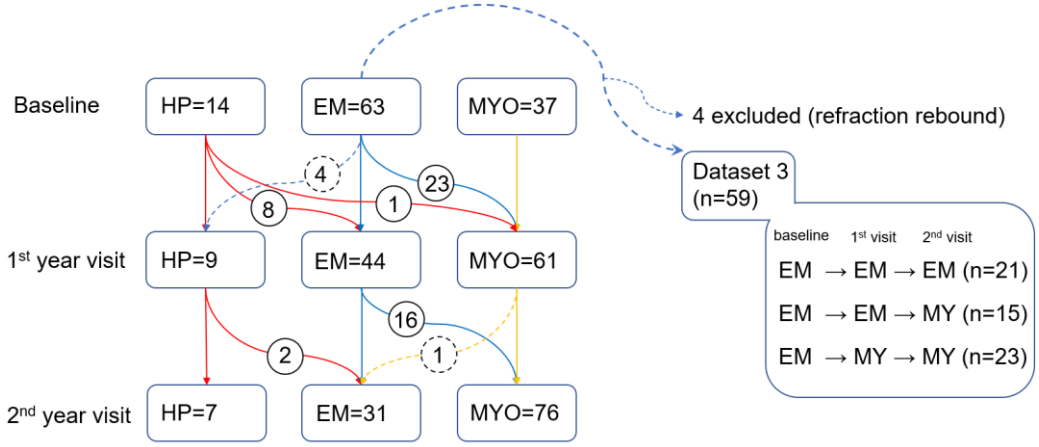


Figure 3-5. Longitudinal refractive status changes (HP: SER > +0.5 D; EM: −0.5 D ≤ SER ≤ +0.5 D; MYO: SER < −0.5 D). Boxes: participant counts per visit. Solid circles: myopic progression. Dashed circles: hyperopic rebound (4 EM→HP: +0.38 ± 0.14 D; 1 MYO→EM: +0.18 D). Four subjects with refraction rebound were excluded from analysis.

### 3.2.2 Procedure

All subjects undergo VPR 2D peripheral refraction measurements (see details in Chapter 2). Only the right eye was measured, with the left eye covered by an eye patch. Zernike coefficients were derived from a 4-mm diameter pupil area.

In addition to peripheral refraction, each subject underwent measurements of axial length (LENSTAR LS 900, Haag-Streit AG, Koeniz, Switzerland), multimodal fundus imaging (DRI OCT Triton, Topcon, Oakland, US), intraocular pressure, and subjective refraction at each visit. All assessments were conducted under cycloplegia, achieved by instilling Alcaine eye drops (Alcon, Japan) followed by two drops of 1% cyclopentolate (Alcon, Japan).

All experimental protocols adhered to the tenets of the Declaration of Helsinki and received approval from the Institutional Review Board of Aier Eye Hospital. Participants and their parents or guardians were fully informed about the study and provided written consent prior to the trial's initiation.

### 3.2.3 Visual behavior information

Visual behavior monitoring was performed using the Clouclip wearable device (Glasson Technology Co Ltd, China) [123, 124], which was mounted on the right temple of a spectacle frame. This device continuously recorded both viewing distance (range: 0–204 cm; sampling interval: every 5 seconds) and ambient light intensity (range: 1–65,336 lux; sampling interval: every 2 minutes) along the user’s line of sight. Data collection spanned a full week, beginning at 8:30 a.m. on Monday and concluding the following Monday. Participants were instructed to wear the device throughout the day, removing it only for activities such as bathing or sleeping. For emmetropic participants, lensless spectacle frames were provided to accommodate the device.

In addition to distance and light measurements, the Clouclip incorporates a three-axis accelerometer (X, Y, and Z axes). If no movement was detected for over 40 seconds, the device would enter a sleep mode and pause data recording, resuming only when angular motion was detected. Only data collected between 7:00 a.m. and 8:00 p.m. were verified and analyzed, and datasets were included in the final analysis only if data availability exceeded 80%.

Each participant's visual behavior was quantified using the following parameters:
(1) Mean viewing distance – the weekly average distance from the eyes to the target;
(2) Mean ambient light intensity – the weekly average level of light exposure;
(3) Mean near viewing distance – the average distance during near work (defined as <60 cm);
(4) Duration of near work – the average daily time spent at a viewing distance under 60 cm;
(5) Outdoor light exposure time – the average daily duration spent under light levels exceeding 1,000 lux.

## 3.2.4 Data analysis

Two types of analyses were performed: one involving the full cohort of participants, and another restricted to individuals who completed all follow-up visits. In the first analysis, participants were categorized based on their baseline central SER into three refractive groups: hyperopes (SER > +0.50 D), emmetropes (−0.50 D ≤ SER ≤ +0.50 D), and myopes (SER < −0.50 D). Within each refractive category, participants were further stratified according to the rate of central refractive change over time into three progression groups: slow (lowest 33.3% of myopic progression), moderate (middle 33.3%), and fast (highest 33.3%).

To assess group differences in peripheral refraction, two-dimensional peripheral refraction maps were divided into a 3×3 grid (Figure 3-6b). The average value within each grid region was calculated and used for statistical analysis. Each region was labeled with a letter (S, M, or L) denoting its vertical location—superior, middle, or lower, respectively—followed by a number (1, 2, or 3) indicating its horizontal position—nasal, central, or temporal. This segmentation was defined by horizontal lines at 5.5° above and below the horizontal meridian, and vertical lines at 10.5° nasal and temporal. Data points located near the optic nerve head ($13.5° < x < 21.5°$, $3.5° < y < 5.5°$) were excluded from analysis.

Data were presented as mean ± 1 standard deviation unless otherwise specified. To compare differences between the fast and slow progression groups, a two-tailed t-test was used. One-way ANOVA was employed to compare peripheral refraction differences across the three progression groups. If the data did not follow a normal distribution, the Kruskal-Wallis test was used. Pearson correlation analysis was performed to evaluate the relationship between peripheral refraction in each zone and changes in myopia or axial length, with p-values corrected using the false discovery rate (FDR) method.

The second analysis focused exclusively on participants who completed two full follow-up assessments. In this analysis, subjects were classified based on their refractive status at each time point rather than the rate of myopic progression. Three refractive transition categories were defined:

- Category 1 (EM-EM-EM): consistently emmetropic across all visits,
- Category 2 (EM-EM-MY): emmetropic at baseline and first follow-up, but myopic by the second follow-up,
- Category 3 (EM-MY-MY): emmetropic at baseline, progressing to myopia by the first follow-up and remaining myopic thereafter.

The same statistical procedures were employed to compare relative peripheral

refraction among these three groups at each time point. Additionally, repeated measures ANOVA (RM-ANOVA) were used to evaluate longitudinal changes in relative peripheral refraction across the three visits, with Bonferroni-adjusted post-hoc tests applied for pairwise comparisons.

# 3.3 Results

## 3.3.1 Baseline vs. Single-Timepoint Comparative Analysis

Figure 3-6a illustrates the average two-dimensional refraction maps for each group from baseline to the first-year visit, while Figure 3-6b shows the corresponding changes from baseline to the second-year visit. These visual results are supplemented by statistical analyses provided in tables S1 through S4, which detail the findings for each case. In these analyses, the retinal maps were segmented into nine distinct regions for quantitative comparison.

As anticipated, hyperopic children showed greater relative hyperopic defocus in the central retina, regardless of the extent of myopic progression during the study period. This relative hyperopia tended to follow a spatial distribution from the superior-nasal to the inferior-temporal retina. At baseline, no significant differences in mean refraction across the nine retinal regions were observed among the different progression groups. However, when examining peripheral refraction changes from baseline to follow-up, the earliest alterations appeared in the temporal-superior retinal area. This regional change became increasingly prominent with higher progression rates, being more evident in the fast progressors compared to the slow ones.

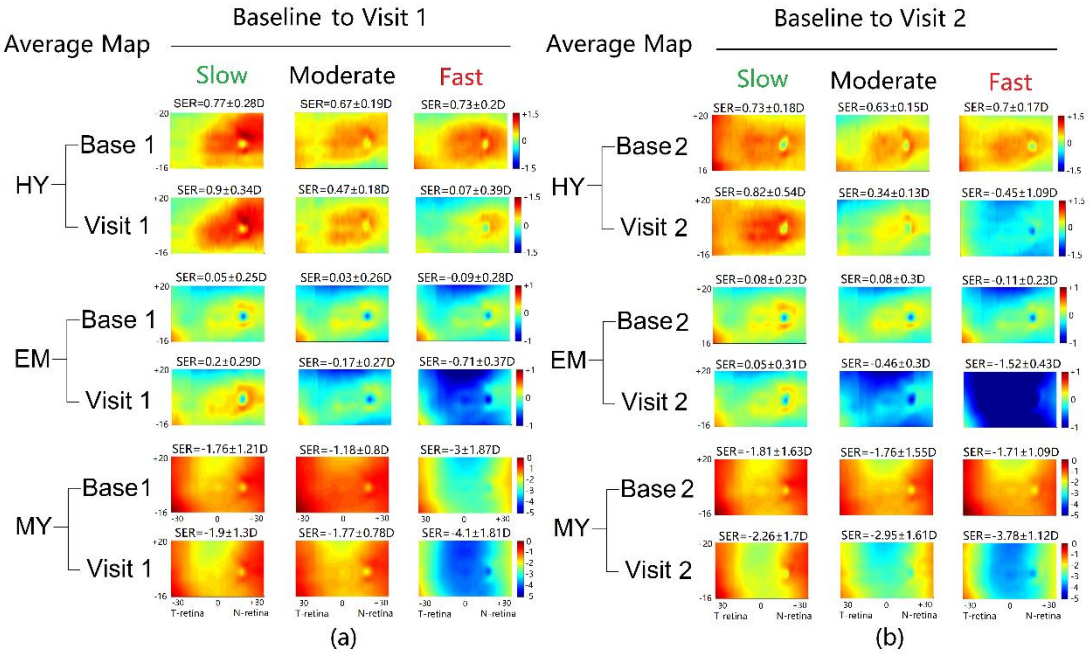


Figure 3-6. Change of 2D peripheral refraction map in two years. (a) From baseline to the first follow-up visit. (b) From baseline to the second follow-up visit. According to the central refraction at baseline and the progression of myopia in one or two years, the average 2D maps were divided into three primary rows (hyperopes/HP, emmetropes/EM, myopes/MY) and three columns (slow/moderate/fast myopia progression groups) for left and right panels.

In emmetropic children, the overall peripheral refraction distribution resembled that of hyperopes but showed generally lower levels of hyperopia across the retinal map. A key distinction, however, was that baseline peripheral refraction in the superior retina significantly differed among the progression groups—unlike in hyperopes. In the 1-year follow-up, the mean peripheral refraction in the superior retina was -0.14 ± 0.41 D for the slow progression group, -0.27 ± 0.35 D for the moderate group, and -0.44 ± 0.38 D for the fast group (p-ANOVA = 0.041). Moreover, children in the fast progression group exhibited slightly but significantly more myopic central refraction compared to those in the slow and moderate groups (mean central refraction: 0.13 ± 0.23 D for slow, 0.10 ± 0.27 D for moderate, and -0.04 ± 0.27 D for fast; p-ANOVA = 0.046). A similar

trend was also seen specifically at the central retinal location (0.05 ± 0.25 D, 0.03 ± 0.26 D, and -0.09 ± 0.28 D for slow, moderate, and fast groups, respectively; p-ANOVA = 0.043). In addition, a significant correlation was observed between peripheral refraction and myopia progression within the middle column of retinal regions. This correlation was strongest in the superior region and progressively weakened toward the inferior retina. Specifically, the correlation coefficients (r-values) for changes in refraction during the first year were 0.308 (superior), 0.256 (central), and 0.243 (inferior), while the corresponding r-values for axial length changes were -0.385, -0.379, and -0.310, respectively. Notably, the correlation was weaker when analyzing relative peripheral refraction (RPR) compared to peripheral refraction (PR). The baseline distribution pattern observed in the 1-year study closely matched that of the 2-year study.

Among myopic children, peripheral refraction along the horizontal meridian generally showed a pattern of relative hyperopia in the peripheral retina, with this effect extending into both the superior and inferior regions. On average, relative peripheral hyperopia at 30 degrees eccentricity was less than 2.00 D. During the 1-year follow-up, children in the fast progression group demonstrated significantly greater central myopia compared to those in the slow and moderate progression groups. Specifically, central refraction values were -1.76 ± 1.21 D for the slow group, -1.18 ± 0.80 D for the moderate group, and -3.00 ± 1.87 D for the fast group ($\chi^2 = 14.996$, $p < 0.001$). However, by the 2-year visit, no significant differences in central refraction were observed among the groups, with values of -1.81 ± 1.63 D, -1.76 ± 1.55 D, and -1.71 ± 1.09 D for the slow, moderate, and fast groups, respectively ($F = 0.019$, $p = 0.981$). Across all segmented retinal regions, mean refraction showed a significant correlation with central myopia progression.

## 3.3.2 Baseline vs. Multi-Timepoint Sequential Change Analysis

Figure 3-7a illustrates the evolution of relative peripheral refraction (RPR) in subjects

who completed all measurements over the two-year period. The subjects were divided into three categories: those who remained emmetropic throughout the two years (EM-EM-EM), those who developed myopia in the second year (EM-EM-MY), and those who became myopic in the first year (EM-MY-MY). At baseline, although all three groups were emmetropic, there was a small but significant difference in central refractive error ($F=22.266$, $p<0.001$; table S6). On average, category 3 (EM-MY-MY) was 0.43 D more myopic than category 1 (EM-EM-EM) and 0.25 D more myopic than category 2 (EM-EM-MY).

At baseline, the 2-D maps for category 3 showed more relative hyperopic defocus than those for category 1 in regions S1, S3, M1, M3, L1, L2, and L3 (as determined by a two-tailed t-test), though no significant differences were observed among the three categories across all peripheral regions. During the first follow-up visit, similar results were found when comparing the two extreme categories (Category 1 vs. Category 3) using two-tailed t-tests. One-way ANOVA revealed significant differences in regions S3, M1, M3, L1, and L3 among the three groups. By the second follow-up visit, significant differences were observed across all peripheral regions except for S2. See more statistical details in table S5.

Figure 3-7b shows the 2-D maps for absolute peripheral refraction in the three categories at baseline and the two follow-up visits. The impact of myopia progression first appeared in the superior retina, slightly extending toward the temporal direction, and later progressed to the central-vertical regions. This figure demonstrates the remarkable temporal evolution of peripheral refraction with myopia progression, with effects gradually extending to the central retina.

The results for RPR and absolute PR are detailed in Tables S5, S6, S7, and S8. Additionally, a two-tailed t-test was conducted to compare RPR before [(1st follow-up in category 2) vs. (baseline in category 3)] and after the onset of myopia [(2nd follow-

up in category 2) vs. (1st follow-up in category 3)], but no significant differences were found between the groups.

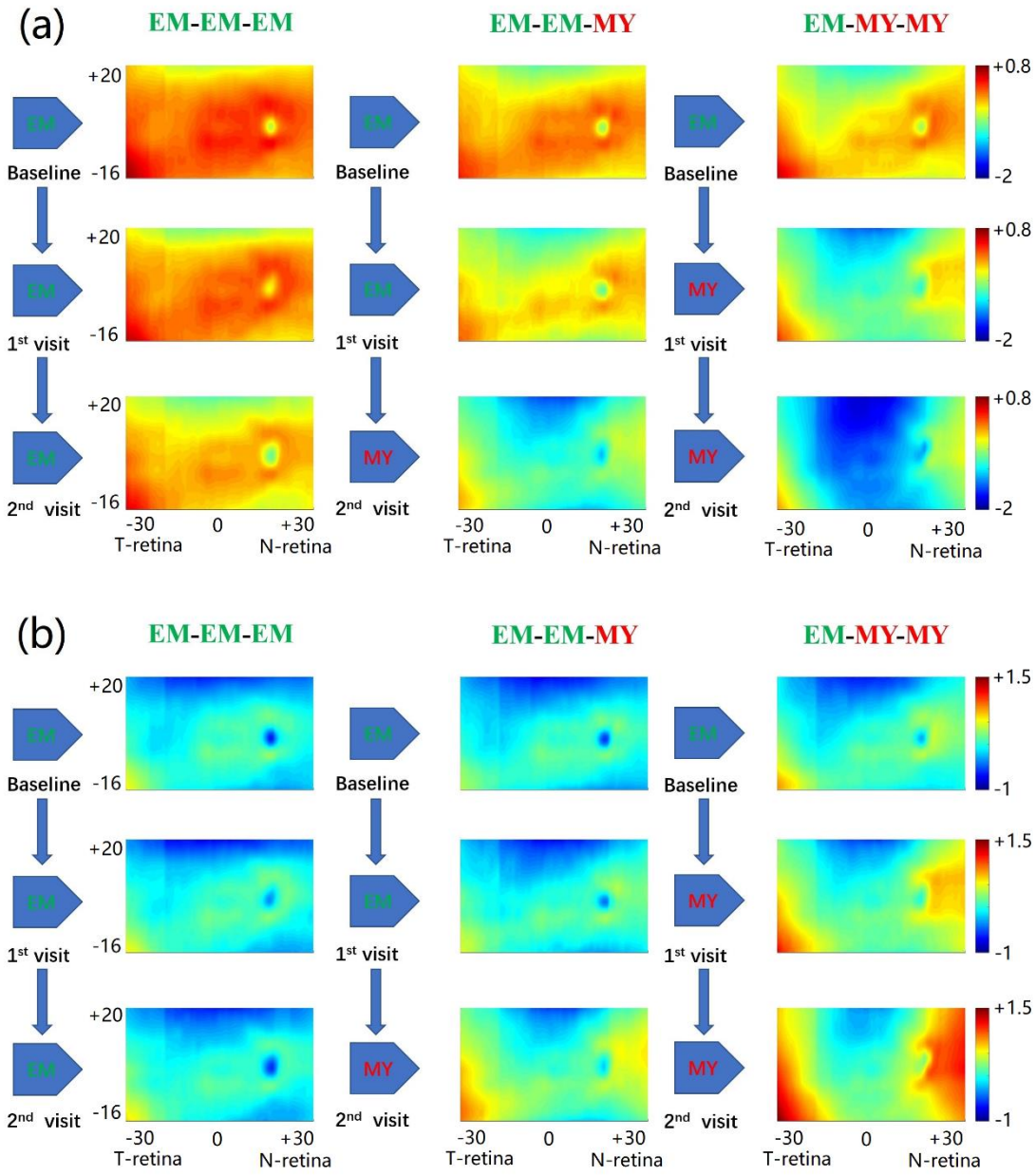


Figure 3-7. Average 2-D peripheral refraction maps showing (a) relative and (b) absolute values for emmetropic children from baseline to the second follow-up visit. Participants were grouped based on changes in their central refractive status over the two-year period. *Category 1 (EM-EM-EM)* includes children who remained

emmetropic throughout the study. *Category 2 (EM-EM-MY)* comprises those who were emmetropic at baseline and at the first follow-up but became myopic by the second follow-up. *Category 3 (EM-MY-MY)* includes those who were emmetropic at baseline but developed myopia by the first follow-up.

Table 3-1. The demographics for the emmetropic subjects from baseline with full observation

| Category (N=59) | Category 1 (EM-EM-EM) (N=21) | Category 2 (EM-EM-MY) (N=15) | Category 3 (EM-MY-MY) (N=23) | Statistics | *p* |
|---|---|---|---|---|---|
| Age | 11.76±1.09 | 11.27±1.49 | 11.35±1.47 | $F$=0.756 | 0.474 |
| Gender (Male/Female) | 52.4%/47.6% | 46.7%/53.3% | 34.8%/65.2% | $\chi^2$=1.434 | 0.488 |
| SER-B0 | 0.19±0.23 | 0.01±0.22 | -0.24±0.19 | $F$=22.266 | <0.001 |
| SER-F1 | 0.08±0.22 | -0.28±0.18 | -0.86±0.26 | $F$=95.794 | <0.001 |
| SER-F2 | -0.09±0.23 | -0.95±0.32 | -1.48±0.54 | $F$=67.075 | <0.001 |
| AL-B0 | 23.27±0.72 | 23.1±0.67 | 23.29±0.59 | $F$=0.446 | 0.642 |
| AL-F1 | 23.37±0.73 | 23.32±0.72 | 23.65±0.56 | $F$=1.431 | 0.248 |
| AL-F2 | 23.54±0.75 | 23.69±0.72 | 23.99±0.56 | $F$=2.58 | 0.085 |

This table presented the demographics of emmetropic children from baseline that completed all measures. The subjects were assigned to three categories based on the status of central refractive error. 'Category 1 (EM-EM-EM)' corresponding to the group that keep emmetropic during the whole observation. 'Category 2 (EM-EM-MY)' corresponding to the group that keep emmetropic in the baseline and the first follow-up but developed myopia in the second follow-up. 'Category 3 (EM-MY-MY)' corresponding to the group that was emmetropic in the baseline but developed myopia in the first follow-up visiting. SER and AL represent spherical equivalent refraction and axial length, separately. The suffix -B0, -F1, -F2 mean the data from baseline, the first follow-up and the second follow-up, separately. Chi-square test and one-way ANOVA test were used for the evaluation of gender distribution or SER/AL distribution among the categories. All quantitative data were expressed with Mean ± Standard Deviation.

### 3.3.3 Local values of peripheral refraction and myopia progression

At the beginning of the analysis, the map was divided into 9 rows and 12 columns, each corresponding to a small, segmented region of 5°×4° (see figure 3-8). The mean refraction in each region was then correlated with central myopia progression over one year. The results are presented below. The numbers in the rectangles represent the r-values from the correlation analysis for RPR (left) and PR (right) data. As previous analysis indicated significant relationship solely in emmetropes, only the results from this group of population were demonstrated. Overall, the results indicate that both PR and RPR are correlated with myopia progression, with the strongest correlation observed in the central superior field.

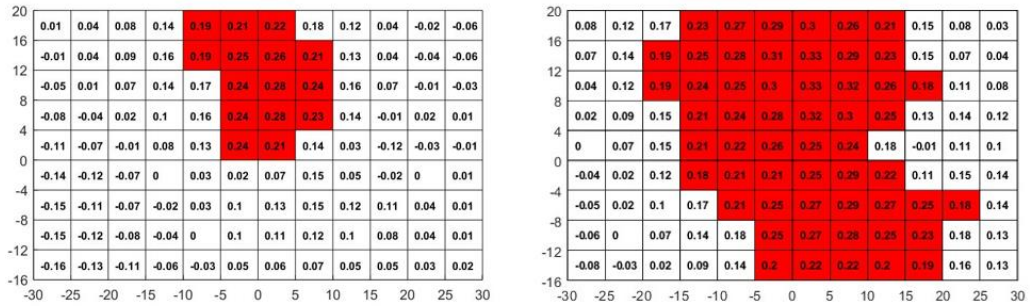


Figure 3-8. Correlation analysis between RPR (a), PR (b), and myopia progression in each segmented region for emmetropes. The map was divided into a grid of 9×12 regions, with each region representing a field of 5°×4°. The mean value in each region was correlated with changes in central retinal refraction over one year. Regions where the correlation was statistically significant are highlighted with a red background to emphasize the results. The r-value for each region is displayed within the corresponding area.

Based on the results mentioned above, we focused the statistical analysis on the superior retina, specifically within the rectangular region [from superior 8° to superior 12°, from

nasal 3° to temporal 3°], examining the correlation with changes in central refraction and axial length. The analysis was conducted in emmetropes and myopes. However, only the data from emmetropic group shows statistical significance. In the emmetropic group (red symbols in Figure 3-9), children with greater peripheral myopia in the superior retina experienced significant myopia progression. Over the 2-year follow-up period, superior defocus accounted for 21.2% of the myopic change ($r=0.46$, $p<0.001$) and 25% of the axial elongation ($r=0.5$, $p<0.001$). Further details are provided in the plots below.

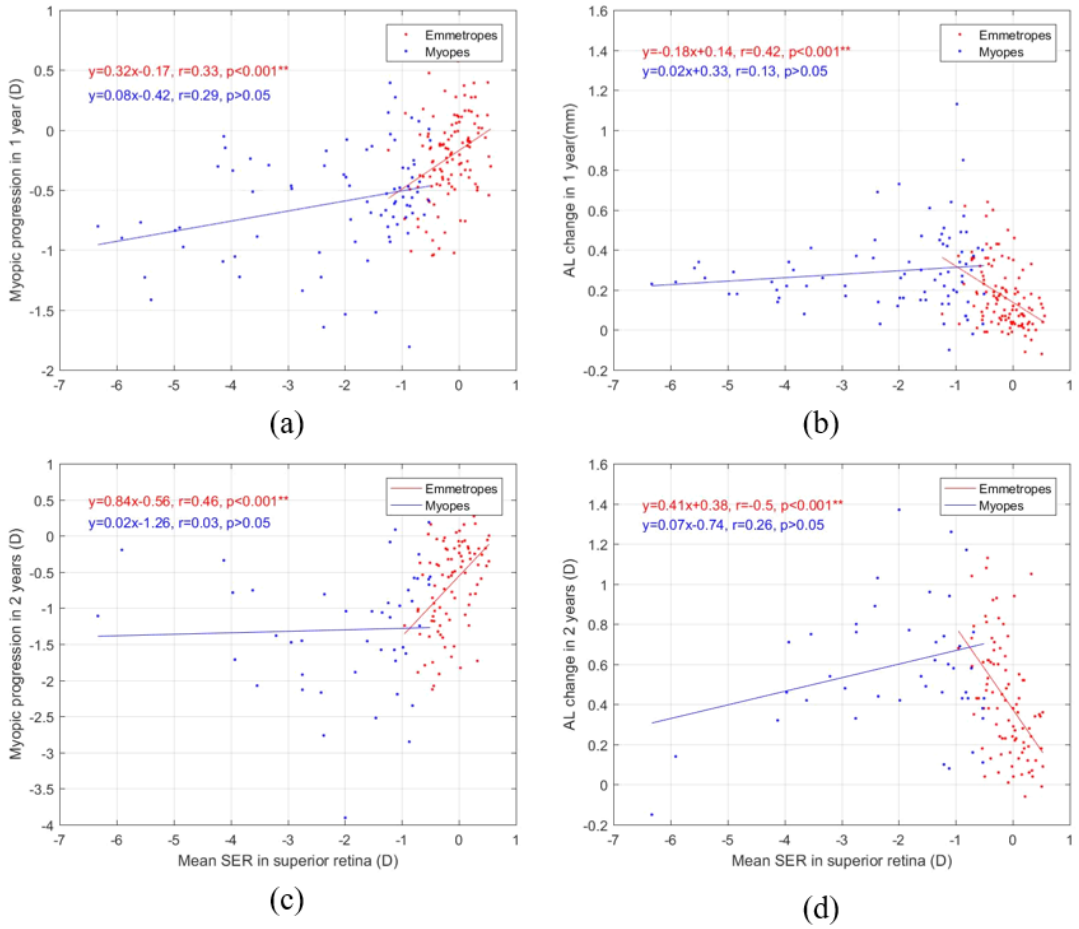


Figure 3-9. The relationship between superior refraction and myopia progression in two years. (a/c) depict changes in central refraction as a function of superior refraction over one and two years, respectively. (b/d) show changes in axial length as a function of superior SER over the same periods. Superior retinal refraction was calculated as the average SER within a representative region defined by coordinates [$-3 \leq x \leq 3$ and

$8 \leq y \leq 12$], comprising a total of 35 data points. Data points from emmetropic and myopic children are shown as red and blue dots, respectively, along with their corresponding fitted trend lines. Hyperopic subjects were excluded from the analysis due to the small sample size.

## 3.3.4 Analysis of confounding factors

There are multiple factors that may influence the progression of myopia during the observational period. Thus, we conducted a parallel analysis to investigate those confounding factors such as central refraction, age, sex, axial length, visual behavior related data, family history of myopia. The results are summarized in table S9.

For hyperopic subjects, there is no significant correlation found in any of the investigated factors.

For emmetropic subjects, significance appeared in average viewing distance over a week (for slow, moderate, and fast progression group: $59.62 \pm 32.74$ cm, $58.27 \pm 30.96$ cm, and $77.21 \pm 25.5$ cm, respectively; $F = 4.753$, $p < 0.01$). A similar pattern was found in near viewing distance ($16.19 \pm 8.86$ cm, $15.02 \pm 8.91$ cm, and $19.94 \pm 6.66$ cm for the respective groups, $F = 3.723$, $p < 0.05$). Baseline age and central retinal refraction are also significant differences in various progression groups. However, the differences are minor and unlikely to be clinically significant for the study (around 0.5 years old difference in baseline age and 0.1 D difference for baseline central refraction).

For myopic subjects, children in the fast-progression subgroup had a significantly longer axial length at baseline compared to those in the slow and moderate progression subgroups. The mean axial lengths were $23.72 \pm 0.81$ mm for the slow group, $23.49 \pm 0.70$ mm for the moderate group, and $24.62 \pm 0.93$ mm for the fast group ($F = 13.712$, $p < 0.001$).

# 3.4 Discussion

To the best of our knowledge, this is the first large-scale clinical study to investigate the evolution of high-resolution 2D peripheral refraction maps over two years during the critical age of myopia progressive population (12 years old). The study includes a comprehensive examination of ophthalmic tests for potential confounding factors, in addition to peripheral refraction maps. The key finding is that peripheral refraction across the entire central vertical field is correlated with myopia progression in the emmetropic population. Myopia progression, in this context, refers to the development of central retinal refraction and the elongation of axial length. The phenomenon is pronounced in the superior retina, where more myopic defocus is related with more myopia progression. This finding is especially important given that the study population was genetically homogeneous, and potential confounding factors showed no significant differences among groups with varying levels of refractive change.

## 3.4.1 General discussion for the 2-D refraction maps

The 2-D peripheral refraction patterns were similar between emmetropes and hyperopes. Both groups exhibited relatively myopic defocus in the periphery, particularly in the superior and inferior retina. In contrast, the peripheral refraction in bilateral regions (nasal or temporal) along the horizontal meridian appeared relatively flat, with no obvious relative defocus. In hyperopes, a distinct "island" of relatively hyperopic refraction was observed in the central field. As the process of emmetropization began, peripheral refraction tended to become more myopic, especially in the superior and nasal retina. An interesting phenomenon was the transition between myopic defocus and hyperopic defocus in the superior retinal region of hyperopes and myopes. In hyperopes, this transition formed an arc with its center pointing inferiorly, whereas in emmetropes, the arc pointed superiorly. This suggests that the evolution of peripheral refraction started in the superior retina and gradually extended to the central retina.

For the myopic population, relative hyperopic defocus was observed in the peripheral field beyond 15 degrees in horizontal direction (see Figure 3-6b, MY-Baseline 2 maps). The development of peripheral refraction primarily occurred in the central field and then expanded to the periphery in the nasal and temporal directions. This trend is evident when comparing the evolution patterns across different progression groups in myopes.

An intriguing observation was that the 2-D peripheral refraction maps displayed notable asymmetry across the retina, particularly in emmetropic children. This asymmetry appears to be closely associated with refractive error status and the degree of central myopia progression over the subsequent two years. Our findings align with previous research reporting asymmetries along either the horizontal or vertical meridians [81-83, 94, 97], with a common trend of relatively more myopic defocus in the superior retina. At least one prior 2D peripheral refraction study covering 42° x 32° visual field identified significant superior-inferior asymmetry in hyperopes, but not in emmetropes for the population around 29 years old [97]. Differences in age and ethnicity between the studies may help explain this discrepancy. Overall, these findings indicate that ocular dimensional changes are not uniform across the retina. As a result, relying solely on measurements along the horizontal or vertical meridians may be insufficient to fully characterize peripheral refraction.

To maintain comparability between different studies, it is recommended to select emmetropes without any optical intervention to avoid any change of peripheral refraction pattern in myopes and hyperopes. Meanwhile, we also provided single vision glasses for children with refractive errors to ensure the visual behavior did not change due to myopia onset.

We performed a correlation analysis for peripheral refraction at local region in step of

5 degrees visual field, but no significant relationship was verified in either hyperopes or myopes (see tables S2 and S4). In contrast, a significant relationship was found in the upper retina of emmetropes, which indicates that more myopia progression is associated with more myopic defocus. Those findings are indeed surprising as it appears to contradict with previous studies with optical interventions (extrinsic optical defocus), which generally assumed that myopic defocus in periphery is a protective factor for controlling myopia progression.

### 3.4.2 Relative myopia in the superior retina as a cause of myopia?

We propose two hypotheses to explain the role of relative peripheral myopia in the superior retina as a potential cause of myopia progression. For the intrinsic peripheral refraction hypothesis, the observed superior retinal myopia is considered the driver of myopia progression. However, this theory contradicts previous animal studies suggesting that relative peripheral myopia protects against myopia development. This discrepancy could be explained by different mechanisms of retinal response to peripheral defocus in emmetropes versus myopes. For instance, recent findings indicate that the sensitivity to detect defocus differs between emmetropic and myopic eyes [142]. The mean difference in superior retinal defocus between fast progression group and slow progression group was approximately 0.3D ($p=0.017$). While this degree of defocus may cause only mild retinal blur, it could nonetheless be sufficient to trigger axial elongation. Consequently, preserving emmetropic refraction in the peripheral retina may represent an effective approach for preventing the onset of central myopia in emmetropic individuals.

The second hypothesis, based on additional peripheral refraction, suggests that the optics encountered by the human eye in its visual environment contribute to myopia progression. This type of peripheral optics cannot be directly measured by a peripheral refractor but can be inferred from the subject's visual environment. For example, when

a child is doing homework, the superior retina is exposed to the optics of near objects like the table surface and textbooks. If the image from this near work is perfectly focused on the fovea, then relative peripheral hyperopia might be present in the superior retina as accommodation alters peripheral refraction in parallel [100]. Conversely, when the eye looks downward, relative peripheral myopia may be exposed to the inferior retina, as light from the ceiling or sky, which is nearly 0 D, converges.

The detected average working distance for near tasks is from 16 cm to 20 cm, corresponding to approximately 5 D of accommodative stimulation. If there is an accommodative lag in emmetropic eyes, the superior retina could be dominated by hyperopic defocus and potentially promote local axial elongation. The local response to local defocus has been found in previous animal studies [143, 144]. In China, school-aged children typically face considerable academic pressure, leading to prolonged time spent on near tasks like homework and decreased time for outdoor activities [125]. This might explain why children with faster myopia progression present more myopic defocus in superior retina. Additionally, children with early-onset myopia often show more variability for accommodative lag than emmetropes [145], which is consistent with another finding by Gwiazda et al. [121] that 0.5 D accommodative lag is sufficient to accelerate myopia development in emmetropes.

### 3.4.3 Relative myopia in the superior retina as an outcome of myopia development?

An alternative interpretation for the observed relative myopia in the superior retina could be linked to the end point of myopia development. When myopization is initialized, the human eye might preferentially start in the superior retinal region, and then subsequently extend toward the posterior pole and later involving nasal/temporal quadrants. This directional expansion may be more strongly associated with inherent

growth mechanisms than with locally induced optical defocus signals.

The evidence comes from the study that the change of eyeball is more pronounced in vertical meridian than horizontal meridian when emmetropic children just developed myopia [146]. Additionally, findings from our previous publication regarding the most common types of 2D refractive patterns in emmetropic children [32] offer additional support. The fast progression group from current research strongly resembled category 2 (bilateral hyperopia pattern) from the study, which accounted for 14% of emmetropic population.

### 3.4.4 Summary

The key advantage of this research lies in its longitudinal assessment of peripheral refraction across a two-dimensional retinal area, utilizing high-resolution spatial sampling. We also considered various potential confounding variables, though none showed a significant impact on the outcomes. Additionally, the genetic and environmental consistency within the participant group strengthens the reliability and comparability of the findings among different progression subgroups.

In summary, our results suggest that emmetropic children exhibiting relatively higher myopia in the superior retinal region may undergo more rapid axial myopia progression. In contrast, no distinct peripheral refraction profiles were found to correlate with refractive changes in children who remained hyperopic or had already developed myopia. Notably, relative myopic defocus in the superior retina—approximately 10 degrees eccentricity—emerged as a meaningful indicator of future myopia onset. These insights may support the development of optical interventions designed to sustain relative emmetropia in the superior visual field as a preventive approach to against childhood myopia.

# Chapter 4. Accommodation responses with modified peripheral optics

## 4.1. Introduction

A popular hypothesis for the mechanism of peripheral defocus-based techniques is related to the intervention of the accommodation response. It has been hypothesized that greater accommodative lag results in more relatively hyperopic defocus in the periphery, thereby promoting myopia progression. To investigate this issue, we conducted an experiment to examine the accommodation response dynamically through a double-pass instrument for three commercially available myopia control lenses. The spectacles include MiYOSMART (Hoya), Stellest (Essilor), and MyoCare (ZEISS). Additionally, four types of regular single vision (SV) glasses were tested, with refractions of 0 D, +3D defocus, -3D defocus, and -3D astigmatism. The central distant correction zone materials were removed to focus solely on the impact of peripheral refraction modification on accommodation response.

## 4.2. Methods

### 4.2.1. Subjects

The inclusion criteria include:

1. Age≤38 years old (adults) or age ≤14 years old (children)
2. Astigmatism no more than 1.5 D
3. BCVA better than 0.8 (decimal) or less than 0.1 (LogMAR)
4. Generally, in good health. No history of eye disease, refractive surgery and systemic disease
5. No experience of application of myopia control lenses

The exclusion criteria include:

1. The amplitude of accommodation less than 5.0D (adults) or 10 D (children)
2. The subject cannot follow the instruction with the practitioner
3. The subject has difficulty to fix on the target

Subjects were divided into three groups. The first group consisted of all the adults (n=13, mean age=28±4.5 years) and was aimed at testing the accommodation response across different myopia control spectacles. The second group was a subset of the first, including only emmetropes (n=7) and one low myope (n=1) with contact lens correction, with the purpose of testing the accommodation response with partially excised spectacles. The third group comprised 9 children (mean age=9.8 years) with the same testing purpose as the first group. Details are listed in table 4-1.

Table 4-1. The demographics of the subjects in three groups (M±SD).

| | Group 1 (N=13) | Group 2 (N=8) | Group 3 (N=9) |
|---|---|---|---|
| Age (years) | 28±4.5 | 27.9±5.3 | 9.8±1.7 |
| Gender (female:male) | 6:7 | 5:3 | 6:3 |
| SER (D) | -2.5±2.3 | -1.4±1.2 | -0.13±0.3 |
| Distance VA | 1±0.1 | 1±0.2 | 1±0 |
| AA (D) | 7±1.2 | 7.2±1.2 | 16±4 |
| Race | 3 Asians, 10 White/Caucasian | 1 Asian, 7 White/Caucasian | 9 White/Caucasian |
| SER, Spherical Equivalent Refraction; VA, visual acuity; AA, amplitude of accommodation; Group 1 and group 3 were for testing the dynamic accommodation response among varies myopia control spectacles. Group 2 was for testing the dynamic accommodation response among different partially excised regular glasses. | | | |

All participants or their legal guardians received comprehensive information regarding the experimental procedures. All procedures adhered to the principles outlined in the Declaration of Helsinki. Ethical approval for the study was granted by the Institutional Review Board of the University of Murcia (M10/2023/080).

4.2.2. Experimental procedure

The testing procedure involved two steps:

1. Determining the best focus value: In this initial step, the device introduced defocus from -10 D to +10 D in 0.25 D increments.
2. Recording the dynamic accommodation response: This step involved recording the eye's dynamic accommodation response. The testing range for the through-focus images was set based on the best focus value, adjusted to [-6 D to +1 D] in 0.25 D increments for adults and [-7 D to +1 D] for children. During this phase, a CCD camera can record 33 images within 0.65 seconds, corresponding to a dynamic measurement frequency of 1.54 Hz. Further details about the instrument can be found in section 2.2.

The measurement was performed by changing the fixation sequentially at distant, near, and distant again for the dynamic response. The distant target was placed 3 meters away. The near target was attached to a board controlled by a stepper motor, placed at a distance of 0.22 meters (4.5 D) for adults and 0.18 meters (5.5 D) for children. The distance from the near target to the eye was adjustable by moving the stepper motor box along a 1-meter rail. The distant, near, and distant targets were presented for 3 s → 5 s → 3 s sequentially. The testing environment is presented as figure 4-1.

4.2.3. Myopia control spectacles

The lenses were uncut, so customized frames were 3D-printed (Form 3L, Formlabs, United States). To investigate the effect of peripheral refraction on accommodation response in foveal vision, the lenses could be shifted laterally by 1.5 cm (figure 4-1).

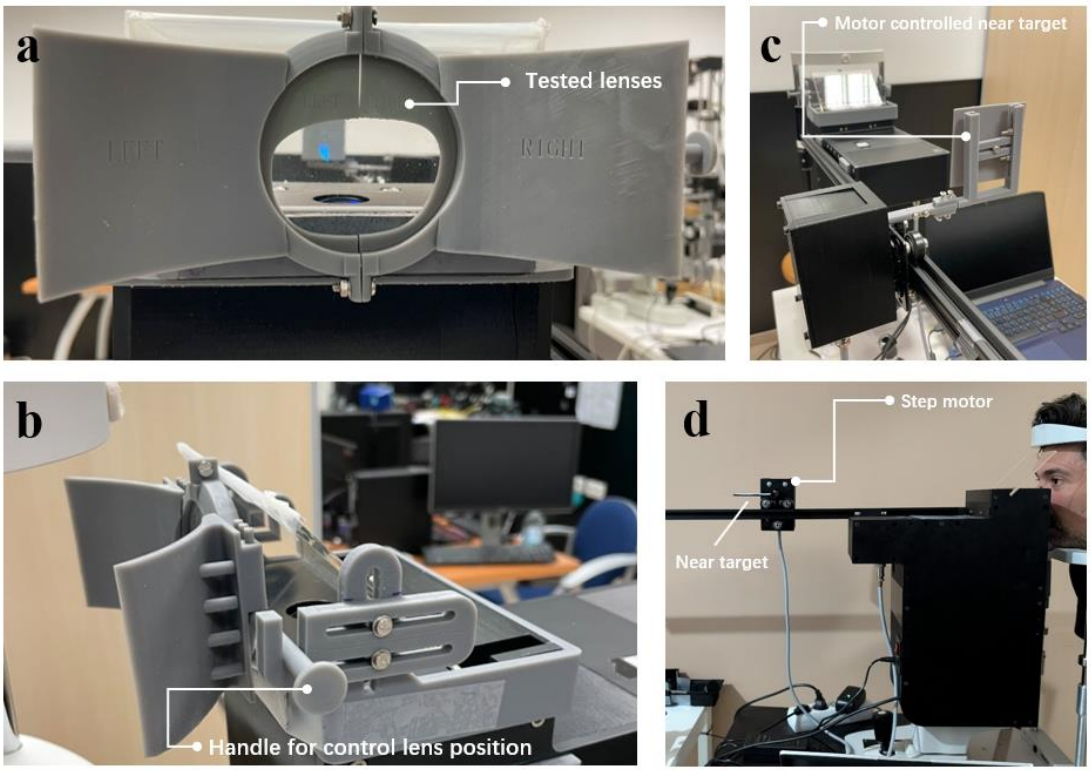


Figure 4-1. The set up for the measurement of accommodation along with the 3D-printed accessories for controlling the position of the lenses. a). A front view from the side of subjects. b). A side view of the 3D-printed accessories for controlling the position of lenses. c). A back view demonstrates how does the device controls the near target. d). The lateral view of the device.

4.2.4. Partially excised spectacles

In addition to the micro lenslets-based spectacles, regular SVG can also alter peripheral refraction (figure 4-2) in a broad range. However, since the central and peripheral refractions of these glasses are identical, they do not provide relative peripheral refraction for the wearer. To address this, we removed the material in the central area to focus solely on the impact of peripheral refraction on accommodation response. The circular area in the center of the glasses was removed in 12 mm diameter. The refractions of the four glasses used were plano, +3 D peripheral myopia, -3 D peripheral hyperopia, and -3 D astigmatism.

Figure 4-2. A picture shows the appearance of the partially excised SVG.

4.2.5. Experimental procedures

1. Best-corrected visual acuity (BCVA): BCVA was evaluated with an eye chart that attached to the wall. The experiment was performed with their habitual correction. All participants had a visual acuity of 1.0 (decimal)/0.1 (LogMAR) or better.

2. Accommodation amplitude (AA): The AA was evaluated with minus lens technique [147] and push up test [148] for adults and children, respectively. This examination aimed to exclude subjects that are unable to fixate on the near target. One adult subject was found ineligible for the experiment due to an AA of 3.5D.

3. Auto-refraction: The objective refraction of the eye was determined using a double-pass instrument. The test was repeated for myopic subjects wearing their prescribed glasses. This pre-exam was conducted to improve the measurement speed of the dynamic accommodation test.

4. Dynamic accommodation responses: After determining the central refraction, an 11-second dynamic accommodation response test was conducted on the subjects. Details about the hardware device can be found in section 2.2. It is important to note that subjects in group 2 were derived from group 1, so they underwent the test twice. The

first dynamic test was always performed with myopia control spectacles, and the second with partially excised glasses. There was at least a 10-minute rest between the two experiments. The order of the spectacles tested was randomized to avoid visual fatigue effects on the results. Each measurement was repeated three times, and the mean values were used for data analysis. Assessments were conducted solely on the right eye, while the left eye was occluded with an eye patch.

### 4.2.6 Data analysis

The control software in the double-pass instrument was developed in Matlab (MathWorks, USA). After the experiment, the captured through-focus images and accommodation results were exported as '.mat' files for initial analysis in Matlab. This initial analysis involved data cleaning, data integration, manual inspection of best focus images, figure generation, and calculation of PSF image contrast, all performed using customized scripts. Statistical analysis was then conducted using SPSS software. Descriptive data are reported as mean ± standard deviation in the text, while figure plots display values as mean ± standard error. To assess differences in accommodation responses under various lens fitting conditions, a one-way ANOVA was conducted, followed by Bonferroni-adjusted post hoc analyses.

The dynamic accommodation test consisted of three phases: distant target (3 seconds) → near target (5 seconds) → distant target (3 seconds). Based on this sequence, the mean accommodation response was segmented into three distinct time intervals: the initial phase (0–1.5 seconds), representing the first distant fixation, the middle phase (5–6.5 seconds), corresponding to near fixation, and the final phase (9.5–12 seconds), reflecting the return to the distant target. The average from those three phases were considered representative values and were used for comparisons across the different spectacle conditions.

## 4.3. Results

The dynamic accommodation responses are presented in Figure 4-3, with (a) showing results for adults and (b) for children. It is important to note that the near stimulation for children was greater than that for adults (4.5D/0.22m for adults and 5.5D/0.18m for children). Consequently, more through-focus images were captured in one round for children, resulting in fewer sampling points in the dynamic accommodation curve (17 time points for adults and 16 for children). Overall, there was no significant difference observed among the various myopia control spectacles for both adults and children. The accommodative lag for near stimulation was less than 0.5D across all subjects.

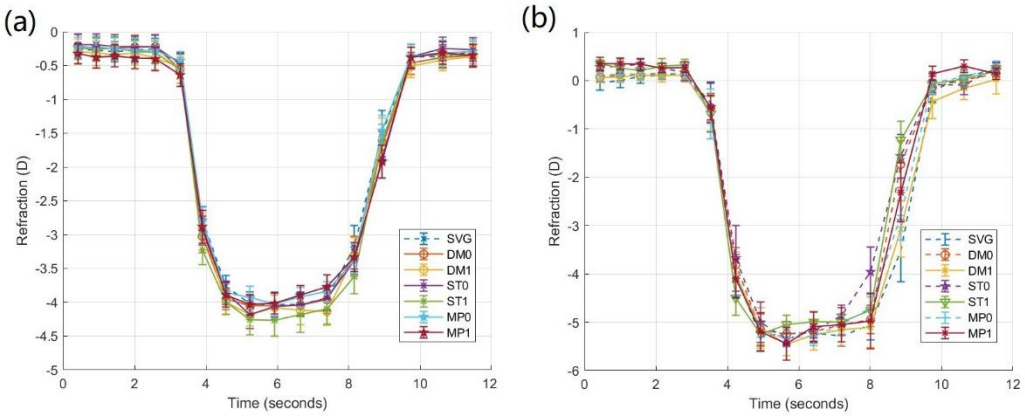


Figure 4-3. Time course of dynamic accommodation responses in adults (a) and children (b). The near target imposed an accommodative demand of 4.5 D for adults and 5.5 D for children. The measurement protocol involved sequential presentation of a distant target (3 seconds), a near target (5 seconds), and a return to the distant target (3 seconds). The legend abbreviations denote the following spectacle types: SVG – single vision glasses; DM0 – centered MiYOSMART; DM1 – decentered MiYOSMART; ST0 – centered Stellest; ST1 – decentered Stellest; MP0 – centered MyoCare; MP1 – decentered MyoCare. Data in the plots are shown as mean ± standard error.

The refractive errors of the participants were corrected to fully stimulate the accommodation response. A stable period for ocular refraction was noticed prior to the

shift of near target (approximately -0.25D for adults and +0.25D for children). The exact values for each phase are summarized in table 4-2.

Table 4-2. The mean amplitude of accommodation response (M±SD) with different spectacles at beginning, middle and late stage of dynamic accommodation

| Adult (N=13) | | | | | | | | | |
|---|---|---|---|---|---|---|---|---|---|
| Stage | SV | CenMiyo | DecMiyo | CenStell | DecStell | CenMyoC | DecMyoC | F | P |
| Early | -0.3±0.5 | -0.2±0.6 | -0.3±0.7 | -0.2±0.6 | -0.2±0.6 | -0.2±0.6 | -0.4±0.6 | 0.27 | 0.95 |
| Middle | -4±0.7 | -4±0.6 | -4.1±0.7 | -4.1±0.7 | -4.2±0.8 | -4±0.6 | -4±0.5 | 0.10 | 0.99 |
| Final | -0.3±0.6 | -0.4±0.6 | -0.4±0.6 | -0.3±0.6 | -0.3±0.6 | -0.3±0.6 | -0.3±0.6 | 0.08 | 0.99 |
| Children (N=9) | | | | | | | | | |
| Stage | SV | CenMiyo | DecMiyo | CenStell | DecStell | CenMyoC | DecMyoC | F | P |
| Early | 0.0±0.1 | 0.1±0.1 | 0.1±0.1 | 0.3±0.1 | 0.3±0.1 | 0.1±0.1 | 0.4±0.1 | 1.37 | 0.24 |
| Middle | -5.2±0.2 | -5.2±0.2 | -5.4±0.2 | -5.3±0.1 | -5.0±0.2 | -5.3±0.2 | -5.3±0.3 | 0.3 | 0.93 |
| Final | 0.1±0.1 | 0±0.1 | -0.1±0.2 | 0±0.1 | 0.1±0.1 | 0.1±0.1 | 0.3±0.1 | 0.88 | 0.51 |

The accommodation response was calculated as the mean value within three specific time windows: the initial phase (0–1.5 seconds, representing distant fixation), the middle phase (5–6.5 seconds, representing near fixation), and the final phase (9.5–12 seconds, representing a return to distant fixation). These mean values served as representative metrics for comparing performance across different spectacle designs. A one-way ANOVA was employed to assess statistical differences in accommodation among the various lens types. The following abbreviations were used: CenMiyo – centered MiYOSMART; DecMiyo – decentered MiYOSMART; CenStell – centered Stellest; DecStell – decentered Stellest; CenMyoC – centered MyoCare; DecMyoC – decentered MyoCare.

Following the transition from a distant to a near target, participants required approximately 2 seconds (corresponding to time points 6 through 9) to achieve a stable refractive state (Figure 4-3a). Upon returning to a distant fixation (time points 13 to 15), it took roughly 1.6 seconds for accommodation to stabilize again. During the near

viewing phase, a slight tendency for the participants to lose focus was noted, which is a commonly reported phenomenon for fixating behavior. The target shift from near to far at the 9 second shows greater variability, potentially reflecting the visual fatigue due to sustained near fixation. Similar accommodative patterns were observed when using spectacles with partially removed zones (Figure 4-4 and Table 4-3). There were no significant differences in the magnitude of accommodation response among the different spectacle designs for different time periods.

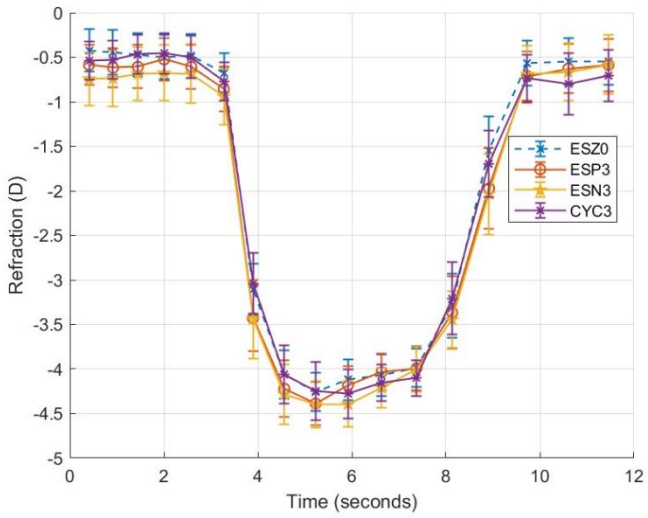


Figure 4-4. The plots of dynamic accommodation responses over time in adults with the partially excised SVG. The legends represent different lenses are: ESZ0 – plano lenses; ESP3 – lenses with +3.00 D spherical power; ESN3 – lenses with –3.00 D spherical power; and CYC3 – lenses with –3.00 D cylindrical power.

Table 4-3. Mean accommodation response (M ± SD) in adults during the early, middle, and late phases of dynamic accommodation using partially excised SVG.

| Stage | ESZ0 | ESP3 | ESN3 | CYC3 | F | P |
|---|---|---|---|---|---|---|
| Early | -0.4±0.7 | -0.6±0.6 | -0.7±0.9 | -0.5±0.6 | 0.23 | 0.88 |
| Middle | -4.1±-0.6 | -4.2±0.6 | -4.3±0.7 | -4.2±0.7 | 0.11 | 0.95 |
| Final | -0.6±0.7 | -0.6±0.8 | -0.6±0.9 | -0.7±0.8 | 0.07 | 0.97 |
| The accommodative response amplitude was calculated as the mean value within three specific time intervals: the initial phase (0–1.5 seconds, corresponding to distant fixation), the middle phase (5–6.5 seconds, corresponding to near fixation), and the final phase (9.5–12 seconds, corresponding to the return to distant fixation). These mean values were used as representative indicators to compare accommodative behavior when viewing through regular spectacles with a central opening. A one-way ANOVA was applied to assess differences in accommodative response across the different lens conditions. The abbreviations ESZ0, ESP3, ESN3, and CYC represent lenses with prescription as plano, +3.00 D peripheral defocus, –3.00 D peripheral defocus, and –3.00 D cylindrical power, respectively. | | | | | | |

## 4.4. Discussion

### 4.4.1. Dynamic accommodation response

We evaluated the accommodation response dynamically with various types of myopia control lenses. The approach provided a fast assessment of refraction evaluation continuously at high speed by easily switching the frame of the lenses. There was one similar study that also evaluates dynamic accommodation but in contact lenses (SVG, MiSight, and Acuvue Moist), which are designed for presbyopia correction. The findings suggest that the mechanism of myopia control for MiSight could be interpretated by altering retinal contrast in the periphery and meanwhile improve the accommodative ability [149]. Another widely used approach for myopia control is Ortho-K, and the treatment effect is assumed to be related to the enhancement of accuracy in accommodation response for near targets [64].

We randomized the experimental sequences and lens positions of those myopia control

spectacles trying to reduce visual fatigue after long tests. The horizontal displacement of the lenses is set as 15 mm as the central clear zone is around 5 mm in radius. This ensured that the central vision of the subject is fully overlapped with the peripheral defocus region of the lenses, and thereby the visual behavior of the wearer can be changed. Nevertheless, we didn't find any significant differences for the accommodation response for different phases in both children and adults. This finding is beyond expectation as previous study found that the retinal image, particularly image contrast, was changed depending on the design of the spectacles [150]. Similar results were validated in our study for through-focus retinal PSF images. Thereby, just the modification of retinal images by those myopia control spectacles is not enough to change the accommodation behavior of the wearer in the current study.

Accommodation demand was set at 4.5D for adults and 5.5D for children, corresponding to 64.2% (4.5D/7D) and 34.3% (5.5D/16D) of the average accommodative amplitude (AA) for the respective cohorts. The threshold value 4.5 D was determined according to the average amplitude of accommodation of the adult population from current study (age 28 – 30 years old). The accommodation stimulation for children was set as 5.5 D, which is limited by the dimension of the device for placing the near target. The setting of the device allows more stable results for the near stimulation and therefore reflects the true response of the study population.

Except for the multi-focus myopia control lenses, a parallel experiment was conducted in a set of partially excised lenses to investigate the influence of uniform distributed peripheral refraction on accommodation behavior. This purpose was ensured by removing the central part of the SVG. Specifically, the optical power of the spectacles is: plano, +3D peripheral hyperopia, -3D peripheral myopia, and -3D astigmatism. Although the optical power differed significantly across various experimental lenses, there is no significant difference noticed among different lenses for any time phase (see Figure 4-4). In summary, the findings from our research indicate that peripheral optical

defocus does not change accommodation behavior. However, this conclusion is subject to a serious experimental condition: peripheral defocus less than 3.5D and short time adaptation to peripheral defocus-based techniques.

Despite clear differences in retinal image quality under varied optical conditions, the dynamic accommodation responses remained remarkably stable throughout the trials. This implies that the human visual system may possess a robust tolerance to blur, enabling effective fixation ability at both near and far distances. It's worth noting that the current generation of myopia control spectacle lenses possess a maximum peripheral defocus of approximately +3.50 D. This opens the possibility of enhancing therapeutic outcomes for myopia control by further increasing defocus power. Thus, it remains unclear whether current lens designs have reached the optimal balance between visual performance and wearer comfort required for clinical application in myopia management.

4.4.2. Strength and limitations

Our research offers several advantages. In primary, the dynamic accommodation response was evaluated in an objective manner by screening the through-focus images. Compared to Hartmann-Shack wavefront sensor, our device provides high confidence for evaluating pupil aberration that interfered with micro-lenslets. This is because our double-pass system can capture the real retinal PSF image in through-focus status without losing any optical information, whereas the wavefront data at pupil plane may miss the information due to the limited resolution of Hartmann-Shack lens array. Furthermore, this feature enabled effective comparisons of image contrast for various research purposes. Finally, we designed a spectacle frame to fix myopia control lenses, which allows for straightforward manipulation of lens positioning to assess peripheral effects without requiring subjects to shift their gaze, thereby minimizing potential sources of measurement variability.

The research had some limitations. First and foremost, the study just included a small number of participants, which means a relatively poor power of test for statistics. Nonetheless, the low variation in accommodation outcomes supports the overall reliability of the findings. Secondly, accommodation was assessed under monocular conditions, with the opposite eye occluded, which might not fully represent the natural binocular visual behavior for their daily activities. Thirdly, our study does not include refractive progressive population (childhood myopia). This special cohort could demonstrate a different accommodation behavior compared to adults and emmetropic children as previous study found different ocular response to peripheral defocus in emmetropes and myopes [142]. Fourthly, the temporal frequency increment (TFI) was fixed at 0.25 D, balancing between measurement speed and dioptric precision. If subtle differences exist between test conditions that fall below this threshold, they may go undetected statistically. Lastly, the dynamic accommodation response was recorded at a relatively modest speed of approximately 1.5 samples per second, limiting the temporal resolution for dynamic analysis. Even so, the measurement principle ensures the reliability of all recorded data.

### 4.4.3 Summary

Our findings suggest that commercially available defocus-based spectacles do not induce changes in dynamic accommodation response over short-term observation periods. This indicates that the human eye may have a higher threshold for adjusting accommodation to blurred images during fixation. Therefore, the mechanisms driving the myopia control effect of peripheral defocus-based spectacles are unlikely to involve alterations in accommodation response.

The direct findings of current research indicate that the peripheral defocus-based spectacles do not affect accommodation response over brief observation periods. This suggests that the capability to adapt to blurred images in the human eye might be higher

than the defocus brings from current commercially available optical products. Therefore, it is unlikely that changes in accommodative response contribute to the myopia control efficacy of peripheral defocus-based spectacles.

# Chapter 5. Retinal contrast with modified peripheral optics

## 5.1 Introduction

This chapter presents an in-depth analysis of the retinal image contrast with myopia control lenses. Retinal contrast represents a novel theoretical framework that may help explain the myopia control effects of peripheral modification in spectacles. Additionally, it is well known that defocused images exhibit a reduction in contrast. Therefore, it is plausible that peripheral defocus-based spectacle lenses prevent myopia progression by reducing peripheral image contrast rather than solely relying on the detection of optical defocus. Furthermore, the double-pass instrument applied in the thesis provides a reliable approach to evaluate the image contrast directly from retina. To investigate the hypothesis regarding the contrast theory, we conducted an analysis of through-focus retinal image contrast with different myopia control spectacles.

## 5.2 Data analysis

Contrast refers to the difference in brightness between various areas of an image. A high-contrast optical system enhances the visibility of an object to the human eye or an image sensor. Since the human eye is more sensitive to contrast than to absolute luminance, we can perceive our surroundings throughout the day, even in relatively low-light conditions [151].

### 5.2.1 Formulas for contrast calculation

Depending on the experiment's purpose or the application environment, there are multiple methods to quantify contrast.

1. RMS contrast

RMS contrast describes the standard deviation of pixel brightness within an image, effectively capturing the dispersion of pixel values. However, this value can be influenced by the absolute luminance of the visual environment or the camera's exposure time.

$$C_{RMS} = \sqrt{\frac{1}{N}\sum_{i=1}^{N}(I_i - \mu)} \quad \text{(Equation 5-1)}$$

Here, N is the number of pixels over the image;$I_i$ represents the brightness of the *i*th pixel; $\mu$ is the average brightness of the image.

2. Michelson contrast ($C_{Michelson}$)

Michelson contrast is primarily used for periodic patterns, such as sine wave patterns. However, this method may not be suitable for calculating contrast in images characterized by irregular variations.

$$C_{\text{Michelson}} = \frac{I_{max} - I_{min}}{I_{max} + I_{min}} \quad \text{(Equation 5-2)}$$

Here, $I_{max}$ is the maximum pixel value of the image, $I_{min}$ is the minimum pixel value of the image.

3. Sobel contrast ($C_{Sober}$)

Sobel contrast is widely used in image processing to detect the edges of a pattern using the Sobel operator.

$$C_{Sober} = \sum_{x,y}\sqrt{\left(G_x(x,y)\right)^2 + \left(G_y(x,y)\right)^2} \quad \text{(Equation 5-3)}$$

Here, $G_x$ and $G_y$ represent the gradient vector differences in the x and y directions, where (x, y) corresponds to the image coordinates.

4. CV (Coefficient of Variation) contrast ($C_{CV}$)

CV contrast is derived from RMS contrast but, unlike RMS contrast, it is not influenced by the absolute brightness of the image. This makes it a useful parameter for comparing different imaging systems or for comparing the performance of healthy eyes versus cataract-affected eyes.

$$C_{CV} = \frac{C_{RMS}}{\mu} \quad \text{(Equation 5-4)}$$

Here, $C_{RMS}$ is the RMS contrast, $\mu$ is the average luminance of the image.

5.2.2 Procedure of contrast calculation

Step 1: Determine the analysis area

S1.1 Select the pixels for calculate weighted center

The center of the analysis area was determined by multiplying pixel values by their coordinates. To minimize the impact of stray light, only pixel values within the 90% to 99% intensity range of the entire image were selected.

S1.2 Calculate the weighted center

$$W_x = \frac{\sum[X \cdot P_{(x,y)}]}{\sum P_{(x,y)}},\ W_y = \frac{\sum[Y \cdot P_{(x,y)}]}{\sum P_{(x,y)}} \quad \text{(Equation 5-5)}$$

Here, $W_x$ and $W_y$ represent the coordinates of the weighted centroid of the PSF image. $X$ is the row of the pixels, $Y$ is the column of the pixels, $P_{(x,y)}$ is the pixel value at $(x, y)$.

S1.3 Select the analysis area

The analysis area was defined as a circular region with a radius equal to 30 pixels [corresponding to a 0.06 degrees visual field (VF) radius].

Step 2: Calculate contrast value

We applied the three contrast formulas: $C_{RMS}$, $C_{Micheleson}$, and $C_{CV}$. The best focus image and through-focus PSF images (with defocus values of -3D, -2D, -1D, 0D, +1D, +2D, +3D) were selected for analysis. As the through-focus images were determined by central refraction around [-6D: 0.25D: +1D] (for adults) during the dynamic accommodation test, negative defocus images were selected when the subject was looking at a distant target, while positive defocus images were selected when the subject was looking at a near target.

Figure 5-1 is an example of integrated through-focus PSF images from the dynamic

accommodation response test of one subject. The red/white asterisks indicate the best focus images calculated by Matlab based on two different algorithms. The white, red, and grey rectangles indicate the selected PSF images with defocus values of -1D, +1D, and -2D, respectively. The choice of defocus image was based on the best focus image at the corresponding time point.

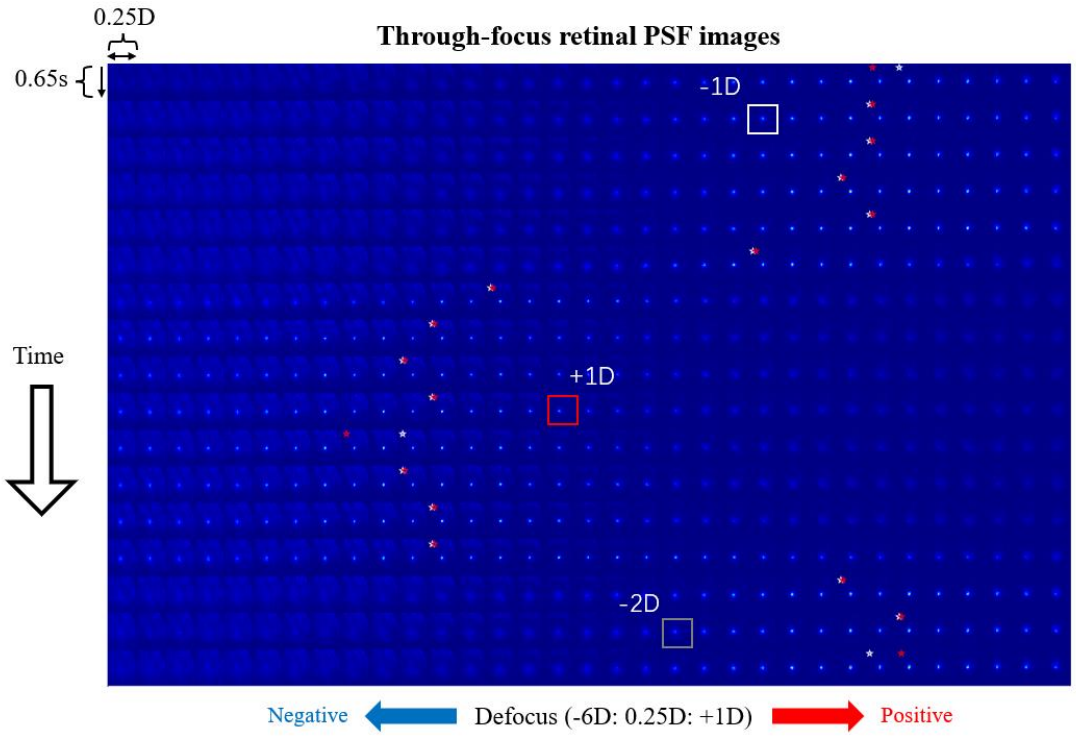


Figure 5-1. Integrated through-focus retinal PSF images. Each row represents a group of through-focus PSF images. The double-pass instrument captures 33 PSF images in approximately 0.65 seconds. The chronological order of measurements is presented from top to bottom. Therefore, the step between two images in the horizontal direction represents a 0.25D increment (equivalent to a 0.02-second time difference) from left to right, while the interval between two images in the vertical direction indicates a 0.65-second time difference.

## 5.3 Results

### 5.3.1 Features of through-focus images

To better understand the PSF images, a few examples of through-focus images are

presented here as figure 5-2. Below shows the best focus images in four subjects. Each column corresponds to one type of spectacles or experimental conditions. The results from MyoCare showed the shape of PSF images resembling a shell placed in horizontal direction. This is because the lens was shifted in horizontal direction, and the concentrical rings in lateral side dominate its power in horizontal direction.

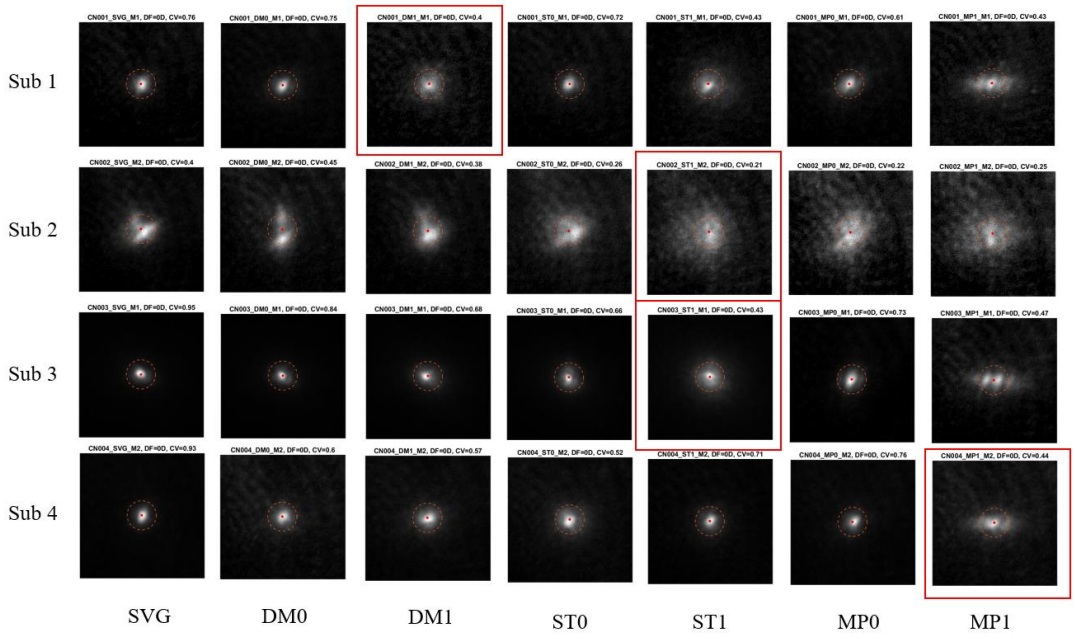


Figure 5-2. Examples of best focus images in four subjects across different experimental conditions. The columns from left to right correspond to PSF image from single vision glasses, DIMS lens, decentered DIMS, Stellest lens, decentered Stellest, MyoCare lens and decentered MyoCare. The red dashed circular around the center of the image indicates the region for contrast analysis (r = 30 pixels/0.06 degrees). The red rectangular in each row highlights the situation with lowest contrast value among the experimental conditions.

Defocused PSFs are also important to understand the optical effects of the myopia control spectacles. As an example, the image from two subjects were presented below as figure 5-3. Best focus images showed the highest contrast compared to defocused images. It seems that the contrast is dominated by added defocus instead of the

peripheral optics of the myopia control spectacles (the micro-lenslets) when there is a significant optical defocus on retina.

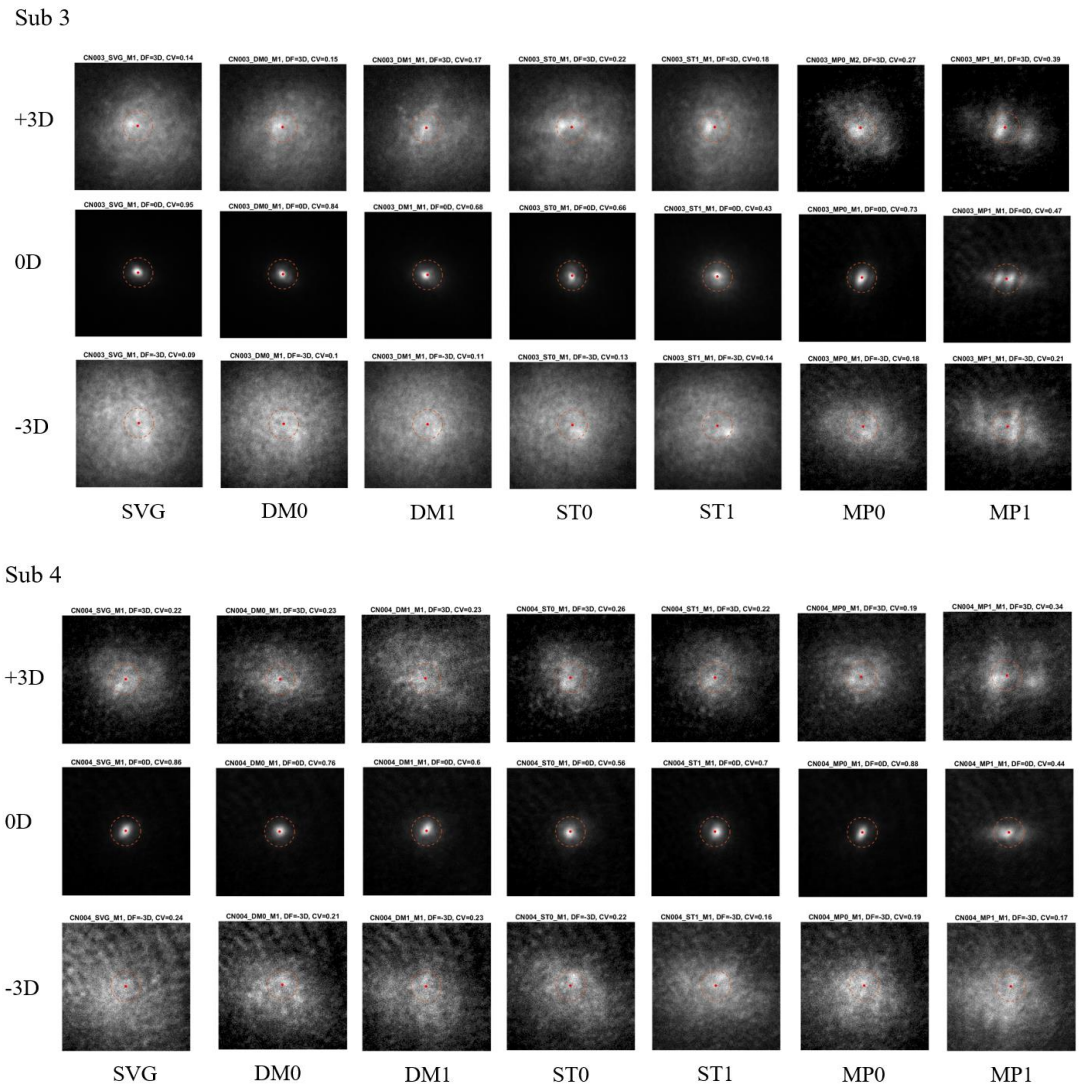


Figure 5-3. Through focus PSF images from two subjects. The graphs in superior/inferior part of the figure indicate the results from subject 3/4. The words SVG, DM0, DM1, ST0, ST1, MP0, MP1 refer to single vision glasses, centered MiYOSMART, decentered MiYOSMART, centered Stellest, decentered Stellest, centered MyoCare, decentered MyoCare.

### 5.3.2 Critical questions before contrast analysis

We will address three questions before comparing contrast.

- First, does accommodation affect retinal contrast in the best-focus image?

- Second, which formula is most appropriate for calculating PSF image contrast?
- Third, what range of the visual field should be used for analysis?
- And last, which image from the through-focus series is the best option for contrast calculation?

To address the first two questions, three histograms in figure 5-4 present contrast values from different spectacles under various accommodation conditions.

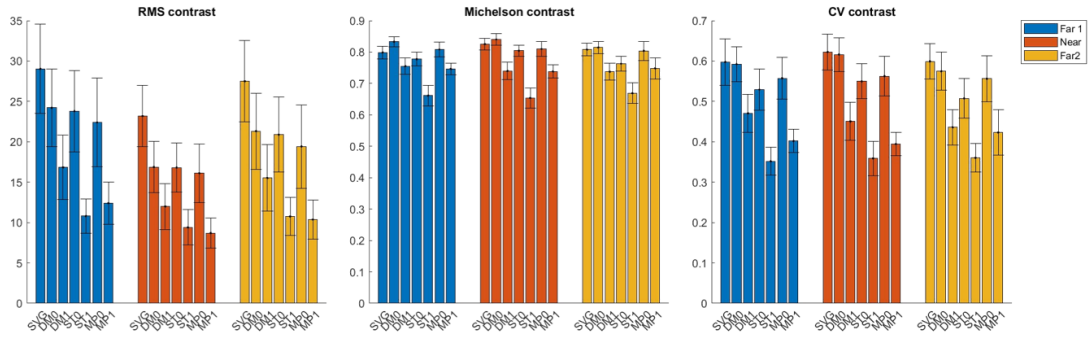


Figure 5-4. The contrast values of best-focus PSF images during near and relaxed accommodation. Subgraphs (a), (b), and (c) display contrast values calculated using RMS contrast, Michelson contrast, and CV contrast, respectively. In each subgraph, the left (blue), middle (red), and right (yellow) bar groups represent values from relaxed accommodation (first time looking far), near accommodation, and relaxed accommodation again (second time looking far). The error bars indicate the standard error across subjects. The labels SVG, DM0, DM1, ST0, ST1, MP0, and MP1 refer to single vision glasses, centered MiYOSMART, decentered MiYOSMART, centered Stellest, decentered Stellest, centered MyoCare, and decentered MyoCare, respectively.

To compare the difference in contrast value between different accommodation statuses, the results are summarized in table 5-1, table 5-2, and table 5-3.

Table 5-1. Contrast values from the best-focus image under different accommodation conditions, calculated using **RMS** contrast (Mean ± Standard Error).

| Spectacles | Far 1 | Near | Far 2 | $t^{\dagger}$ | $P^{\dagger}$ | $t^{※}$ | $P^{※}$ |
|---|---|---|---|---|---|---|---|
| SVG | 29.0±5.5 | 23.2±3.8 | 27.5±5.03 | 2.31 | 0.0389* | 0.76 | 0.46 |
| DM0 | 24.2±4.5 | 16.9±3.18 | 21.3±4.72 | 3.08 | 0.0095** | 2.0 | 0.068 |
| DM1 | 16.8±4.0 | 12.0±2.85 | 15.5±4.11 | 2.61 | 0.0225* | 1.5 | 0.236 |
| ST0 | 23.8±5.05 | 16.9±3.03 | 20.9±4.63 | 2.81 | 0.0156* | 1.89 | 0.082 |
| ST1 | 10.8±2.12 | 9.41±2.21 | 10.8±2.37 | 1.42 | 0.1816 | 0.08 | 0.936 |
| MP0 | 22.4±5.49 | 16.1±3.64 | 19.4±5.18 | 2.83 | 0.0149* | 0.49 | 0.028* |
| MP1 | 12.4±2.62 | 8.7±1.87 | 10.4±2.42 | 2.89 | 0.0136* | 2.56 | 0.025* |

A paired t-test was used to compare the differences between relaxed accommodation (Far 1) and near accommodation (Near), as well as the differences in relaxed accommodation between the beginning (Far 1) and the end (Far 2) of the measurement.

$t^{\dagger}$ and $P^{\dagger}$: The statistics for Far 1 vs Near, $t^{\dagger}$ and $P^{\dagger}$ refer to the t-statistic and significance level of the test results.

$t^{※}$ and $P^{※}$: The statistics for Far 1 vs Far 2, $t^{※}$ and $P^{※}$ refer to the t-statistic and significance level of the test results.

The labels SVG, DM0, DM1, ST0, ST1, MP0, and MP1 correspond to single vision glasses, centered MiYOSMART, decentered MiYOSMART, centered Stellest, decentered Stellest, centered MyoCare, and decentered MyoCare, respectively.

*Indicate the P-value<0.05, and ** means the P-value<0.01.

Table 5-2. Contrast values from the best-focus image under different accommodation conditions, calculated using **Michelon** contrast (Mean ± Standard Error).

| Spectacles | Far 1 | Near | Far 2 | $t^{\dagger}$ | $P^{\dagger}$ | $t^{※}$ | $P^{※}$ |
|---|---|---|---|---|---|---|---|
| SVG | 0.799±0.02 | 0.825±0.019 | 0.808±0.021 | -1.62 | 0.130 | -0.68 | 0.51 |
| DM0 | 0.833±0.016 | 0.84±0.018 | 0.815±0.02 | -0.51 | 0.62 | 1.18 | 0.259 |
| DM1 | 0.755±0.026 | 0.74±0.028 | 0.737±0.027 | 0.63 | 0.535 | 0.91 | 0.382 |
| ST0 | 0.777±0.022 | 0.8±0.018 | 0.763±0.023 | -1.62 | 0.132 | 0.95 | 0.36 |
| ST1 | 0.661±0.033 | 0.654±0.032 | 0.669±0.033 | 0.22 | 0.832 | -0.49 | 0.63 |
| MP0 | 0.808±0.023 | 0.81±0.024 | 0.804±0.304 | -0.17 | 0.866 | 0.24 | 0.811 |
| MP1 | 0.747±0.018 | 0.738±0.021 | 0.748±0.034 | 0.34 | 0.742 | -0.06 | 0.954 |

A paired t-test was used to compare the differences between relaxed accommodation (Far 1) and near accommodation (Near), as well as the differences in relaxed accommodation between the beginning (Far 1) and the end (Far 2) of the measurement.

$t^{\dagger}$ and $P^{\dagger}$: The statistics for Far 1 vs Near, $t^{\dagger}$ and $P^{\dagger}$ refer to the t-statistic and significance level of the test results.

$t^{※}$ and $P^{※}$: The statistics for Far 1 vs Far 2, $t^{※}$ and $P^{※}$ refer to the t-statistic and significance level of the test results.

The labels SVG, DM0, DM1, ST0, ST1, MP0, and MP1 correspond to single vision glasses, centered MiYOSMART, decentered MiYOSMART, centered Stellest, decentered Stellest, centered MyoCare, and decentered MyoCare, respectively.

$^{*}$Indicate the P-value<0.05, and $^{**}$ means the P-value<0.01.

Table 5-3. Contrast values from the best-focus image under different accommodation conditions, calculated using **CV** contrast (Mean ± Standard Error).

| Spectacles | Far 1 | Near | Far 2 | $t^{\dagger}$ | $P^{\dagger}$ | $t^{※}$ | $P^{※}$ |
|---|---|---|---|---|---|---|---|
| SVG | 0.598±0.058 | 0.623±0.045 | 0.599±0.044 | -0.57 | 0.582 | -0.04 | 0.966 |
| DM0 | 0.592±0.043 | 0.616±0.042 | 0.575±0.047 | -0.81 | 0.434 | 0.78 | 0.453 |
| DM1 | 0.471±0.047 | 0.45±0.047 | 0.436±0.043 | 0.62 | 0.549 | 1.28 | 0.223 |
| ST0 | 0.529±0.051 | 0.55±0.043 | 0.508±0.049 | -0.63 | 0.54 | 0.93 | 0.372 |
| ST1 | 0.352±0.034 | 0.359±0.043 | 0.36±0.035 | -0.18 | 0.859 | -0.48 | 0.646 |
| MP0 | 0.557±0.052 | 0.563±0.05 | 0.556±0.057 | -0.2 | 0.844 | 0.05 | 0.963 |
| MP1 | 0.402±0.029 | 0.395±0.029 | 0.423±0.056 | 0.22 | 0.829 | -0.40 | 0.694 |

A paired t-test was used to compare the differences between relaxed accommodation (Far 1) and near accommodation (Near), as well as the differences in relaxed accommodation between the beginning (Far 1) and the end (Far 2) of the measurement.

$t^{\dagger}$ and $P^{\dagger}$: The statistics for Far 1 vs Near, $t^{\dagger}$ and $P^{\dagger}$ refer to the t-statistic and significance level of the test results.

$t^{※}$ and $P^{※}$: The statistics for Far 1 vs Far 2, $t^{※}$ and $P^{※}$ refer to the t-statistic and significance level of the test results.

The labels SVG, DM0, DM1, ST0, ST1, MP0, and MP1 correspond to single vision glasses, centered MiYOSMART, decentered MiYOSMART, centered Stellest, decentered Stellest, centered MyoCare, and decentered MyoCare, respectively.

$^{*}$Indicate the P-value<0.05, and $^{**}$ means the P-value<0.01.

RMS contrast results revealed significant differences between relaxed and near accommodation in most experimental conditions. However, Michelson contrast and CV contrast did not show any significant differences under any conditions, whether comparing Far 1 vs Near or Far 1 vs Far 2. For the comparison between Far 1 and Far 2, only RMS contrast demonstrated significant differences in MP0 and MP1 (centered and decentered MyoCare spectacles). Similar statistical results were observed for Michelson contrast and CV contrast.

A more sensitive formula can detect subtle changes in image contrast, which could be beneficial for comparisons in certain cases. To illustrate this, table 5-4 showing the variation in describing image contrast is presented below.

Table 5-4. The coefficient of variation (CV) describing the variability of formulas (Mean ± SD)

| Formulas | Far 1 | Near | Far 2 |
|---|---|---|---|
| RMS contrast | 0.416 ± 0.147 | 0.437 ± 0.129 | 0.467 ± 0.132 |
| Michelson contrast | 0.105 ± 0.049 | 0.104 ± 0.048 | 0.106 ± 0.051 |
| CV contrast | 0.256 ± 0.09 | 0.262 ± 0.09 | 0.26 ± 0.096 |
| The coefficient of variation was calculated for each subject for the variation among different spectacles for the three formulas. | | | |

The table results indicate that RMS contrast demonstrated maximum variability compared to Michelson contrast and CV contrast. The variation of the formula is similar between relaxed accommodation status and near accommodation stimulation. Michelson contrast shows minimal variation among the formulars.

The choice of visual field may affect the contrast value. Thus, the results from two different radius were generated to compare the difference (figure 5-5 for SVG, figure 5-6 for myopia control lenses).

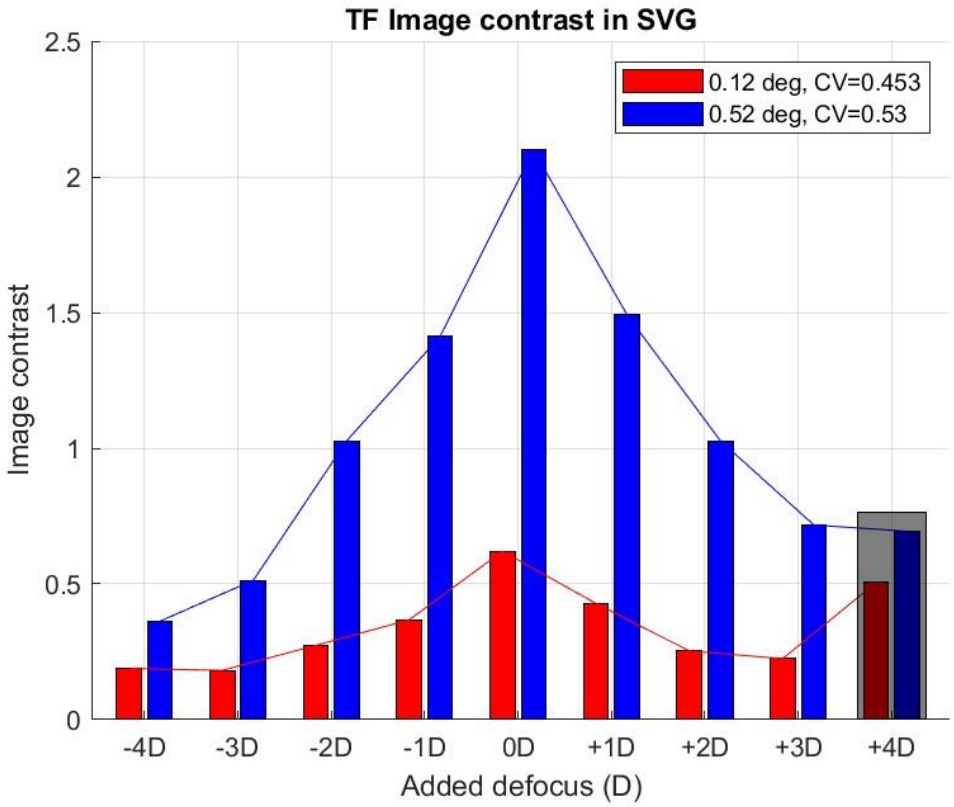


Figure 5-5. Through-focus image contrast calculated using the CV formula. Results were obtained with a radius of 30 pixels (0.12 degrees VF, blue bars) and 128 pixels (0.52 degrees VF, red bars). The CV values in the figure legend represent the variation of TF contrast within the analyzed region. The tops of the bars (mean values) are connected to show the trend of contrast across TF images. The bar at the +4D position is masked with a black rectangle due to an unavoidable internal reflection detected in that defocus range, making the data unreliable. The best-focus image was calculated when subjects were looking at a distant target.

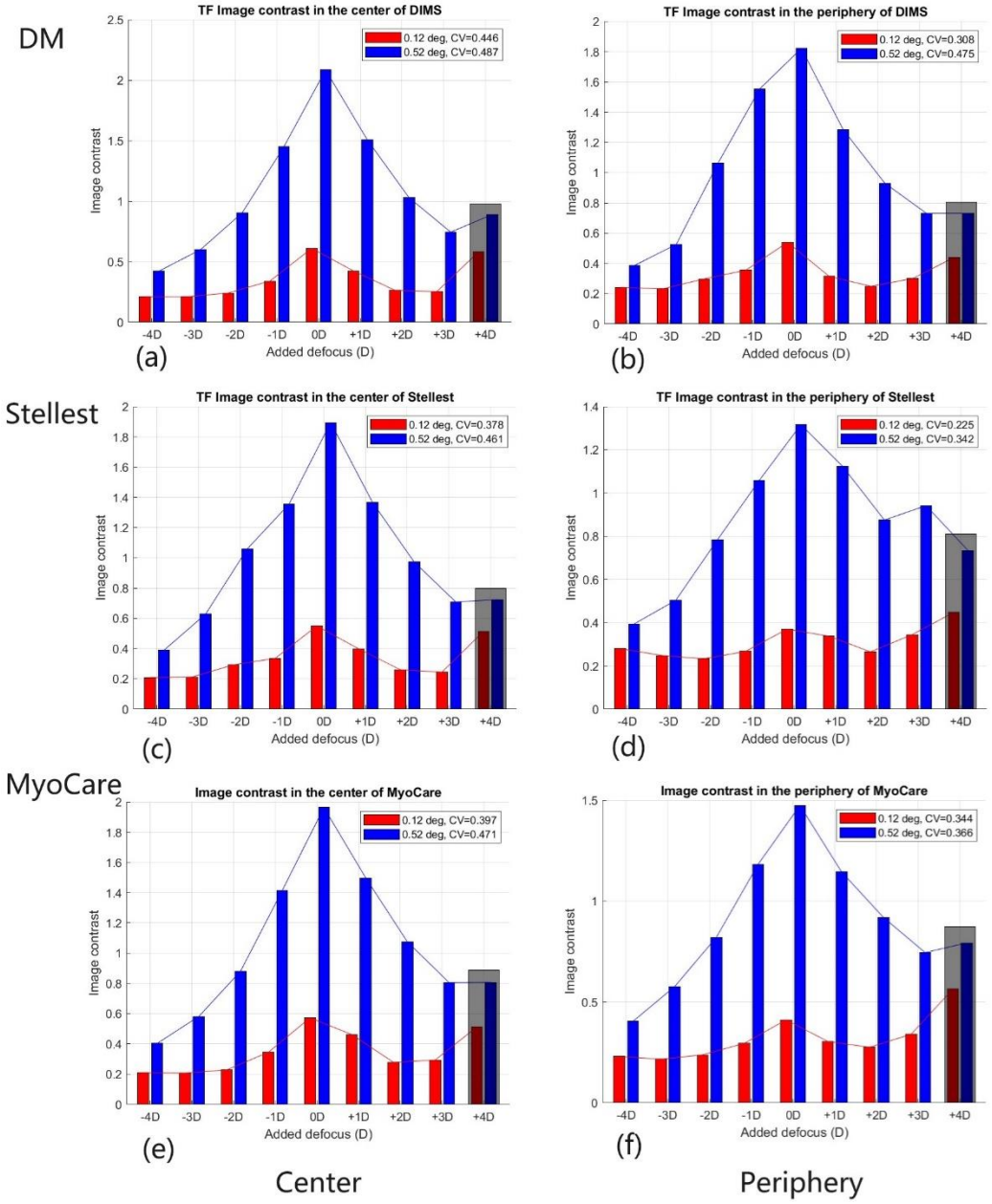


Figure 5-6. Through-focus image contrast calculated using the CV formula. Subgraphs (a), (c), and (e) are the results from well-centered DIMS, Stellest, and MyoCare, respectively, while subgraphs (b), (d), and (f) display the results from decentered DIMS, Stellest, and MyoCare, respectively. Results were obtained with a radius of 30 pixels (0.12 degrees VF, blue bars) and 128 pixels (0.52 degrees VF, red bars). The CV values in the figure legend represent the variation of TF contrast within the analyzed region. The tops of the bars (mean values) are connected to show the trend of contrast across

TF images. The bar at the +4D position is masked with a black rectangle due to an unavoidable internal reflection detected in that defocus range, making the data unreliable. The best-focus image was calculated when subjects were looking at a distant target.

### 5.3.2 Contrast calculations

The comparison of TF image contrast is important to understand the optical mechanisms of various myopia control lenses. As presented in figure 5-7, single vision glasses provided the highest retinal image contrast compared to other spectacles. Contrast values consistently decreased as the absolute defocus increased (though the contrast value at +4D for ST1 appeared to increase, the high variability makes these results questionable). The contrast curve in the through-focus images is generally symmetrical around the best-focus value for all experimental conditions.

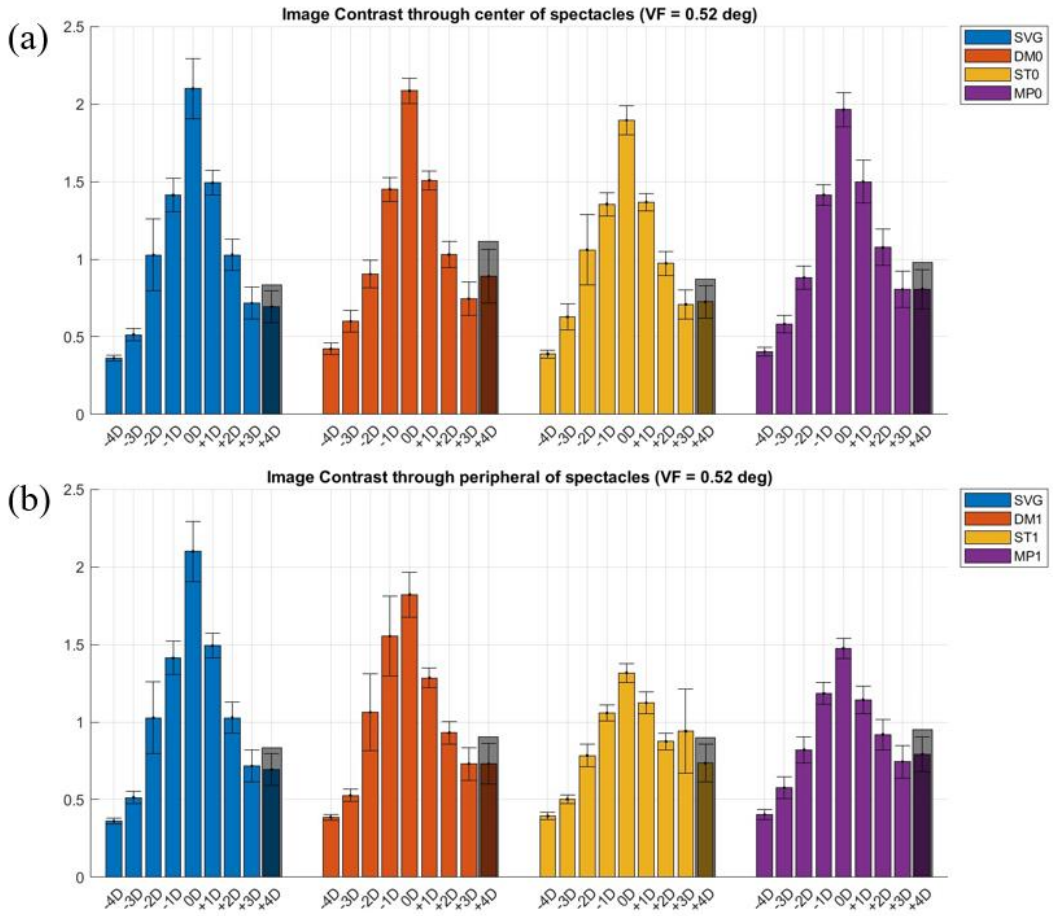


Figure 5-7. Comparison of through-focus image contrast between spectacles. Contrast was calculated using the CV formula with a radius of 128 pixels (0.52 degrees VF). The bar at the +4D position is masked with a black rectangle due to an unavoidable internal reflection detected in that defocus range, making the data unreliable. The best-focus image was obtained when subjects were looking at a distant target. The labels SVG, DM0, DM1, ST0, ST1, MP0, and MP1 represent single vision glasses, centered MiYOSMART, decentered MiYOSMART, centered Stellest, decentered Stellest, centered MyoCare, and decentered MyoCare, respectively.

As the contrast curves are symmetrical among different lenses in through-focus images, the value at the peak of the curve, which also represents the best focus image, may be representative to the lens. Thus, A One-Way ANOVA test was applied to compare the difference among different experimental conditions for the best focus image. The

descriptive results are presented in figure 5-8 and the statistics are summarized in table 5-3. In general, decentered Stellest shows the lowest contrast value compared to MyoCare, DIMS, and SVG. Furthermore, the comparison between well centered lens and decentered lens indicates that, as expected, significant differences were found in Stellest and MyoCare. Nevertheless, a non-significant difference was found in DIMS (table 5-7).

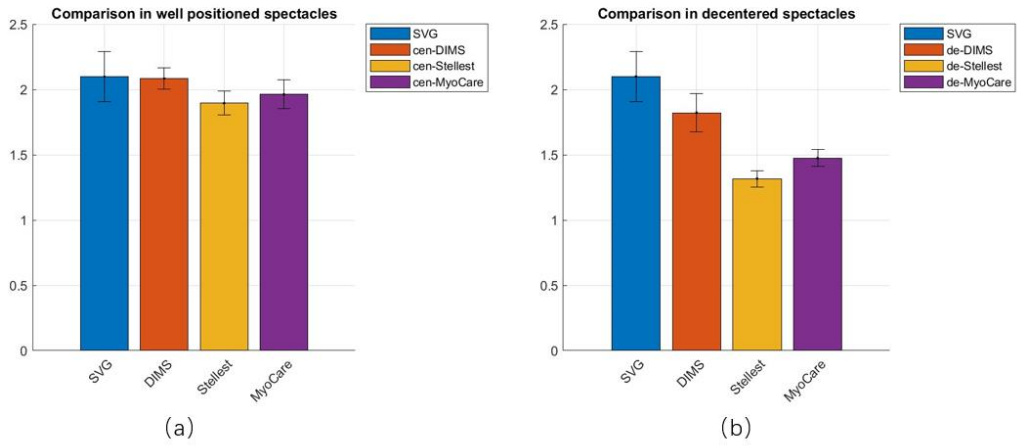


Figure 5-8. Contrast of best focus image in myopia control spectacles. The best focus value was calculated when subject was looking at distant target. (a) The comparison in well positioned spectacles. (b) The comparison in decentered spectacles. The prefix cen-/de- represent well positioned, or decentered spectacles.

Table 5-5. One-way ANOVA test for the comparison of image contrast in well positioned lenses (Mean±Standard error)

| SVG | cen-DIMS | cen-Stellest | Cen-MyoCare | F | P |
|---|---|---|---|---|---|
| 2.1±0.19 | 2.08±0.08 | 1.89±0.09 | 1.96±0.11 | 0.596 | 0.620 |
| Post-hoc comparison:<br>Not applicable | | | | | |

Table 5-6. One-way ANOVA test for the comparison of image contrast in decentered lenses (Mean±Standard error)

| de-DIMS | de-Stellest | de-MyoCare | F | P |
|---|---|---|---|---|
| 1.82±0.15 | 1.32±0.06 | 1.47±0.06 | 6.879 | 0.03* |
| Post-hoc comparison:<br>DIMS vs Stellest, mean difference = 0.51, p = 0.003**<br>Stellest vs MyoCare, mean difference = -0.16, p = 0.796<br>DIMS vs MyoCare, mean difference = 0.34, p = 0.052 | | | | |

Table 5-7. Paired-t test for the comparison between centered position and decentered position

| | ci | t | P |
|---|---|---|---|
| Cen vs Dec (DM) | [-0.062, 0.588] | 1.7589 | 0.104 |
| Cen vs Dec (ST) | [0.365, 0.792] | 5.892 | <0.001 |
| Cen vs Dec (MY) | [0.286, 0.691] | 5.2541 | <0.001 |
| A paired t-test was used to compare the difference in image contrast between the center and the periphery of the spectacles. "Cen" and "Dec" indicate well-centered and slightly decentered spectacles, respectively. "DM," "ST," and "MC" refer to DIMS, Stellest, and MyoCare lenses. "ci" refers to the confidence interval for the mean difference, while "t" and "P" represent the t-statistic and significance level, respectively. | | | |

## 5.4 Discussion

The contrast of the retinal image can be an important concept for myopia research. High contrast means the image can be easily recognized. Conversely, low image contrast can cause blurring. Therefore, image contrast is essential for the human eye to detect the details of the world. In clinical practice, it was once common to prescribe glasses to prevent myopia, as they provide sharp, high-contrast images in the central fovea.

However, with advances in myopia control strategies, eye care professionals are increasingly opting for additional interventions such as low-dose atropine or peripheral defocus-based spectacles. In underdeveloped areas, like parts of Africa, single-vision prescription glasses remain the primary solution for myopia [31]. It is widely believed that the myopia control effect of these spectacles is due to modifications in peripheral retinal defocus. Several myopia control spectacles, such as DIMS, Stellest, and MyoCare, have been commercialized based on this theory. However, a newly developed myopia control lens, DOT [113], which uses diffractive technology, seems to challenge this peripheral defocus theory.

The DOT lens doesn't alter peripheral retinal refraction but reduces image contrast over a wide-angle field using microscopic diffusers on the lens surface. The CYPRESS clinical trial showed that, compared to a control group, DOT lenses significantly reduced axial length progression by up to 50% in the first year, and this effect was sustained throughout the 36-month follow-up period [113].

This significant myopia control efficacy raises an important question: Do peripheral defocus-based spectacles control myopia through the same mechanism as DOT lenses? To explore this, it's essential to first capture retinal images and then analyze the retinal contrast produced by different lenses. In this study, we used a double-pass instrument to capture through-focus PSF images from the retina, which provided a useful approach for studying retinal image contrast. A critical question arises before comparing contrast: How do we quantify image contrast on the retina? This question can be addressed by answering the questions:

1. Which formula would be appropriate to calculate contrast?
2. What is the recommended visual field size for contrast calculation?
3. Does accommodation affect the contrast of the best focus image on retina?

4. Which image from the through-focus series is the best option for contrast calculation?

To answer the first question, we first analyzed the differences in best focus image between near accommodation and relaxed accommodation, as well as the first-time relaxed accommodation and the second time relaxed accommodation (figure 5-4 and table 5-1) by using three formulars: RMS contrast, Michelon contrast, and CV contrast. The data showed that RMS contrast significantly differed between near and relaxed accommodation in most cases. However, Michelon contrast and CV contrast showed no significant differences in best focus images in any cases. This aligns with expectations from physical eye models when only axial length is altered to simulate accommodation. In human eye, astigmatism was primarily induced by cornea and crystalline lens, thus, we could expect a minor change of astigmatism during accommodation process (notice that larger astigmatism could induce reduction of image contrast). To valid data this issue, a paired-t test was analyzed to compare the difference in astigmatism between in near accommodation status (20 cm gaze distance with Open-view autorefractor WAM5500, Grand Seiko, Japen) and in relaxed accommodation status (Close-view Autorefractor KR800, Topcon, Japen), and non-significant result was found (The data was from Chapter 6 regarding the eye tracker with 15 adult subjects). Thus, there should be no difference between near accommodation and relaxed accommodation in the contrast of best focus images. The statistics from Michelon contrast and CV contrast align with this expectation. Thus, the results from Michelon contrast and CV contrast are likely more accurate.

As a similar performance was found between CV contrast and Michelon contrast, the next step would be to evaluate the sensitivity of the formula to evaluate the inter-group difference. For example, the ability to tell the difference among DIMS, Stellest and MyoCare. Here we used the metric CV, which uses the same calculation as CV contrast. The CV was calculated with data from different experimental conditions for each subject for their best focus images, and the results are presented in table 5-4. The higher

value indicates more variability, or more sensitivity of the formula. RMS contrast shows greatest variability/sensitivity of its capacity, likely because it's affected by absolute brightness. Michelson contrast shows smaller variations compared to CV contrast. This might be because Michelson contrast only considerate the maximum brightness and the minimum brightness. However, in figure 5-2 and figure 5-3, the PSF images clearly showed that the distribution pattern of the brightness is irregular across the field. CV contrast, which accounts for all pixels, could explain the higher CV value compared to Michelson contrast. In summary, RMS contrast exhibited too much variably, Michelson contrast is not as sensitive as CV contrast, therefore, it is recommended to use CV formula to describe the contrast of PSF images from double-pass instrument.

The size of the visual field to be analyzed is another important consideration. Figure 5-5 shows the results from two visual field sizes: 0.12 degrees and 0.52 degrees. The CV formular was applied again to compare the trend of contrast plots across TF images. We first compared the trend of TF contrast among different experimental conditions. When the image was de-focused, the contrast value also decreased, and the general trend is similar among different experimental conditions. However, an abnormal trend was found in +4D defocus. After checking the original PSF images, we confirmed that the issue was caused by the internal lens reflection of the instrument. Thus, the results from +4D are not trustable, and a black rectangular was masked with the bar of +4D in figure 5-5. The abnormal trend was not obvious when the visual field expanded to 0.52 degrees, which seems to minimize the error estimation caused by the reflection. The CV value, representing the variability of contrast across through-focus images, is higher in a larger visual field, indicating increased sensitivity to the field size. In summary, the results indicated that a larger visual field provides more reliable data, as long as it remains within the sensor's available area.

For the final question—Which image from the series of through-focus images is the best option to calculate contrast? As figure 5-7 proved that the general trend of contrast

plot is always similar across different experimental conditions, and the best focus image always demonstrates highest contrast value in through focus images, therefore, the contrast of the best-focus image is used to compare different conditions (Figure 5-8, Table 5-3).

Based on the known importance of image contrast in central vision and peripheral retina for myopia treatment, it's beneficial for myopia control spectacles to provide high contrast in the center and lower contrast in the periphery. A one-way ANOVA (table 5-5) showed no significant difference in central image sharpness between the myopia control spectacles and single-vision glasses. However, in the periphery, Stellest lenses exhibited significantly lower contrast than DIMS (mean difference = 0.51, p=0.003), and MyoCare also showed a trend toward lower contrast compared to DIMS (table 5-6). No significant difference was found between Stellest and MyoCare. A paired t-test revealed significant differences between the centered and decentered positions of Stellest and MyoCare lenses, but not for DIMS. This could be a false negative result due to the relatively high variability of data or small simple size. The difference between centered position and decentered position in Stellest or MyoCare are significant, which is easy to expect before running the test.

Finally, regarding the comparison between myopia control efficacy and the reduction of retinal contrast among those three myopia control spectacles: DIMS lens showed highest image contrast (less contrast reduction), followed by MyoCare, and finally Stellest (lowest contrast). However, the myopia control effectiveness of these lenses did not follow this order. For example, the efficacy for refractive control in DIMS [152], MyoCare [153], and Stellest [76] are 50%, 21% and 74%, respectively, and the axial length progression rate are 60%, 23% and 50%, respectively, based on the published data. A higher value indicates better treatment effect. While these results should be interpreted with caution due to different study populations, but at least, it suggests that the image contrast should not be the sole factor influencing the myopia control

mechanism of these spectacles. A supplementary experiment was conducted by the current double-pass instrument with an emmetropic artificial eye showing the curve of contrast from through-focus images (figure 5-9).

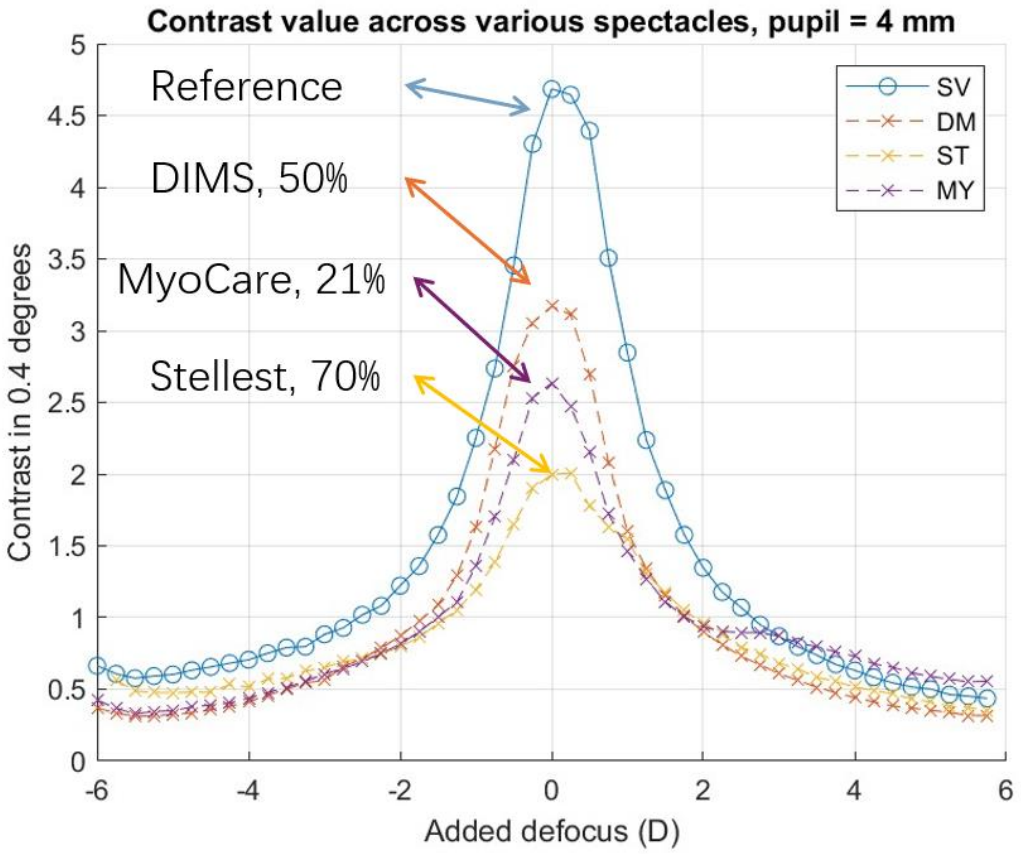


Figure 5-9. The contrast value of through-focus images from an emmetropic artificial eye with various spectacles. SV, DM, ST and MY refer to single vision glasses, DIMS, Stellest and MyoCare. The numbers nearby the plots show the myopia control efficacy in refractive change in 1-year based on the clinical studies. The evaluation of contrast in myopia control spectacles was conducted in decentered lenses.

What could be the confounding optical factor that explains the clinical treatment discrepancies among these myopia control spectacles, beyond defocus and contrast? One hypothesis is astigmatism. As shown in figure 5-10, the best-focus image from a horizontally displaced lens exhibits a power distribution resembling a shell with its long

axis oriented horizontally. In the corresponding eccentricity of the human eye, the cylindrical power defocuses the image along the horizontal axis but with a negative sign. Consequently, peripheral retinal astigmatism may be partially compensated with MyoCare lenses, reducing the image-blurring effect and potentially weakening the myopia control efficacy. A simple way to validate this hypothesis would be to either rotate the cylindrical axis of MyoCare or maintain the current axis while changing the positive refraction to negative. More experiments are needed to confirm this theory.

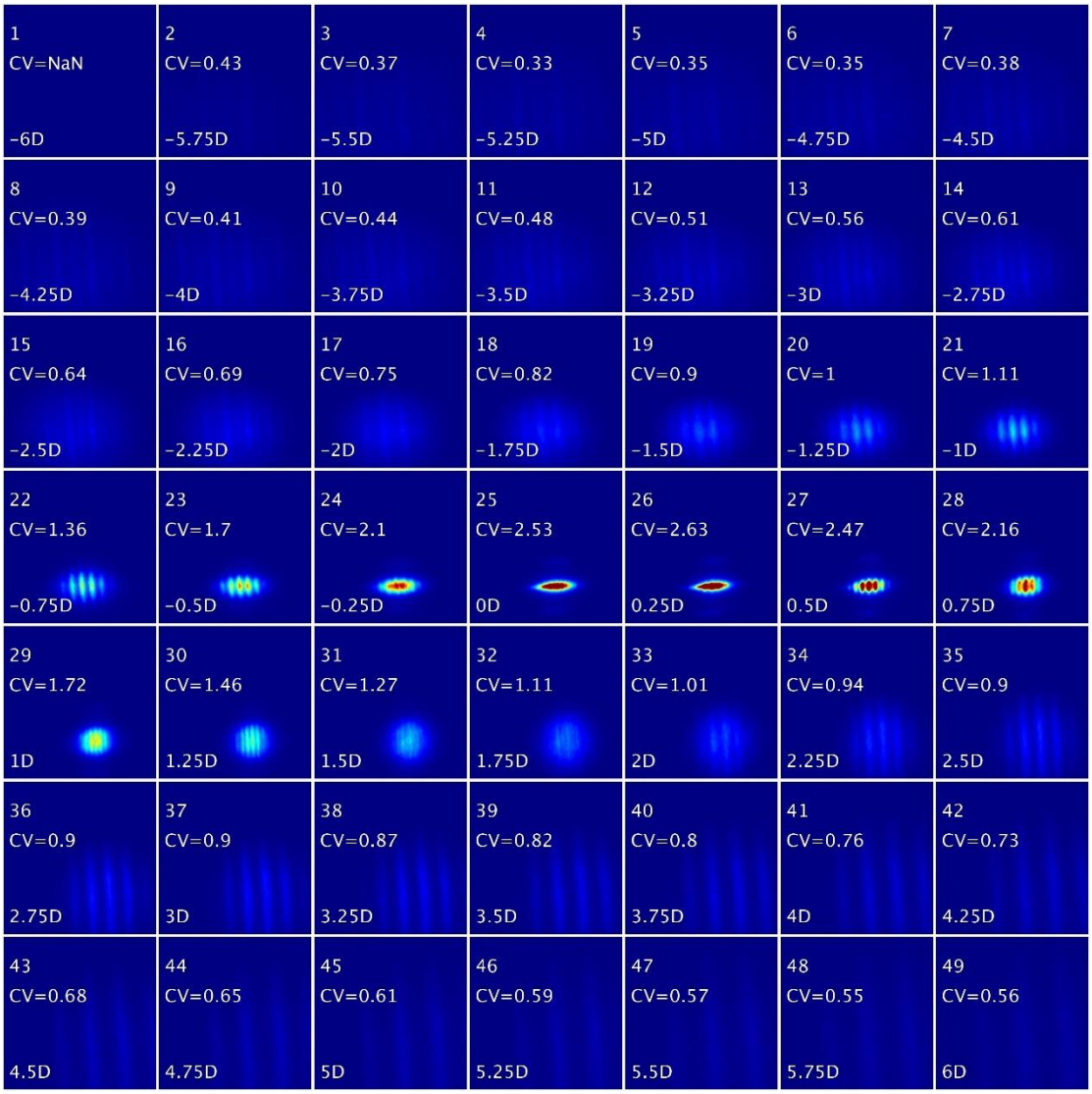


Figure 5-10. The through-focus images with MyoCare in an emmetropic artificial eye. The CV value indicates the contrast of image, and the number in the below-left corner represents the added defocus. The image was captured with a 4-mm aperture.

A cautious should be aware by the investigators that PSF image could be affected by the optical characteristics of a real eye, especially in peripheral retina. This may explain why we did not observe the classic defocus pattern of myopia control spectacles in the central field, as previous studies have shown (figure 5-11, Figures 5-2 and 5-3). Additionally, human peripheral refraction exhibits greater variability. Therefore, future custom-designed myopia control spectacles should consider peripheral refraction for improved treatment outcomes in myopia management.

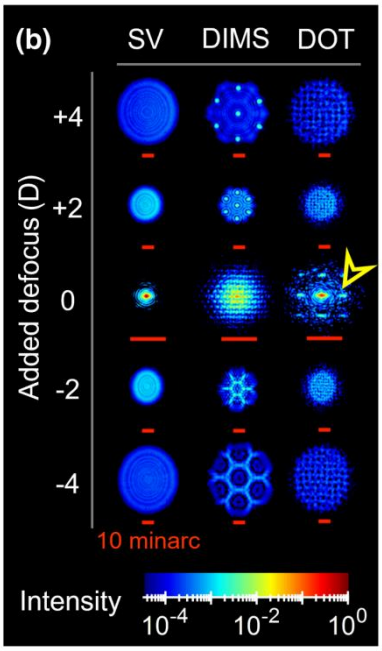


Figure 5-11. The first pass through-focus image of SV, DIMS and DOT lenses [150].

## 5.5 Conclusions

We analyzed retinal image contrast in wearers of different myopia control lenses using a double-pass instrument. The calculation procedure was extracted from multiple contrast formulas to ensure a reliable comparison and minimize the artifacts of stray light from the device. Our findings revealed that the ranking of contrast values among different lenses did not correspond to their reported myopia control efficacy in clinical trials. This suggests that additional optical factors, such as astigmatism or light scattering, may influence the effectiveness of myopia treatment. Therefore, neither

image contrast nor peripheral defocus alone is likely to be the sole determining factor in myopia management.

# Chapter 6. The development of a novel portable eye tracker

## 6.1. Introduction

Visual behavior is an important contributing factor to myopia progression. It is linked to accommodative lag, which ultimately leads to hyperopic defocus in peripheral retina and thereby promotes axial myopia. In chapter 3, we explored the evolution of peripheral refraction in a cohort of children for two years, and we found that the relatively myopic defocus in superior retina is a risk factor for myopia development. We proposed a hypothesis that the relatively myopic defocus is a consequence of looking-down visual behavior that mostly happened in near work activities such as reading.

To verify this hypothesis, a wearable device is required to accurately record visual behavior, particularly gaze distance. However, to the best of our knowledge, no existing device is capable of directly measuring gaze distance; instead, available technologies primarily assess facing distance based on head orientation. To bridge this gap, we developed a wearable eye tracker designed to provide precise estimations of gaze distance. In this chapter we evaluated the performance of the eye tracker under both central and eccentric viewing conditions, aiming to establish it as a robust tool for future visual behavior research that linked to the superior retinal myopic defocus. Additionally, we examine various visual functions to investigate their potential influence on the performance of gaze distance-based measurement devices.

## 6.2. Methods

### 6.2.1. Subjects

The experiment was conducted at the Aier Eye Hospital Groups in Changsha, China from March 2024 to October 2024 with an initial enrollment of 20 adult participants from Aier Hospital. The inclusion criteria for recruiting subjects: 1). Best corrected visual acuity >1.0 (decimal). 2). Normal visual function. 3). Good compliance with the experiment. 4). Generally good health status.

Before proceeding to the gaze distance examination, participants were required to undergo a series of basic ophthalmic tests. This included objective refraction and interpupillary distance measurements (Topcon KR800, Japan), subjective refraction (Phoropter), eye position assessment (Maddox Rod Test), accommodation amplitude and near point of convergence (Push Up Test), and accommodative lag measurement (WAM5500, Grand Seiko, Japan). Accommodative lag was measured at three distances: 20 cm, 25 cm, and 33 cm. After completing the preliminary tests, participants were fitted with a customized eye tracker, and the experimental protocol was explained to them by the practitioner. The ethical review was approved by Changsha Aier Eye Hospital (KYPJ040). Trial lenses were inserted into the eye tracker based on each participant's prescription from the phoropter. Visual acuity was verified once more prior to the gaze test to ensure optimal visual quality during the experiment.

After data inspection, 4 subjects were excluded from the analysis due to unstable soft issues. Thus, 16 subjects were included in the final data analysis. The demographic data is summarized in table 6-1 and table 6-2.

Table 6-1. Demographics of general data (N=16; M ± SD)

| | |
|---|---|
| Gender | 11 females, 5 males |
| Interpupillary distance (mm) | 62.7 ± 3.4 |
| Age (years) | 28.3 ± 4.6 |
| Near point of convergence (cm) | 7.2 ± 2.2 |
| Accommodation amplitude – OD (D) | 16.8 ± 3.5 |
| Accommodation amplitude - OS (D) | 16.9 ± 3.3 |
| Accommodation amplitude - OU (D) | 16.9 ± 3.2 |
| Eye position – near (Δ) | -1.3 ± 8.6 |
| Eye position – far (Δ) | 0.2 ± 2.9 |

Table 6-2. Demographics of refractive data (N=16; M ± SD)

| | Sphere (D) | Cylinder power (D) | SER |
|---|---|---|---|
| ObjR-OD | -3.2 ± 2.7 | -0.8 ± 0.8 | -3.6 ± 2.9 |
| ObjR-OS | -3.0 ± 2.7 | -1.0 ± 0.8 | -3.5 ± 2.8 |
| SubR-OD | -3.2 ± 2.7 | -0.7 ± 0.8 | -3.6 ± 2.9 |
| SubR-OS | -2.9 ± 2.6 | -0.8 ± 0.8 | -3.3 ± 2.8 |
| ACC 33 | -1.9 ± 0.5 | -0.7 ± 0.6 | -2.3 ± 0.5 |
| ACC 25 | -2.8 ± 0.4 | -0.7 ± 0.7 | -3.2 ± 0.5 |
| ACC 20 | 3.7 ± 0.5 | -0.9 ± 0.7 | -4.1 ± 0.5 |
| The refractive data from autorefractor or phoropter. ObjR – Objective refraction; SubR – Subjective refraction; OD - right eye; OS – left eye; ACC 33, ACC 25 and ACC 20 represent accommodation response of right eye for targets at 33 cm, 25cm and 20 cm, respectively (Open View autorefractor WAM 5500). | | | |

6.2.2. Data Analysis

1. Accuracy of the instrument in the three directions (±25˚ and 0˚)

The mean and standard deviation of measurements for each preset distance (0.5D, 1D, 2D, 3D, 4D, 5D, and 6.7D), along with measurement bias (measured value – standard distance), were calculated for descriptive analysis. A general linear model with repeated measures was applied to assess inter- and intra-group differences, as well as trends in bias relative to the standard values (SPSS statistics, IBM Corp, NY, USA). This model also evaluated variations across different directions and preset distances.

2. Repeatability of the instrument

A Bland-Altman plot was used to visualize the repeatability of the instrument across two separate measurements in three directions. Additionally, an intraclass correlation coefficient (ICC) analysis was conducted to assess overall measurement consistency.

3. Post-calibration of gaze distance

Given the common occurrence of convergence lag in the human eye, gaze distance measurements may be overestimated. However, with the experimental setup described in Chapter 2, accuracy can be improved using known distances of the preset targets. To quantify this improvement, we applied a simple linear fitting between measured and reference distances to assess the effectiveness of the post-calibration method.

4. Correlation between estimated gaze distance and accommodation response

Theoretically, there should be a strong correlation between the measured dioptric gaze distance and the accommodation response. However, the results can be affected by error estimation of the device, lag of convergence and lag of accommodation. To explore this, we collected accommodation response data using a commercialized open-view autorefractor and performed a correlation analysis to assess the relationship between dioptric distance and directly measured accommodation response. This analysis was repeated using the calibrated measurements.

5. Correlation between visual function metrics and device performance

Visual dysfunction could be a confounding factor affecting the instrument's accuracy in estimating gaze distance. Therefore, we conducted visual function tests, including eye position, accommodation amplitude, and near point of convergence. A correlation analysis was performed to determine whether there is a significant relationship between the lag in gaze distance (reference - measured value) at far (near stimulation = -0.5D) and near distance (near stimulation = -6.7D).

## 6.3. Results

### 6.3.1. Examples of plots of estimated gaze distance

To demonstrate how the device works, a few examples with estimated gaze distance and reference lines are presented in figure 6-1.

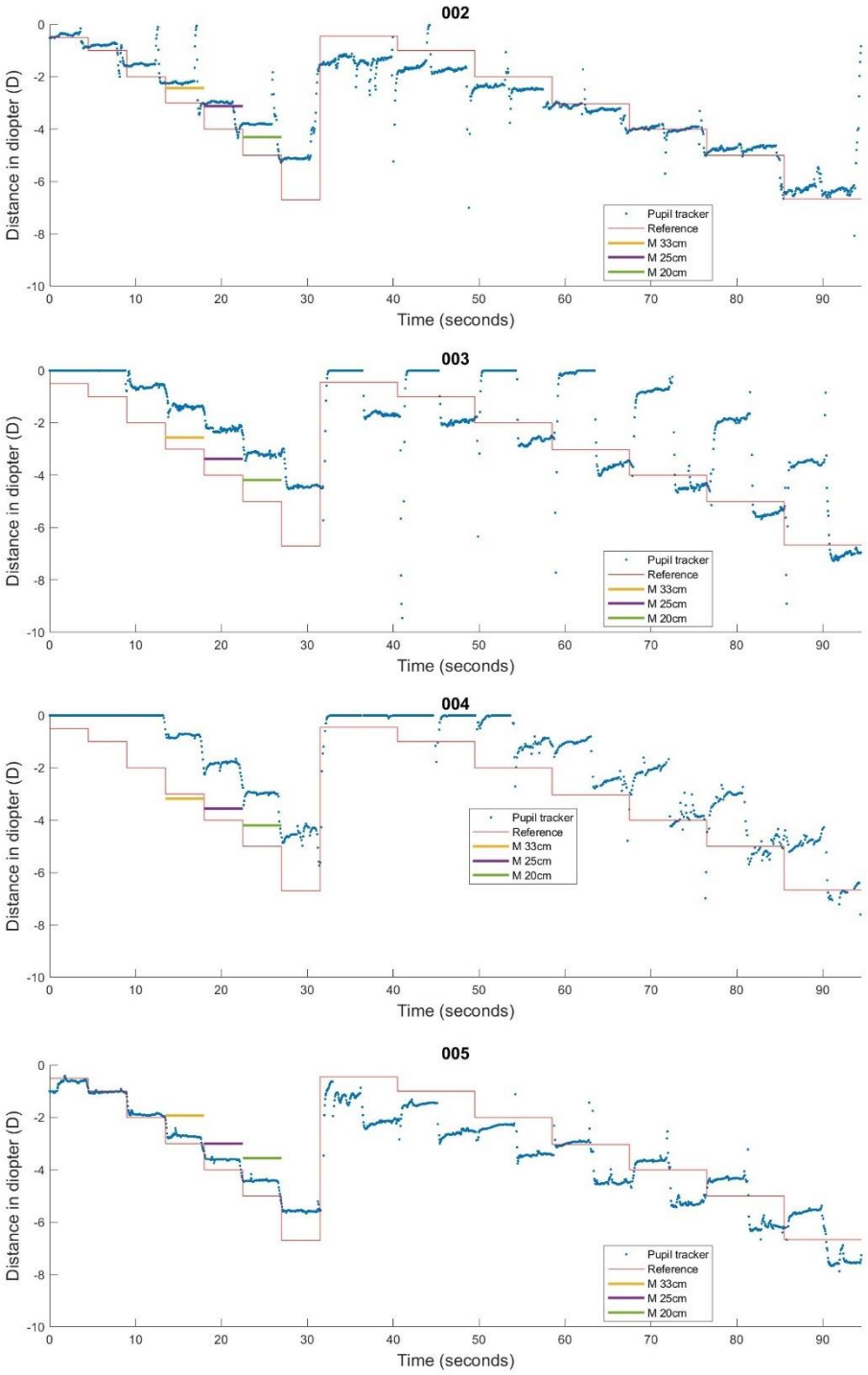


Figure 6-1. Examples of the recorded gaze distances from subjects 002, 003, 004, and 005. The x-axis represents time in seconds, while the y-axis indicates the dioptric gaze distance. The red line represents the preset distance from the targets to the midpoint between the pupils. The blue dots show the recorded gaze distances for each subject. The horizontal bars in yellow, purple, and green correspond to the measured

accommodation responses at 33 cm, 25 cm, and 20 cm, respectively, as measured by the Open View autorefractor WAM5500. The plots are constrained to the time frame of the experiment.

6.3.2. Evaluation of the accuracy of the instrument

Figure 6-2 shows the general trend of estimated gaze distance in the three directions. In central direction, the measure bias reflects the lag of convergence with approach of near targets. In peripheral directions, the plot shows different trends compared to central direction and exhibits asymmetric pattern between left and right directions. Specifically, the results from the right targets are closer to reference for mean value but with greater variability. The results from the left targets display a flatter inclination, indicating minimal change as the near targets approach.

The correlation between reference and estimated gaze distance are presented in figure 6-3. For central, left and right directions, the correlation values are 0.94, 0.41, 0.77. All p-values are < 0.001.

The exact values of mean bias from each preset target are summarized in table 6-3 and the 95% confidence interval (95CI) is presented as shaded plots in figure 6-4.

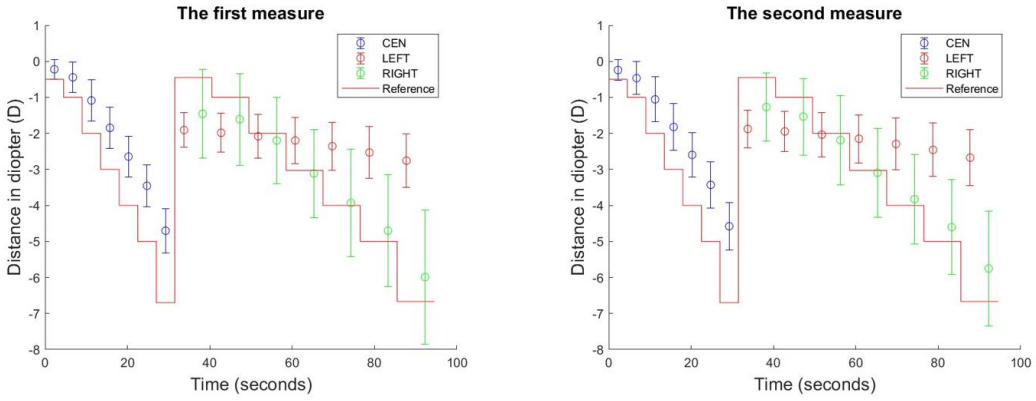


Figure 6-2. Mean and standard deviation of the average samples from each period. The measurements taken from the central portion of each period (the middle 3.5 seconds of

the 4.5-second period) were averaged to generate representative data. The mean and standard deviation of these values were then used to create the plots for both the first and second measurements. Blue, red, and green circles and error bars represent the results for the central (on-axis), left (nasal 25 degrees), and right (temporal 25 degrees) targets, respectively. The left plot shows the results from the first measurement, while the second measurement was conducted 5 minutes later.

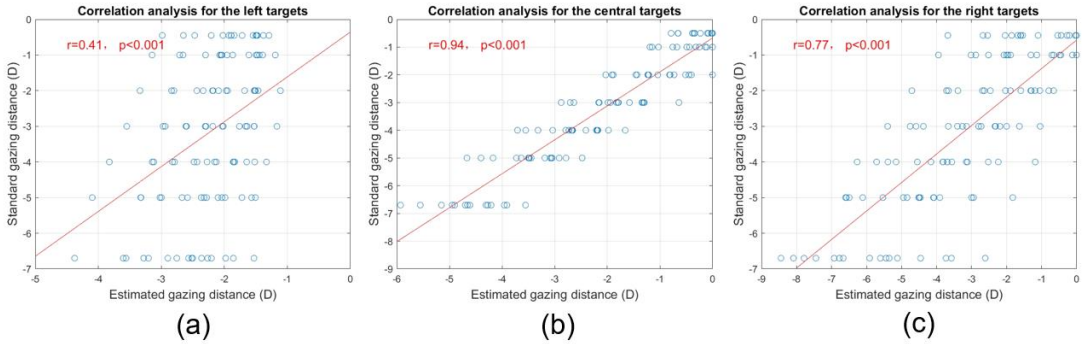


Figure 6-3.Correlation analysis for estimated dioptric gaze distance and standard distance for the left (a), central (b) and right (c) targets.

Table 6-3. The bias of estimated gaze distance at each preset distance (D)

| | Left | Central | Right |
|---|---|---|---|
| 0.5 D / 2 m | -1.44 | 0.27 | -0.91 |
| 1 D / 1 m | -0.97 | 0.54 | -0.57 |
| 2 D / 0.5 m | -0.06 | 0.93 | -0.19 |
| 3 D / 0.33 m | 0.83 | 1.16 | -0.1 |
| 4 D / 0.25 m | 1.67 | 1.38 | 0.12 |
| 5 D / 0.20 m | 2.51 | 1.56 | 0.35 |
| 6.7 D / 0.15 m | 3.98 | 2.06 | 0.83 |
| The bias of estimated gaze distance was calculated by (measured value – preset value). Thus, positive results indicate more hyperopia of the instrument (overestimate distance), whereas negative results represent more myopia of the instrument | | | |

(underestimate distance). The results from the two measured were combined in the table.

For the general trend of measure bias in all directions, a repeated measures ANOVA was conducted in SPSS, with preset distances as the between-subjects factor and target directions as the within-subjects variance. The results are summarized in table S10 (appendix). Overall, there was a significant difference in measurement bias across various distances (Table S10C, $F=479.573$, $P<0.0001$) and directions (Table S10A, $F=8.989$, $P<0.001$). Additionally, a significant trend was observed in the measured values across different distances for various fitting orders (Table S10D). The interaction between distance and direction was also significant (Table S10C, $F=94.222$, $P<0.001$). Greenhouse-Geisser correction was applied, as the sphericity test indicated non-significance (Table S10B, W-value=0.000, $P<0.0001$).

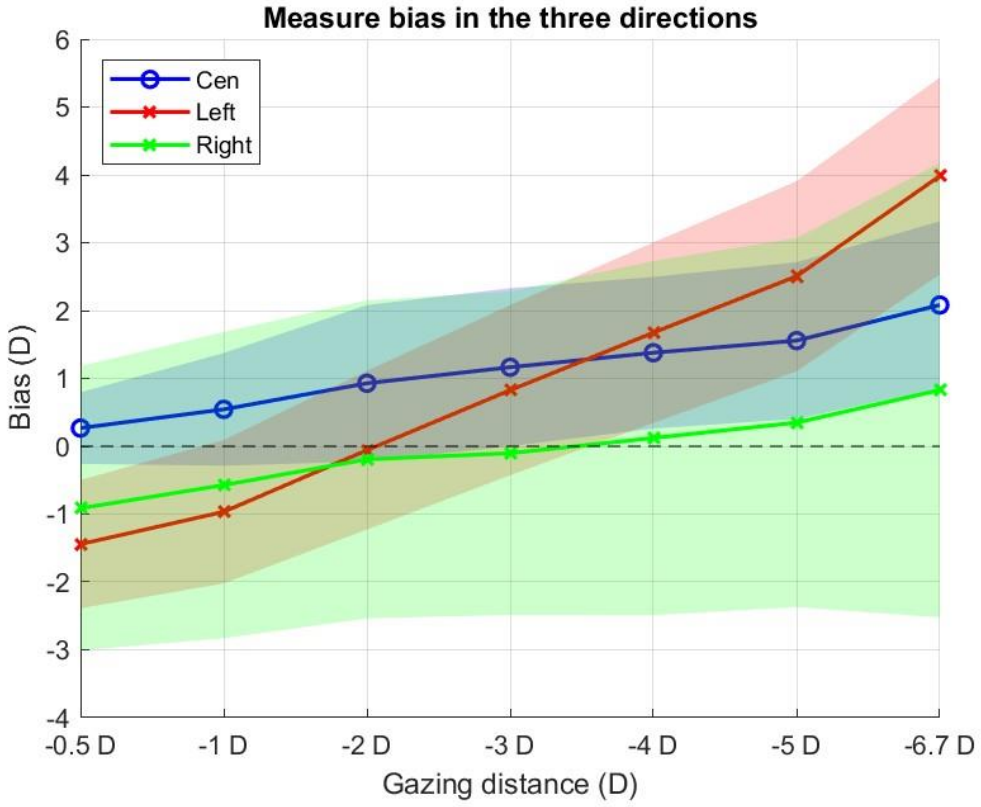


Figure 6-4. Measure bias of gaze distance in the three directions. The blue, red and

green colored plots represent the means of measuring bias for the left, central, and right targets. The shaded areas correspond to the 95% confidence intervals for the measurement bias under each condition.

6.3.3. Repeatability of the instrument

The Bland-Altman plots in figure 6-5 demonstrate excellent consistency in the measurements for the left and central targets, with the 95CI of differences remaining within 0.5D and a mean bias close to 0D. However, the results for the right targets show less consistency compared to the central and left targets, with the 95CI expanding to ±1D.

Details about ICC values are summarized in table 6-4. The ICC value is relatively high across all directions. The mean ICC value is highest for the central targets, followed by the right targets, and then the left targets. However, the 95CI for the right targets shows twice the variability compared to the central and left targets.

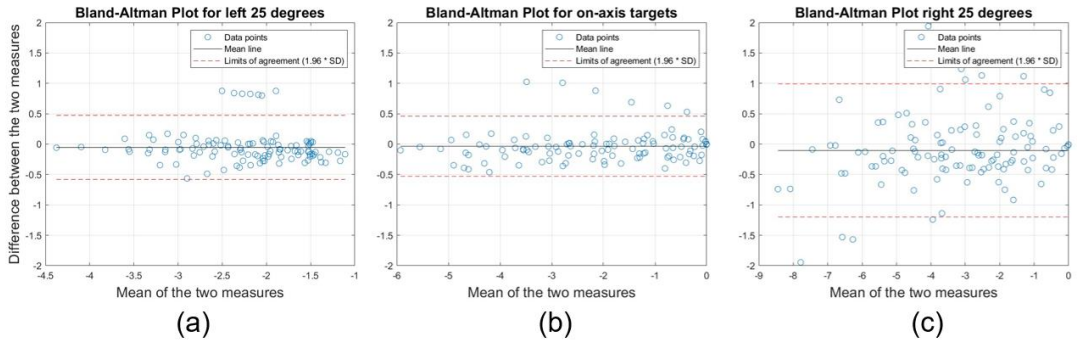


Figure 6-5. Bland-Altman plots for the repeatability of two measures in the three directions. Subgraph (a), (b) and (c) represent data from the targets at left (25 degrees), central, and right (25 degrees) directions, respectively.

Table 6-4. The consistency indicated by ICC value between two measures

| | Left targets | Central targets | Right targets |
|---|---|---|---|
| Mean Bias (D) | -0.05±0.27 | -0.05 ± 0.25 | -0.1 ± 0.56 |
| 95% CI of Bias (D) | [-0.58, 0.47] | [-0.53, 0.46] | [-1.20, 1.00] |
| ICC value | 0.92 | 0.99 | 0.96 |
| 95% CI of ICC value | [0.87, 0.95] | [0.98, 0.99] | [0.94, 0.97] |
| The ICC value was calculated using data from all distances for the left, central, and right targets. The bias was defined as the difference between the two measurements (measure 1 – measure 2). | | | |

6.3.4. Post-calibration based on the standard distance

Accommodation/convergence lag commonly exists in human eye [121, 154, 155]. Therefore, it is recommended to implement a calibration protocol for the instrument to improve gaze distance estimation accuracy. Given the well-calibrated experimental setup, where the distance between the targets and the subjects was precisely measured, we performed a linear calibration between the recorded gaze distance and the standard value. The choice of linear fitting was based on the results from the repeated measures ANOVA, where the F-value for linear fitting was the highest compared to other models (Table S10D).

In summary, data from the first measurement were used to generate a fitting function for each subject, which was then applied to the second measurement. This approach was deemed appropriate, as the instrument demonstrated good repeatability between the two sets of measurements.

A significant reduction in measurement bias was observed after calibration (Figure 6-6 and figure 6-7). Prior to calibration, measurement bias showed a noticeable trend of

increasing as distance decreased (ranging from 0.3D to 2.1D). After calibration, this trend disappeared, and the measurement bias remained consistently below 0.25D across all testing distances.

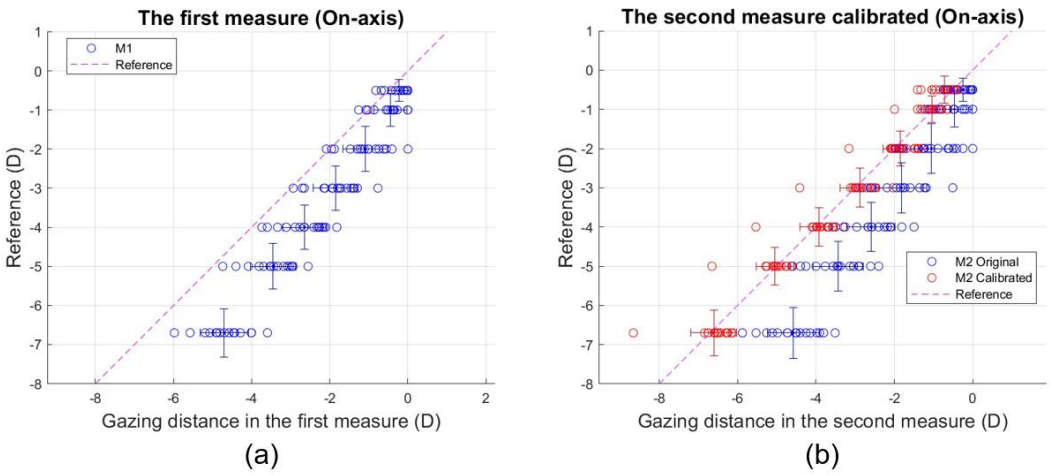


Figure 6-6. Measured gaze distance in diopters as a function of standard values set by experimental setup. (a) Shows the first measurement for all subjects (blue circular markers). (b) Displays both the second measurement (blue circular markers) and the calibrated second measurement (red circular markers). The error bars represent the standard deviation. The calibration of the second measurement was based on the linear fitting derived from the first measurement.

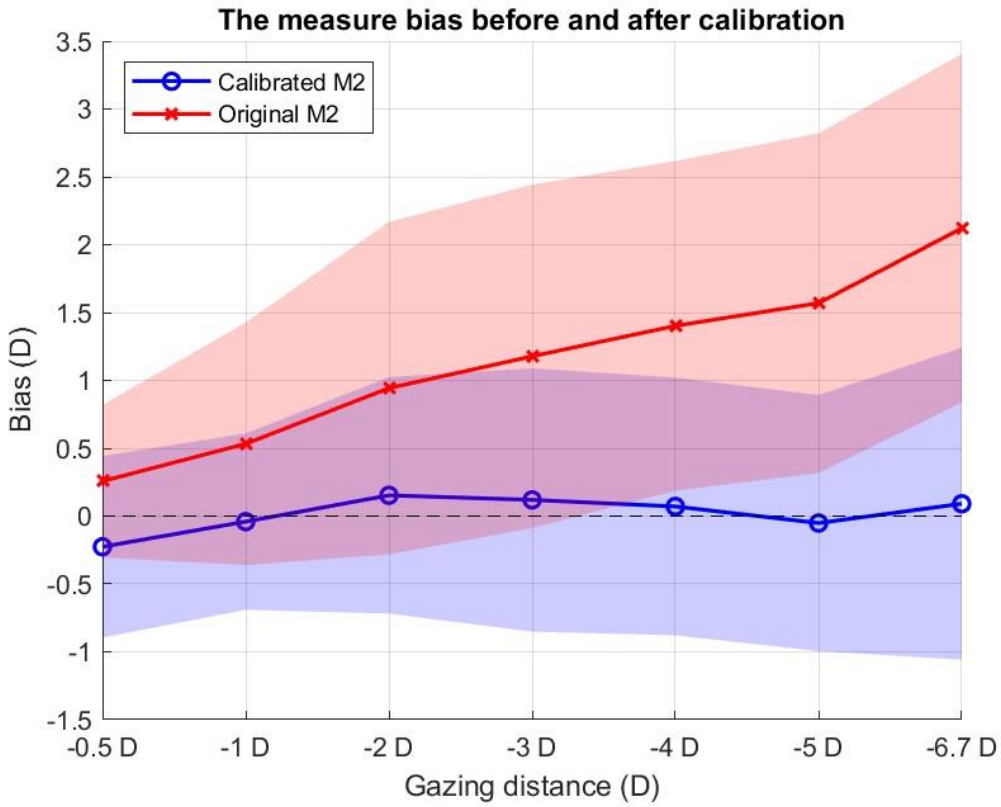


Figure 6-7. The measurement bias of the second measurement before (red) and after (blue) calibration. The shaded areas represent the 95% confidence intervals of the bias at each distance. The bias was calculated as the difference between the measured value and the standard value.

6.3.5. The relationship between accommodation response and convergence

Accommodation response is significantly associated with estimated gaze distance provided by the eye tracker ($R=0.34$, $p<0.001$, figure 6-8). After the linear calibration with reference, the correlation improved from 0.34 to 0.53 (coefficient of determination).

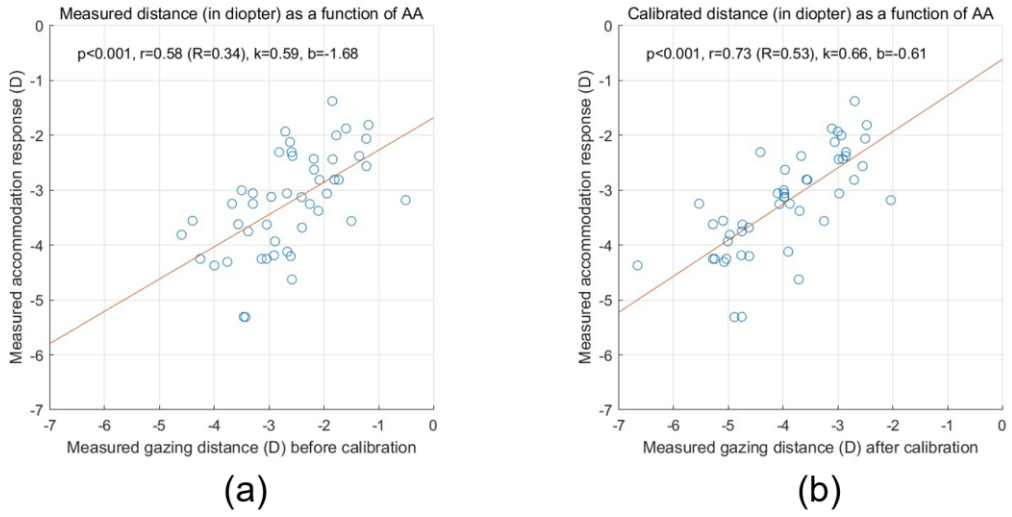


Figure 6-8. The relationship between estimated distance (in diopters) and accommodation response. (a) Shows the results using the original data, and (b) presents the results with calibrated data. The data corresponds to the second measurement from the eye tracker for each subject, while the accommodation response was measured using the WAM5500. The red line represents the fitted relationship between the two variables. The R-value, r-value, p-value, k-value, and b-value represent the coefficient of determination, correlation coefficient, significance, slope of the fit, and intercept of the fit, respectively. These values were calculated using Matlab.

6.3.6. The relationship between visual functions and measuring bias

The analysis of visual functions reveals a significant relationship between the error estimation of gaze distance and the near point of convergence (NPC) value. The correlation is even stronger when the subject is viewed through a near distance (figure 6-9).

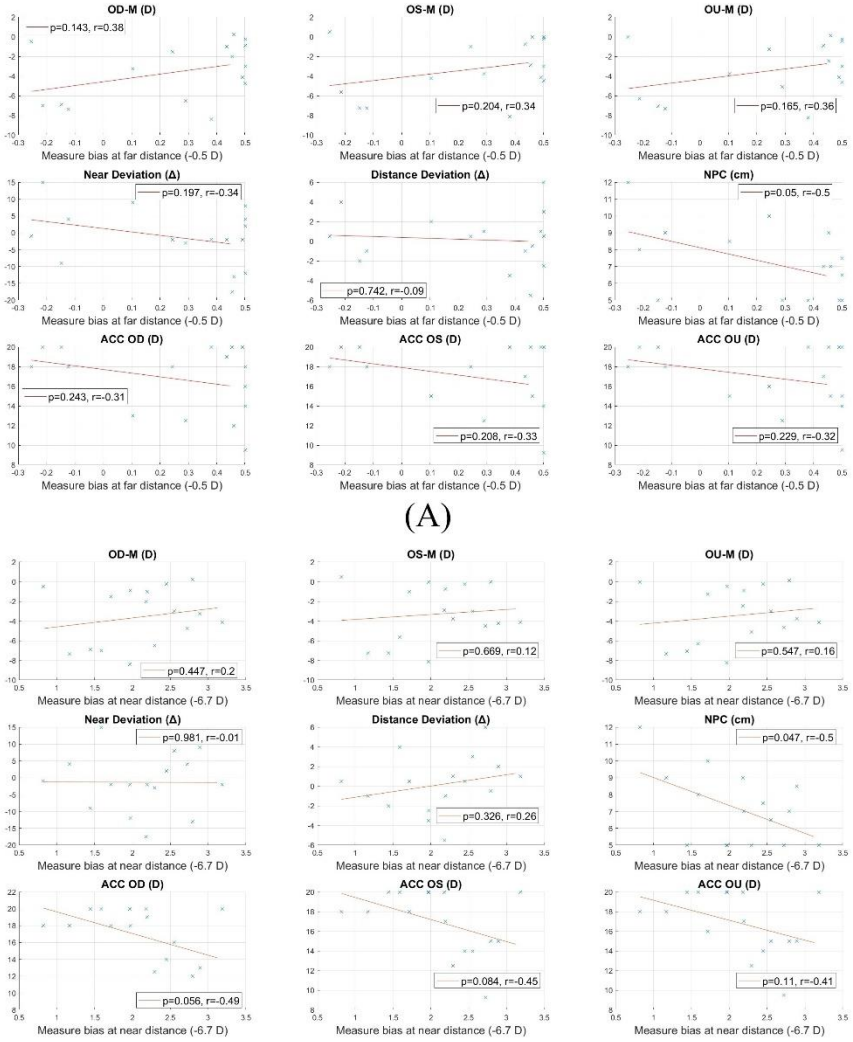


Figure 6-9. The error estimation of gaze distance (in diopters) as a function of potential confounding factors. The error estimation is labeled on the x-axis. The analysis was conducted for a distance of -0.5D (relatively far distance) in subgraph (A) and a distance of -6.7D (relatively near distance) in subgraph (B). The lag of GD was calculated as [measured value – standard value (in negative diopters)]. OS-M, OD-M, and OU-M represent the subjective refraction for the left eye, right eye, and the average of both eyes, respectively. NPC refers to the near point of convergence. ACC OD, ACC OS, and ACC OU indicate the amplitude of accommodation for the right eye, left eye, and both eyes, respectively.

6.3.7. Head rotation during the test

Given the asymmetric trend of measure bias, a retrospective examination was conducted on a video recording (only 1 subject has video recording). In figure 6-10, we can estimate the degree of head rotation caused by the asymmetric head position. The distance across the inside of the head-chin rest is approximately 208 mm, suggesting a head radius of about 104 mm. The prominent part of the eye tracker on the right side, indicated by the red arrow, corresponds to an extra length of 10 mm. This results in a head orientation bias of approximately 5.5 degrees. According to this hypothesis, the true angles for subjects with head rotation in the left, central, and right directions would be -30, -5, and +20 degrees, respectively.


Figure 6-10. The photo shows slightly rotation of head to the right side of the subject. (a) Photo was taken from the left side of the subject. (b) Photo was taken from the right side of the subject. The red arrow indicates the slightly difference on head orientation in left and right side.

## 6.4. Discussion

We developed a novel wearable eye tracker designed to record the subject's gaze distance. The calculation was based on simple geometric principles of the gaze triangle, using the positions of the two pupils and the gaze object. An experimental setup was constructed to verify the distance from the gaze object in central and peripheral directions at 25 degrees. We found a strong correlation and agreement between the standard distance and the estimated distance for the central targets ($r=0.94$, $p<0.001$, mean difference=-1.1±0.77D), but relatively lower correlation and agreement for the peripheral targets ($r=0.41$ for the left and $r=0.77$ for the right targets, p-values $<0.001$; mean differences=-0.9±1.9D and 0.1±1.4D for the left and right targets, respectively). A significant trend was observed between the estimated gaze distance and the progression of near targets (Table S10C, $F=479.573$, $p<0.001$), suggesting that error estimation can be reduced through simple calibration. The instrument demonstrated high repeatability across two measurements for all directions (ICC value=0.92, 0.99, 0.96 for the left, central, and right targets, respectively). Additionally, the true accommodation response was correlated with the estimated gaze distance ($R=0.34$, $p<0.001$). Measurement bias was found to be associated with the near point of convergence (NPC) visual function, with a stronger correlation observed when viewing closer distances.

Near visual behavior plays a critical role in myopia progression. However, previous instruments used to record visual distance have been based solely on head orientation, rather than pupil gaze direction. This discrepancy between the two methods can lead to significant measurement bias, potentially resulting in incorrect conclusions. Therefore, gaze distance is a more suitable metric for evaluating visual behavior, particularly in studies where measurement accuracy is paramount. For example, visual distance may be overestimated when the object has a small reflective area, compared to results obtained from head-orientation-based devices.

To comprehensively evaluate the instrument's performance, the testing targets were placed at central and bilateral 25-degree positions. However, the results indicated different measurement bias trends between the left and right targets. After reviewing photos taken during the experiment by the practitioner, it was suspected that some subjects slightly rotated their heads to the right during the experiment. This head rotation likely occurred because the width of the head-chin rest was smaller than the width of the instrument fitted to the subjects' heads in most cases. Most subjects tended to place their heads first on the left side, followed by the right. On average, the results from the right and central targets were closer to the standard values. The slight rotation may explain why the right and central target results were similar, while differing from those of the left targets. As a consequence of the rightward rotation, the actual angle for the right targets may have been smaller than that for the left targets (figure 6-10).

Nguyen D. et al. found that accommodation response and binocular convergence differ between central and peripheral directions. Specifically, the gain of the AC/A ratio (accommodation/convergence) decreases while the bias of convergence-accommodation increases with greater eccentricity [154]. According to their study, accommodation and convergence are balanced when the gaze is directed along the mid-sagittal plane. However, when the gaze is directed towards peripheral angles, the stimuli for the left and right eyes become unequal, and cross-links between accommodation and convergence compensate for these mismatches, which increase with gaze-azimuth. The authors provided a diagram illustrating this concept (Figure 6-11).

For example, if an object moves from the mid-sagittal plane (location ‘A’) to location ‘D’ along an iso-accommodation circle (similar to the setup in the current study), the convergence angle would decrease from α to δ. Our eye tracker, which calculates gaze distance based solely on convergence, may overestimate the gaze distance (i.e., underestimate the dioptric distance) due to this reduced convergence. However, real-

world conditions are likely more complex than this idealized model. For instance, accommodative lag is a common phenomenon in the human eye, but the model does not account for this factor.

To better understand the mechanisms of convergence response at different angles and distances, and to improve the accuracy of the instrument, it is recommended to repeat the experiment with more different angles. Additionally, using a bite bar instead of a head-chin rest would help prevent horizontal head rotation, further reducing potential sources of error.

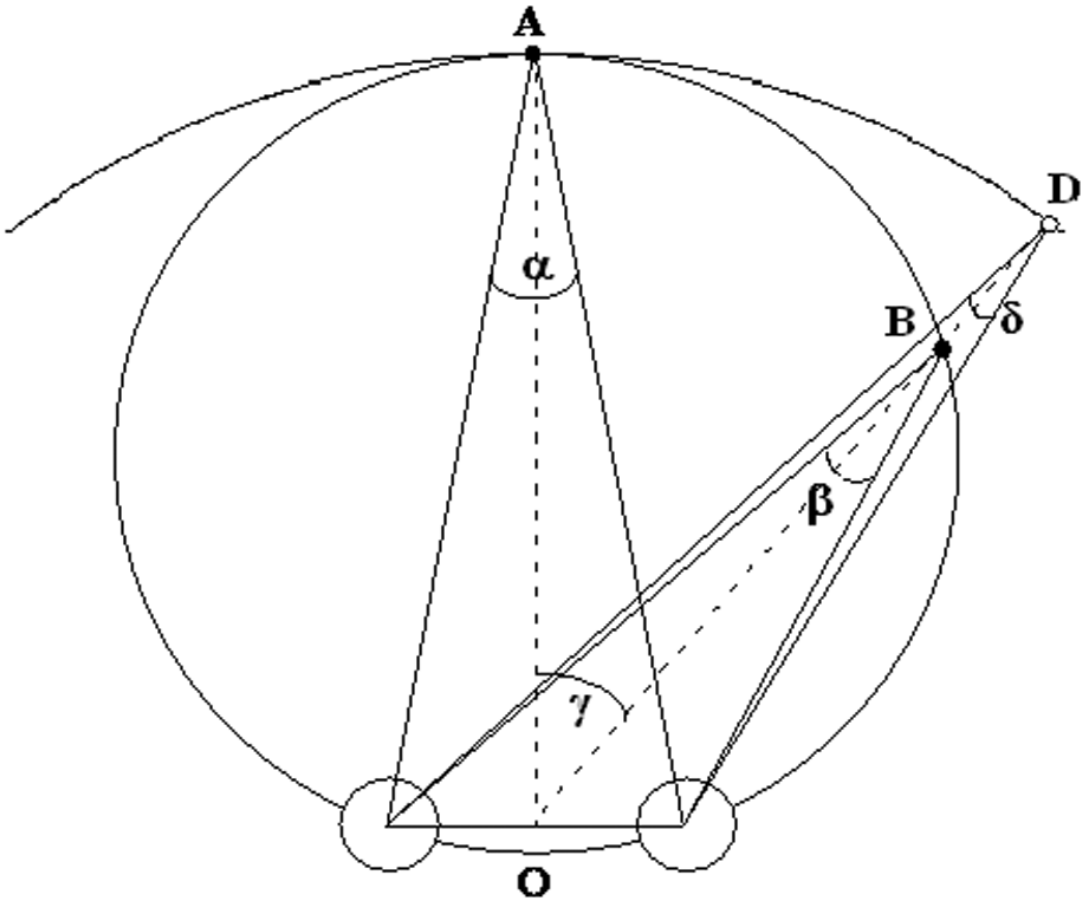


Figure 6-11. Plan view of iso-vergence circle, iso-accommodation circle and various azimuth angles[154]. The large curve in superior indicates the iso-accommodation circle with point O as the center of the circle. The complete big circle represents iso-vergence circle. The two small circles in below represent the eyes. Point A&B have the

same amount of convergence (angle α = angle β). Point A&D have the same amount of accommodation.

The trend of measurement bias is similar between the results from the central and right targets (Figure 6-4). This is likely due to head rotation, which shifts the initial calibrated pupil position, resulting in a displacement of the starting point. The bias in gaze angle is likely more pronounced for the left targets, with the extended eccentricities causing nonlinear changes in convergence.

Although the measurement bias is significant for near targets, the correlation between the standard distances and the estimated distances remains clear. Therefore, subjective calibration is feasible to reduce this bias. However, for calibration to be effective, the measurements must demonstrate good repeatability. To assess this, Bland-Altman plots and ICC values were used to evaluate the repeatability of the instrument using two measurements taken at least 5 minutes apart. The results are summarized in Figure 6-5 and Table 6-4.

Bland-Altman plots show good repeatability for the left and central targets, with a 95% confidence interval (CI) ranging from -0.5D to +0.5D, and no significant trend in the differences was observed. The Bland-Altman plot for the right targets, however, shows more variation, with a 95% CI ranging from -1.1D to +1.0D. The ICC value indicates excellent repeatability for the central targets (ICC = 0.99). Given the good repeatability in the central direction, a post-calibration was conducted based on the experimental setup, and the fitting coefficients were applied to the second measurement for each subject.

A significant improvement in the instrument's accuracy was observed after calibration with the experimental setup. Individual results are shown in Figure 6-6, and the measurement bias for each distance is illustrated in Figure 6-7. Before calibration, the

estimated dioptric distance was consistently underestimated, but after calibration, the results closely aligned with the ideal values (Figure 6-6b). In Figure 6-7, the measurement bias increased as the target distance decreased, but after calibration, the bias curve flattened, with a mean difference of less than 0.25D. These results provide valuable insights: first, the accuracy of the instrument can be improved through a standardized gaze distance test; second, closer gaze distances result in greater convergence lag. This convergence insufficiency can be attributed to the limited ability of extraocular muscles to converge the eyes toward a near object.

Visual function may play a role in the accuracy of the eye tracker when estimating gaze distance. To explore this, a correlation analysis was performed between measurement bias and several visual function parameters, including ocular refraction, near and distance deviation, NPC, and accommodation amplitude for both eyes. The results indicated that NPC was associated with gaze distance error estimation, but unexpectedly, larger dioptric bias was correlated with smaller NPC values. This finding is counterintuitive, as a smaller NPC value typically suggests a greater ability to turn the eyes inward, which should theoretically result in less bias. Further research is needed to explore this conflicting result.

Accommodation, vergence, and miosis form the "near triad" responsible for visual behavior at near distances. Ideally, accommodation and vergence should contribute equally when focusing on near targets in the mid-sagittal plane, meaning a slope ratio of 1 would be expected in a linear fit. A correlation analysis was conducted between the measured accommodation response (Grand Seiko WAM5500) and the estimated dioptric gaze distance (from the eye tracker) at distances of 20 cm, 25 cm, and 33 cm. The results, plotted in Figure 6-8, show a significant relationship in the raw data (first measurement). However, the determination coefficient improved after calibration, suggesting that accommodation response is more closely related to gaze distance than binocular vergence alone. Despite the improvement in the R value from 0.34 to 0.53,

gaze distance only accounts for 53% of the accommodation response, with the remaining 47% likely influenced by pupil miosis (due to environmental illumination) and retinal neural functions. Therefore, a precise estimation of gaze distance should consider not only binocular vergence but also other visual functions.

Although the instrument is designed to estimate gaze distance, for studies related to myopia and visual behavior, researchers may be more interested in the actual accommodation response in different scenarios. Specifically, while the gaze object represents an external condition in the real world, the accommodation response is the physiological reaction that directly affects the human eye. If optical factors, such as relative peripheral myopia or hyperopia, are critical in influencing myopia progression, it is important to also consider the light coming from the environment and analyze its optical characteristics in combination with the subject's intrinsic peripheral refraction in daily life. This would be a challenging task and would require the development of new instruments that integrate distance detection with stereo camera functionality.

The strength of the study:

To the best of our knowledge, this is the first study to use a pupil camera within a wearable device to estimate gaze distance, with its accuracy rigorously evaluated using standard values from a customized experimental setup. Compared to other devices like Clouclip, which rely on head orientation to estimate gaze distance, this instrument provides more reliable data for assessing visual behavior.

The limitations of the study:

1. Weight: The total weight of the instrument is around 90 grams, whereas regular spectacles typically weigh between 15 to 30 grams. We also observed some discomfort on the wearer’s nose after the experiment, indicating that the instrument may not be suitable for extended wear due to its weight, which limits its practical application as an eye tracker.

2. Head rotation: In some subjects, the width of the instrument after fitting was wider than that of the head-chin rest, likely causing the differences in measurement bias trends between the left and right directions. To address this, future studies should use a bite bar to stabilize head position rather than relying on a head-chin rest.
3. Limited range of angles: This study only investigated visual targets at the mid-sagittal plane and 25 degrees peripherally. However, to fully understand the mechanisms of accommodation and convergence at different eccentricities, more angles should be studied. Our research focused on three directions because of space limitations between targets, making it difficult to insert additional near objects with a servo motor. Future studies should optimize the testing system to cover a wider range of eccentricities and distances.

## 6.5. Conclusions

1. We developed a wearable device to estimate gaze distance. The instrument demonstrated good accuracy for targets in the central direction but performed less well for peripheral targets, likely due to different mechanisms in the accommodation-vergence cross-link at the periphery.
2. The device can achieve excellent accuracy in estimating gaze distance with simple post-calibration using preset objects at various distances.
3. The instrument showed good repeatability for both central and peripheral targets.
4. Accommodation response was related to estimated dioptric distance calculated using binocular vergence. However, this correlation is more like a consequence of vergence response to the gaze objects, as a stronger correlation was found with the true gaze distance.
5. Visual function, particularly the near point of convergence (NPC), may influence the eye tracker’s performance.

# Research achievements during the doctoral studies

**Publications** (as first author*, or first co-author†):

1. Tang Y†, **Lin Z**†, Zhou L, et al. AI sees beyond humans: automated diagnosis of myopia based on peripheral refraction map using interpretable deep learning. *Journal of Big Data*. 2024;11(1)doi:DOI:10.1186/s40537-024-00989-4.
2. **Lin Z***, Christaras D, Duarte-Toledo R, et al. Dynamic accommodation responses in subjects wearing myopia control spectacles modifying peripheral refraction. *Invest Ophthalmol Vis Sci.* 2025;66(1):55-55. doi:10.1167/iovs.66.1.55
3. **Lin Z***, Xi X, Wen L, et al. Relative myopic defocus in the superior retina as an indicator of myopia development in children. *Invest Ophthalmol Vis Sci*. 2023;64(4):16-16. doi:10.1167/iovs.64.4.16
4. **Lin Z***, Lu Y, Artal P, Yang Z, Lan W. Two-dimensional peripheral refraction and image quality for four types of refractive surgeries. *Journal of refractive surgery (Thorofare, NJ : 1995)*. Jan 2023;39(1):40-47. doi:10.3928/1081597x-20221115-01
5. **Lin Z***, Lan W, Yang Z, et al. A Review of Peripheral Refraction in Myopia Research. Journal of Bio-optics 2025, 1(1), 3.

**International patent**

SORIANO PLA, Weizhong L, MARTINEZ EJF, **Zhenghua L**, Zhikuan Y. Ophthalmic instrument for measuring optical quality of eye. US Patent App. 17/920,791; 2024.

**Paper presentation**

1. Two-years evolution of two-dimensional peripheral refraction in Children, 2022, The Association for Research in Vision and Ophthalmology (ARVO), May 1-4, Denver, USA.
2. Two-years evolution of two-dimensional peripheral refraction in Children, 2022, 18th International Myopia Conference (IMC), Sep 4-7, Rotterdam, Netherlands.
3. Two-years evolution of two-dimensional peripheral refraction in Children, 2022, 10th Visual and Physiological Optics Meeting, Aug 29-31, Cambridge, England.
4. Accommodation response with myopia control spectacles modifying peripheral optics, 2024, 19th International Myopia Conference (IMC), Sep 23-28, Sanya, China.
5. Retinal contrast reduction induced by different myopia-control spectacles, 2025, The Association for Research in Vision and Ophthalmology (ARVO), May 4-8, Salt Lake city, USA.

**Chinese patent**

[1] 爱尔眼科医院集团股份有限公司. 一种屈光检测系统:CN202411814533.3[P]. 2025-01-10.

[2] 湖南爱尔眼视光研究所,爱尔眼科医院集团股份有限公司,爱尔眼科医院集团股份有限公司长沙爱尔眼科医院. 一种近视防控效果预测系统及设备:CN202411560495.3[P]. 2025-02-14.

[3] 爱尔眼科医院集团股份有限公司. 一种模型眼装置:CN202323115253.7[P]. 2024-08-06.

[4] 湖南爱尔眼视光研究所. 一种矫正镜片设计设备、存储介质及镜片:CN202311812924.7[P]. 2024-02-13.

[5] 爱尔眼科医院集团股份有限公司. 近视发展进化树建立方法及近视发展风险评估装置:CN202011529654.5[P]. 2024-07-26.

[6] 爱尔眼科医院集团股份有限公司. 一种模型眼装置以及周边屈光检查设备校准和评估方法:CN202311540122.5[P]. 2024-01-12.

[7] 湖南爱尔眼视光研究所. 一种裸眼视网膜屈光度拟合装置、镜片、方法及存储介质:CN202211474938.8[P]. 2023-12-01.

[8] 北京九辰智能医疗设备有限公司. 屈光度测量系统、方法及电脑验光仪:CN202211373195.5[P]. 2023-04-07.

[9] 北京九辰智能医疗设备有限公司. 振镜扫描角度标定系统、方法及眼科视光检测设备:CN202211599081.2[P]. 2023-04-07.

[10] 湖南爱尔眼视光研究所. 一种裸眼视网膜屈光度拟合装置、镜片、方法及存储介质:CN202211474938.8[P]. 2023-03-07.

[11] 北京九辰智能医疗设备有限公司. 振镜扫描角度标定系统、方法及眼科视光检测设备:CN202211599081.2[P]. 2023-01-24.

[12] 爱尔眼科医院集团股份有限公司. 一种用于防控近视的镜片及装置:CN202123042402.2[P]. 2022-11-15.

[13] 北京九辰智能医疗设备有限公司. 屈光度测量系统、方法及电脑验光仪:CN202211373195.5[P]. 2022-12-02.

[14] 爱尔眼科医院集团股份有限公司. 一种用于防控近视的镜片及装置:CN202111470686.7[P]. 2022-02-08.

[15] 爱尔眼科医院集团股份有限公司. 一种近视发生风险评估装置:CN202011529628.2[P]. 2021-03-19.

[16] 爱尔眼科医院集团股份有限公司. 测量眼睛的光学质量的眼科仪器:CN202110862091.X[P]. 2021-11-09.

[17] 爱尔眼科医院集团股份有限公司. 近视发展进化树建立方法及近视发展风险评估装置:CN202011529654.5[P]. 2021-04-06.

[18] 爱尔眼科医院集团股份有限公司. 一种角膜接触镜:CN202011529643.7[P]. 2021-04-06.

# Acknowledgments

The four-year PhD period in Spain marks one of the most valuable times in my life. I will always cherish this experience, as I have not only pursued a doctoral degree but also enhanced my professional skills, shaped my personality, and developed a clear vision for my career. Throughout this long journey, I received tremendous support, assistance, and encouragement from many individuals. At this moment, as I complete my doctoral thesis, I wish to express my deepest gratitude to all those who have supported me along the way.

First and foremost, I sincerely thank my supervisor, Professor Pablo Artal. Back in 2020, shortly after finishing my master's degree, I initially applied for a PhD position at Central South University in China. Unfortunately, the sudden outbreak of COVID-19 disrupted my plans and seemed to destroy all my efforts and aspirations. At that critical moment, Pablo encouraged me to apply for a PhD position in Murcia and suggested pursuing an FPI scholarship from the Spanish government. Eventually, we successfully passed the committee’s evaluation, and I secured the pre-doctoral contract. This incredible moment reignited my academic passion and restored my confidence.

My gratitude towards Pablo extends far beyond the opportunity to earn a doctoral degree. His visionary academic insights, generous research support, and wonderful personality significantly impacted my academic and personal growth. During the early stage of my PhD, I initially worked on peripheral refraction and considered exploring binocular vision. Pablo wisely advised me that similar work had previously been done, guiding me instead toward double-pass instrumentation and accommodation responses, which turned out to be a promising academic direction. As a result, we successfully published two papers in IOVS, which was an immense achievement for me as a PhD

student. Under his guidance, I also developed valuable skills in 3D modeling, 3D printing, optical simulations, and programming. Words cannot fully express my heartfelt gratitude to Professor Pablo Artal.

I would also like to extend my sincere appreciation to my master's supervisor, Professor Weizhong Lan (Bruce Lan). The accomplishments during my PhD could not have been achieved without his continual support. He provided substantial assistance by arranging volunteers and materials from Aier Eye Hospital for my experiments. For example, in 2023, when Bruce visited the University of Tübingen in Germany, he personally delivered a set of myopia control lenses to Murcia, enabling me to continue my experiments smoothly. His support during the 19th IMC meeting also allowed me to present my research internationally. His generosity has benefited me greatly.

Living abroad presented significant challenges, as Murcia is more than 10,000 kilometers from my hometown. Everything was new and unfamiliar. I sincerely thank Dr. Vahid for helping me adapt to life in Murcia during the early stages of my PhD. He introduced me to an international student community where I met many new friends, helping me overcome initial loneliness. Together we explored the city, enjoyed local ice cream, and experienced various campus canteens. His empathy and friendship remain deeply meaningful to me.

My special thanks go to Santiago Sager, who has been like a co-supervisor to me. Although my supervisor had many responsibilities and limited availability for technical assistance, Santiago always provided selfless and prompt help, particularly in optical modeling and experimental setups. I have admired and learned greatly from his outstanding English communication skills. Our joint three-month academic trip to China was unforgettable, and I am confident our friendship will last forever.

I also express heartfelt appreciation to Dr. Raul Duarte Toledo, who always offered

immediate and generous support whenever we faced difficulties in Murcia. His assistance was crucial for me and the Chinese research group, especially for Xinyu and myself. Raul and his car often seemed like our lifesavers—I cannot count how many times he rescued us. I look forward to the day he visits China, so I can proudly introduce him to my homeland and return the favor by being his driver.

Special thanks to Dr. Dimitrios and Haris Ginis for their excellent contributions related to the double-pass instrument. Approximately one-third of my thesis involved studying dynamic accommodation responses, and their instrument was essential for exploring these scientific questions effectively and publishing high-quality research papers. Their professional insights and contributions with various prototypes significantly enhanced my research.

I would also like to thank the software engineers at LOUM, including Juan Mompean, Arturo, and Adrian. PhD life is unpredictable and full of challenges. Whenever I encountered software issues, they were always available to assist. Remarkably, they even updated software functionality based on my suggestions and provided remote support for my experiments in China, which was incredibly helpful.

My thanks also go to Luis Artal, who helped me adapt to life in Murcia. Luis and Vahid are good friends; we frequently visited different campus canteens together. During the first year of my PhD, when I often worked at Voptica's office, Luis always took me to the best campus canteen (the one with the balcony) in his impressive two-door luxury car, driving fast yet safely. I vividly recall our visit in 2019 to a church located high in the mountains, where I first tasted the iconic Murcian dish, "Marinera."

I am grateful to my dear friends at LOUM: Rosa, Alba, Dibyendu Pusti, Pien, Xinyu, Lichuan, Alejandra, Alexandra, Pedro, Augusto, Clara Isabel, and Elsa. Your friendship has helped me overcome loneliness, enriching my life during these years in Murcia.

Thank you for brightening my PhD journey. I also thank professors at LOUM, including Pedro, Josua, Silvestre, Juan Tabernero, Eloy, Oscar, Juanma, and Esther. Your constructive feedback, knowledge sharing, and dedication have contributed significantly to my thesis and created a supportive academic environment. Additionally, I appreciate my colleagues at Voptica, such as Shoaib, Sunil, Consuelo, Rosa M. Miras, Lucía, Jose Ortega, Jose Belmonte, and David, whose professionalism helped solve many critical experimental issues, leading to the ultimate success of my research.

My deepest gratitude goes to my parents. Without their unconditional support, I would never have been able to pursue my academic dreams in this distant land, so far from home.

Finally, I sincerely thank my pre-doctoral funding institution, Ministerio de Ciencia e Innovación (FPI2020). Without this grant, I could not have undertaken this wonderful journey, developed valuable scientific skills, or gained experience for my future career.

I am grateful to everyone who appeared in my PhD life. Although this marks the completion of my doctoral studies, my academic journey continues. I firmly believe that we will meet again in the future and continue contributing to this beautiful world together.

# References


1. Huang J, Wen D, Wang Q, McAlinden C, Flitcroft I, Chen H, Saw SM, Chen H, Bao F, Zhao Y *et al*: **Efficacy comparison of 16 interventions for myopia control in children: A network meta-analysis**. *Ophthalmology* 2016, **123**(4):697-708.
2. Flitcroft DI, He M, Jonas JB, Jong M, Naidoo K, Ohno-Matsui K, Rahi J, Resnikoff S, Vitale S, Yannuzzi L: **IMI - Defining and classifying myopia: A proposed set of standards for clinical and epidemiologic studies**. *Invest Ophthalmol Vis Sci* 2019, **60**(3):M20-M30.
3. Jo E, Kim SM, Kim JM, Han SY: **Changes in ocular biometrics following cycloplegic refraction in strabismic and amblyopic children**. *Medicine* 2024, **103**(20):e38143.
4. Han X, Liu C, Chen Y, He M: **Myopia prediction: A systematic review**. *Eye (Lond)* 2022, **36**(5):921-929.
5. Chen Y, Zhang J, Morgan IG, He M: **Identifying children at risk of high myopia using population centile curves of refraction**. *PloS one* 2016, **11**(12):e0167642.
6. Lin H, Long E, Ding X, Diao H, Chen Z, Liu R, Huang J, Cai J, Xu S, Zhang X *et al*: **Prediction of myopia development among Chinese school-aged children using refraction data from electronic medical records: A retrospective, multicentre machine learning study**. *PLoS medicine* 2018, **15**(11):e1002674.
7. Chen Y, Han X, Guo X, Li Y, Lee J, He M: **Contribution of genome-wide significant single nucleotide polymorphisms in myopia prediction: Findings from a 10-year cohort of Chinese twin children**. *Ophthalmology* 2019, **126**(12):1607-1614.
8. Lin Z, Lu Y, Artal P, Yang Z, Lan W: **Two-dimensional peripheral refraction and image quality for four types of refractive surgeries**. *J Refract Surg* 2023, **39**(1):40-47.
9. Chua SY, Sabanayagam C, Cheung YB, Chia A, Valenzuela RK, Tan D, Wong TY, Cheng CY, Saw SM: **Age of onset of myopia predicts risk of high myopia in later childhood in myopic Singapore children**. *Ophthalmic Physiol Opt* 2016, **36**(4):388-394.
10. Wildsoet CF, Chia A, Cho P, Guggenheim JA, Polling JR, Read S, Sankaridurg P, Saw S-M, Trier K, Walline JJ *et al*: **IMI – Interventions for controlling myopia onset and progression report**. *Invest Ophthalmol Vis Sci* 2019, **60**(3):M106-M131.
11. Mutti DO, Hayes JR, Mitchell GL, Jones LA, Moeschberger ML, Cotter SA, Kleinstein RN, Manny RE, Twelker JD, Zadnik K: **Refractive error, axial length, and relative peripheral refractive error before and after the onset of myopia**. *Invest Ophthalmol Vis Sci* 2007, **48**(6):2510-2519.
12. Goss DA, Winkler RL: **Progression of myopia in youth: Age of cessation**. *Am J Optom Physiol Opt* 1983, **60**(8):651-658.
13. Group C: **Myopia stabilization and associated factors among participants in the Correction of Myopia Evaluation Trial (COMET)**. *Invest Ophthalmol Vis Sci* 2013, **54**(13):7871-7884.
14. Sankaridurg P, Bakaraju RC, Naduvilath T, Chen X, Weng R, Tilia D, Xu P, Li W, Conrad F, Smith EL, 3rd *et al*: **Myopia control with novel central and peripheral plus contact lenses and extended depth of focus contact lenses: 2 year results from a randomised clinical trial**.

*Ophthalmic Physiol Opt* 2019, 39(4):294-307.

15. Kim J, Lim DH, Han SH, Chung TY: **Predictive factors associated with axial length growth and myopia progression in orthokeratology**. *PloS one* 2019, **14**(6):e0218140.
16. Wang B, Naidu RK, Qu X: **Factors related to axial length elongation and myopia progression in orthokeratology practice**. *PloS one* 2017, **12**(4):e0175913.
17. Zhong Y, Chen Z, Xue F, Miao H, Zhou X: **Central and peripheral corneal power change in myopic orthokeratology and its relationship with 2-year axial length change**. *Invest Ophthalmol Vis Sci* 2015, **56**(8):4514-4519.
18. Kang P, Swarbrick H: **The influence of different OK lens designs on peripheral refraction**. *Optom Vis Sci* 2016, **93**(9):1112-1119.
19. Queiros A, Amorim-de-Sousa A, Lopes-Ferreira D, Villa-Collar C, Gutierrez AR, Gonzalez-Meijome JM: **Relative peripheral refraction across 4 meridians after orthokeratology and LASIK surgery**. *Eye and vision (London, England)* 2018, **5**:12.
20. Barequet D, Levinger E, Rosenblatt A, Levinger S, Barequet IS: **Intraoperative variability of corneal epithelium thickness in photorefractive keratectomy**. *International ophthalmology* 2024, **44**(1):273.
21. Chen T, Li N, Ge T, Lin Y, Wu X, Gao H, Liu M: **Regional analysis of posterior corneal elevation after laser refractive surgeries for correction of myopia of different degrees**. *Indian journal of ophthalmology* 2024, **72**(6):824-830.
22. Hu H, Zhao G, Wu R, Zhong H, Fang M, Deng H: **Axial length/corneal radius of curvature ratio assessment of posterior sclera reinforcement for pathologic myopia**. *Ophthalmologica* 2018, **239**(2-3):128-132.
23. Holden BA, Fricke TR, Wilson DA, Jong M, Naidoo KS, Sankaridurg P, Wong TY, Naduvilath TJ, Resnikoff S: **Global prevalence of myopia and high myopia and temporal trends from 2000 through 2050**. *Ophthalmology* 2016, **123**(5):1036-1042.
24. Fricke TR, Jong M, Naidoo KS, Sankaridurg P, Naduvilath TJ, Ho SM, Wong TY, Resnikoff S: **Global prevalence of visual impairment associated with myopic macular degeneration and temporal trends from 2000 through 2050: Systematic review, meta-analysis and modelling**. *Br J Ophthalmol* 2018, **102**(7):855-862.
25. Morgan IG, French AN, Ashby RS, Guo X, Ding X, He M, Rose KA: **The epidemics of myopia: Aetiology and prevention**. *Progress in retinal and eye research* 2018, **62**:134-149.
26. Smith TS, Frick KD, Holden BA, Fricke TR, Naidoo KS: **Potential lost productivity resulting from the global burden of uncorrected refractive error**. *Bull World Health Organ* 2009, **87**(6):431-437.
27. Wolffsohn JS, Whayeb Y, Logan NS, Weng R, Group* tIMIA: **IMI—Global trends in myopia management attitudes and strategies in clinical practice—2022 update**. *Invest Ophthalmol Vis Sci* 2023, **64**(6):6-6.
28. Wolffsohn JS, Calossi A, Cho P, Gifford K, Jones L, Jones D, Guthrie S, Li M, Lipener C, Logan NS *et al*: **Global trends in myopia management attitudes and strategies in clinical practice - 2019 Update**. *Cont Lens Anterior Eye* 2020, **43**(1):9-17.
29. Wolffsohn JS, Calossi A, Cho P, Gifford K, Jones L, Li M, Lipener C, Logan NS, Malet F, Matos S *et al*: **Global trends in myopia management attitudes and strategies in clinical practice**. *Cont Lens Anterior Eye* 2016, **39**(2):106-116.

30. Guedes J, da Costa Neto AB, Fernandes BF, Faneli AC, Ferreira MA, Amaral DC, Mora-Paez DJ, Ambrósio R, Jr.: **Myopia prevalence in Latin American children and adolescents: A systematic review and meta-analysis**. *Cureus* 2024, **16**(6):e63482.
31. Kobia-Acquah E, Flitcroft DI, Akowuah PK, Lingham G, Loughman J: **Regional variations and temporal trends of childhood myopia prevalence in Africa: A systematic review and meta-analysis**. *Ophthalmic Physiol Opt* 2022, **42**(6):1232-1252.
32. Lan W, Lin Z, Yang Z, Artal P: **Two-dimensional peripheral refraction and retinal image quality in emmetropic children**. *Sci Rep* 2019, **9**(1):16203.
33. Zhang M, Sun Z, Zhu X, Zhang H, Zhu Y, Yan H: **Sports and myopia: An investigation on the prevalence and risk factors of myopia in young sports-related groups in Tianjin, China**. *Invest Ophthalmol Vis Sci* 2022, **63**(6):27-27.
34. Li S-M, Wei S, Atchison DA, Kang M-T, Liu L, Li H, Li S, Yang Z, Wang Y, Zhang F *et al*: **Annual incidences and progressions of myopia and high myopia in Chinese schoolchildren based on a 5-Year cohort study**. *Invest Ophthalmol Vis Sci* 2022, **63**(1):8-8.
35. He M, Huang W, Zheng Y, Huang L, Ellwein LB: **Refractive error and visual impairment in school children in rural southern China**. *Ophthalmology* 2007, **114**(2):374-382.e371.
36. Hsu CC, Huang N, Lin PY, Tsai DC, Tsai CY, Woung LC, Liu CJ: **Prevalence and risk factors for myopia in second-grade primary school children in Taipei: A population-based study**. *Journal of the Chinese Medical Association : JCMA* 2016, **79**(11):625-632.
37. Sng CC, Lin XY, Gazzard G, Chang B, Dirani M, Chia A, Selvaraj P, Ian K, Drobe B, Wong TY *et al*: **Peripheral refraction and refractive error in Singapore Chinese children**. *Invest Ophthalmol Vis Sci* 2011, **52**(2):1181-1190.
38. Saw S-M, Chan Y-H, Wong W-L, Shankar A, Sandar M, Aung T, Tan DTH, Mitchell P, Wong TY: **Prevalence and risk factors for refractive errors in the Singapore Malay eye survey**. *Ophthalmology* 2008, **115**(10):1713-1719.
39. Fricke TR, Olivier J, Resnikoff S, Tahhan N, Beranger B, Kweon S, Keay L: **Cohort effects on prevalence of refractive error in US and Korean NHANES**. *Invest Ophthalmol Vis Sci* 2023, **64**(8):808-808.
40. Bourne RRA, Dineen BP, Ali SM, Noorul Huq DM, Johnson GJ: **Prevalence of refractive error in Bangladeshi adults: Results of the national blindness and low vision survey of Bangladesh**. *Ophthalmology* 2004, **111**(6):1150-1160.
41. Xu L, Li J, Cui T, Hu A, Fan G, Zhang R, Yang H, Sun B, Jonas JB: **Refractive error in urban and rural adult Chinese in Beijing**. *Ophthalmology* 2005, **112**(10):1676-1683.
42. Munoli K, Harpanalli S, Holkar S, Malkhed SM, Girish B, Vannura KR: **Prevalence of refractive errors among medical students of Raichur institute of medical sciences, Raichur, Karnataka, India**. *Cureus* 2024, **16**(4):e58915.
43. Casson RJ, Kahawita S, Kong A, Muecke J, Sisaleumsak S, Visonnavong V: **Exceptionally low prevalence of refractive error and visual impairment in schoolchildren from Lao People's Democratic Republic**. *Ophthalmology* 2012, **119**(10):2021-2027.
44. Pan CW, Shi B, Zhong H, Li J, Chen Q: **The impact of parental rural-to-urban migration on children's refractive error in rural China: A propensity score matching analysis**. *Ophthalmic epidemiology* 2020, **27**(1):39-44.
45. Yang Y, Chen W, Xu A, Zhao L, Ding X, Li J, Zhu Y, Chen C, Long E, Liu Z *et al*: **Spatial**

**technology assessment of green space exposure and myopia**. *Ophthalmology* 2022, **129**(1):113-117.

46. Li X, Li L, Qin W, Cao Q, Mu X, Liu T, Li Z, Zhang W: **Urban living environment and myopia in children**. *JAMA network open* 2023, **6**(12):e2346999.
47. Wen L, Cheng Q, Cao Y, Li X, Pan L, Li L, Zhu H, Mogran I, Lan W, Yang Z: **The Clouclip, a wearable device for measuring near-work and outdoor time: validation and comparison of objective measures with questionnaire estimates**. *Acta Ophthalmol* 2021, **99**(7):e1222-e1235.
48. Wu PC, Chen CT, Lin KK, Sun CC, Kuo CN, Huang HM, Poon YC, Yang ML, Chen CY, Huang JC *et al*: **Myopia prevention and outdoor light intensity in a school-based cluster randomized trial**. *Ophthalmology* 2018, **125**(8):1239-1250.
49. Rose KA, Morgan IG, Ip J, Kifley A, Huynh S, Smith W, Mitchell P: **Outdoor activity reduces the prevalence of myopia in children**. *Ophthalmology* 2008, **115**(8):1279-1285.
50. Jones-Jordan LA, Sinnott LT, Cotter SA, Kleinstein RN, Manny RE, Mutti DO, Twelker JD, Zadnik K: **Time outdoors, visual activity, and myopia progression in juvenile-onset myopes**. *Invest Ophthalmol Vis Sci* 2012, **53**(11):7169-7175.
51. Flitcroft DI, Harb EN, Wildsoet CF: **The spatial frequency content of urban and indoor environments as a potential risk factor for myopia development**. *Invest Ophthalmol Vis Sci* 2020, **61**(11):42-42.
52. Lan W, Pan W, Wen L, Luo Z, Flitcroft I, Yang Z: **Effect of outdoor scene classrooms on myopia prevention and control: One-year result from a randomized clinical trial**. *Invest Ophthalmol Vis Sci* 2024, **65**(7):129-129.
53. Smith EL, 3rd, Ramamirtham R, Qiao-Grider Y, Hung LF, Huang J, Kee CS, Coats D, Paysse E: **Effects of foveal ablation on emmetropization and form-deprivation myopia**. In: *Invest Ophthalmol Vis Sci.* vol. 48, 2007/08/29 edn; 2007: 3914-3922.
54. Smith EL, 3rd, Hung LF, Huang J, Blasdel TL, Humbird TL, Bockhorst KH: **Effects of optical defocus on refractive development in monkeys: Evidence for local, regionally selective mechanisms**. *Invest Ophthalmol Vis Sci* 2010, **51**(8):3864-3873.
55. Dong F, Zhi Z, Pan M, Xie R, Qin X, Lu R, Mao X, Chen JF, Willcox MD, Qu J *et al*: **Inhibition of experimental myopia by a dopamine agonist: Different effectiveness between form deprivation and hyperopic defocus in guinea pigs**. *Molecular Vision* 2011, **17**:2824-2834.
56. Smith L, Xie PY: **Research updates on a role for retinal contrast in myopia control**. *Chin J Ophthalmol* 2023, **59**(6):488-491.
57. Smith EL, 3rd, Hung LF, Huang J: **Protective effects of high ambient lighting on the development of form-deprivation myopia in rhesus monkeys**. *Invest Ophthalmol Vis Sci* 2012, **53**(1):421-428.
58. Schaeffel F, Glasser A, Howland HC: **Accommodation, refractive error and eye growth in chickens**. *Vision Res* 1988, **28**(5):639-657.
59. Tse DY, To CH: **Graded competing regional myopic and hyperopic defocus produce summated emmetropization set points in chick**. *Invest Ophthalmol Vis Sci* 2011, **52**(11):8056-8062.
60. Tse DY, Lam CS, Guggenheim JA, Lam C, Li KK, Liu Q, To CH: **Simultaneous defocus integration during refractive development**. *Invest Ophthalmol Vis Sci* 2007, **48**(12):5352-

5359.

61. Iii ELS, Arumugam B, Hung LF, She Z, Sankaridurg PJVR: **Eccentricity-dependent effects of simultaneous competing defocus on emmetropization in infant rhesus monkeys**. *Vision Res* 2020, **177**:32-40.
62. H EB, Zeng G, D YT, A JL, Wu Y, To CH, C FW, McFadden SA: **The effect of spectacle lenses containing peripheral defocus on refractive error and horizontal eye shape in the guinea pig**. *Invest Ophthalmol Vis Sci* 2017, **58**(5):2705-2714.
63. Benavente-Pérez A, Nour A, Troilo D: **Axial eye growth and refractive error development can be modified by exposing the peripheral retina to relative myopic or hyperopic defocus**. *Invest Ophthalmol Vis Sci* 2014, **55**(10):6765-6773.
64. Ding C, Chen Y, Li X, Huang Y, Chen H, Bao J: **The associations of accommodation and aberrations in myopia control with orthokeratology**. *Ophthalmic Physiol Opt* 2022, **42**(2):327-334.
65. Cheng X, Xu J, Brennan NA: **Accommodation and its role in myopia progression and control with soft contact lenses**. *Ophthalmic Physiol Opt* 2019, **39**(3):162-171.
66. Maddock RJ, Millodot M, Leat S, Johnson CA: **Accommodation responses and refractive error**. *Invest Ophthalmol Vis Sci* 1981, **20**(3):387-391.
67. McBrien NA, Millodot M: **The effect of refractive error on the accommodative response gradient**. *Ophthalmic Physiol Opt* 1986, **6**(2):145-149.
68. Lin Z, Xi X, Wen L, Luo Z, Artal P, Yang Z, Lan W: **Relative myopic defocus in the superior retina as an indicator of myopia development in children**. *Invest Ophthalmol Vis Sci* 2023, **64**(4):16-16.
69. Smith EL, 3rd, Hung LF, Huang J: **Relative peripheral hyperopic defocus alters central refractive development in infant monkeys**. *Vision Res* 2009, **49**(19):2386-2392.
70. Earl L. Smith III C-sK, Ramkumar Ramamirtham, Ying Qiao-Grider,, Hung L-F: **Peripheral vision can influence eye growth and refractive development in infant monkeys** *Invest Ophthalmol Vis Sci* 2005, **46**(11):3695-3972.
71. Lu Y, Lin Z, Wen L, Gao W, Pan L, Li X, Yang Z, Lan W: **The adaptation and acceptance of defocus incorporated multiple segment lens for Chinese children**. *Am J Ophthalmol* 2020, **211**:207-216.
72. Lam CS, Tang WC, Tse DY, Tang YY, To CH: **Defocus Incorporated Soft Contact (DISC) lens slows myopia progression in Hong Kong Chinese schoolchildren: A 2-year randomised clinical trial**. *Br J Ophthalmol* 2014, **98**(1):40-45.
73. Lam CS, Tang WC, Lee PH, Zhang HY, Qi H, Hasegawa K, To CH: **Myopia control effect of defocus incorporated multiple segments (DIMS) spectacle lens in Chinese children: Results of a 3-year follow-up study**. *Br J Ophthalmol* 2022, **106**(8):1110-1114.
74. Alvarez-Peregrina C, Sanchez-Tena MA, Martinez-Perez C, Villa-Collar C, Ohlendorf A: **Clinical Evaluation of MyoCare in Europe (CEME): Study protocol for a prospective, multicenter, randomized, double-blinded, and controlled clinical trial**. *Trials* 2023, **24**(1):674.
75. Yang B, Liu L, Cho P: **Effectiveness of orthokeratology and myopia control spectacles in a real-world setting in China**. *Cont Lens Anterior Eye* 2024, **47**(3):102167.
76. Bao J, Yang A, Huang Y, Li X, Pan Y, Ding C, Lim EW, Zheng J, Spiegel DP, Drobe B *et al*:

**One-year myopia control efficacy of spectacle lenses with aspherical lenslets**. *Br J Ophthalmol* 2022, **106**(8):1171-1176.

77. Sankaridurg P, Holden B, Smith E, 3rd, Naduvilath T, Chen X, de la Jara PL, Martinez A, Kwan J, Ho A, Frick K *et al*: **Decrease in rate of myopia progression with a contact lens designed to reduce relative peripheral hyperopia: One-year results**. *Invest Ophthalmol Vis Sci* 2011, **52**(13):9362-9367.
78. Kanda H, Oshika T, Hiraoka T, Hasebe S, Ohno-Matsui K, Ishiko S, Hieda O, Torii H, Varnas SR, Fujikado T: **Effect of spectacle lenses designed to reduce relative peripheral hyperopia on myopia progression in Japanese children: A 2-year multicenter randomized controlled trial**. *Jpn J Ophthalmol* 2018, **62**(5):537-543.
79. F. Rempt JH, W. P. H. Hoogenboom: **Peripheral retinoscopy and the skiagram** *Ophthalmologia* 1971, **162**:1-10.
80. J. Hoogerheide FR, W. P. H. Hoogenboom: **Acquired myopia in young pilots**. *Ophthalmologia* 1971, **163**:209-215.
81. Seidemann A, Schaeffel F, Guirao A, Lopez-Gil N, Artal P: **Peripheral refractive errors in myopic, emmetropic, and hyperopic young subjects**. *J Opt Soc Am A Opt Image Sci Vis* 2002, **19**(12):2363-2373.
82. Chen X, Sankaridurg P, Donovan L, Lin Z, Li L, Martinez A, Holden B, Ge J: **Characteristics of peripheral refractive errors of myopic and non-myopic Chinese eyes**. *Vision Res* 2010, **50**(1):31-35.
83. Ehsaei A, Mallen EA, Chisholm CM, Pacey IE: **Cross-sectional sample of peripheral refraction in four meridians in myopes and emmetropes**. *Invest Ophthalmol Vis Sci* 2011, **52**(10):7574-7585.
84. Juan Tabernero AO, M. Dominik Fischer, Anna R. Bruckmann, Ulrich Schiefer, Frank Schaeffel: **Peripheral refraction profiles in subjects with low foveal refractive errors**. *Optom Vis Sci* 2011, **88**(3):388-394.
85. Rosen R, Lundstrom L, Unsbo P: **Sign-dependent sensitivity to peripheral defocus for myopes due to aberrations**. *Invest Ophthalmol Vis Sci* 2012, **53**(11):7176-7182.
86. Li SM, Li SY, Liu LR, Zhou YH, Yang Z, Kang MT, Li H, Yang XY, Wang YP, Zhan SY *et al*: **Peripheral refraction in 7- and 14-year-old children in central China: The anyang childhood eye study**. *Br J Ophthalmol* 2015, **99**(5):674-679.
87. Verkicharla PK, Suheimat M, Schmid KL, Atchison DA: **Peripheral refraction, peripheral eye length, and retinal shape in myopia**. *Optom Vis Sci* 2016, **93**(9):1072-1078.
88. Shen J, Spors F, Egan D, Liu C: **Peripheral refraction and image blur in four meridians in emmetropes and myopes**. *Clin Ophthalmol* 2018, **12**:345-358.
89. Garcia Garcia M, Pusti D, Wahl S, Ohlendorf A: **A global approach to describe retinal defocus patterns**. *PloS one* 2019, **14**(4):e0213574.
90. Tabernero J, Vazquez D, Seidemann A, Uttenweiler D, Schaeffel F: **Effects of myopic spectacle correction and radial refractive gradient spectacles on peripheral refraction**. *Vision Res* 2009, **49**(17):2176-2186.
91. Mathur A, Atchison DA: **Peripheral refraction patterns out to large field angles**. *Optom Vis Sci* 2013, **90**(2):140-147.
92. Mathur A, Atchison DA: **Effect of orthokeratology on peripheral aberrations of the eye**.

*Optom Vis Sci* 2009, **86**(5):E476-484.

93. Charman WN, Mountford J, Atchison DA, Markwell EL: **Peripheral refraction in orthokeratology patients**. *Optom Vis Sci* 2006, **83**(9):641-648.
94. Atchison DA, Pritchard N, Schmid KL: **Peripheral refraction along the horizontal and vertical visual fields in myopia**. *Vision Res* 2006, **46**(8-9):1450-1458.
95. Manuel Rodriguez-Vallejo KN, Juan A. Monsoriu, Vicente, Ferrando WDF: **Two-dimensional relative peripheral refractive error induced by fractal contact lenses for myopia control**. *arXiv preprint arXiv:160906987* 2016.
96. Rodriguez-Vallejo M, Montagud D, Monsoriu JA, Ferrando V, Furlan WD: **Relative peripheral myopia induced by fractal contact lenses**. *Curr Eye Res* 2018, **43**(12):1514-1521.
97. Osuagwu UL, Suheimat M, Atchison DA: **Peripheral aberrations in adult hyperopes, emmetropes and myopes**. *Ophthalmic Physiol Opt* 2017, **37**(2):151-159.
98. Bart Jaeken LL, Pablo Artal: **Fast scanning peripheral wave-front sensor for the human eye**. *Optical Society of America* 2011, **19**(8):7903-7913.
99. Bart Jaeken JT, Frank Schaeffel, Pablo Artal: **Comparison of two scanning instruments to measure peripheral refraction in the human eye**. *J Opt Soc Am A* 2011, **29**(3):258-264.
100. Juan Tabernero FS: **Fast scanning photoretinoscope for measuring peripheral refraction as a function of accommodation**. *J Opt Soc Am A Opt Image Sci Vis* 2009, **26**(10):2206-2210.
101. Bakaraju RC, Fedtke C, Ehrmann K, Falk D, Thomas V, Holden BA: **Peripheral refraction and higher-order aberrations with cycloplegia and fogging lenses using the BHVI-EyeMapper**. *J Optom* 2016, **9**(1):5-12.
102. Zheng X, Cheng D, Lu X, Yu X, Huang Y, Xia Y, Lin C, Wang Z: **Relationship between peripheral refraction in different retinal regions and myopia development of young Chinese people**. *Front Med (Lausanne)* 2021, **8**:802706.
103. Atchison DA, Li SM, Li H, Li SY, Liu LR, Kang MT, Meng B, Sun YY, Zhan SY, Mitchell P *et al*: **Relative peripheral hyperopia does not predict development and progression of myopia in children**. *Invest Ophthalmol Vis Sci* 2015, **56**(10):6162-6170.
104. Rotolo M, Montani G, Martin R: **Myopia onset and role of peripheral refraction**. *Clinical optometry* 2017, **9**:105-111.
105. Hartwig A, Charman WN, Radhakrishnan H: **Baseline peripheral refractive error and changes in axial refraction during one year in a young adult population**. *J Optom* 2016, **9**(1):32-39.
106. Xue M, Lin Z, Wu H, Xu Q, Wen L, Luo Z, Hu Z, Li X, Yang Z: **Two-dimensional peripheral refraction and higher-order wavefront aberrations induced by orthokeratology lenses decentration**. *Transl Vis Sci Technol* 2023, **12**(10):8-8.
107. Lin Z, Duarte-Toledo R, Manzanera S, Lan W, Artal P, Yang Z: **Two-dimensional peripheral refraction and retinal image quality in orthokeratology lens wearers**. *Biomed Opt Express* 2020, **11**(7):3523-3533.
108. Xi X, Hao J, Lin Z, Wang S, Yang Z, Lan W, Artal P: **Two-dimensional peripheral refraction in adults**. *Biomedical optics express* 2023, **14**(5):2375-2385.
109. Wang S, Lin Z, Xi X, Lu Y, Pan L, Li X, Artal P, Lan W, Yang Z: **Two-dimensional, high-resolution peripheral refraction in adults with isomyopia and anisomyopia**. *Invest Ophthalmol Vis Sci* 2020, **61**(6):16-16.

110. Jaeken B, Artal P: **Optical quality of emmetropic and myopic eyes in the periphery measured with high-angular resolution**. *Invest Ophthalmol Vis Sci* 2012, **53**(7):3405-3413.
111. Hiraoka T, Mihashi T, Okamoto C, Okamoto F, Hirohara Y, Oshika T: **Influence of induced decentered orthokeratology lens on ocular higher-order wavefront aberrations and contrast sensitivity function**. *J Cataract Refract Surg* 2009, **35**(11):1918-1926.
112. Paune J, Thivent S, Armengol J, Quevedo L, Faria-Ribeiro M, Gonzalez-Meijome JM: **Changes in peripheral refraction, higher-order aberrations, and accommodative lag with a radial refractive gradient contact lens in young myopes**. *Eye & contact lens* 2016, **42**(6):380-387.
113. Rappon J, Chung C, Young G, Hunt C, Neitz J, Neitz M, Chalberg T: **Control of myopia using diffusion optics spectacle lenses: 12-month results of a randomised controlled, efficacy and safety study (CYPRESS)**. *Br J Ophthalmol* 2023, **107**(11):1709-1715.
114. Logan NS, Radhakrishnan H, Cruickshank FE, Allen PM, Bandela PK, Davies LN, Hasebe S, Khanal S, Schmid KL, Vera-Diaz FA *et al*: **IMI Accommodation and binocular vision in myopia development and progression**. *Invest Ophthalmol Vis Sci* 2021, **62**(5):4.
115. Dhallu SK, Sheppard AL, Drew T, Mihashi T, Zapata-Díaz JF, Radhakrishnan H, Iskander DR, Wolffsohn JS: **Factors influencing Pseudo-Accommodation-The Difference between Subjectively Reported Range of Clear Focus and Objectively Measured Accommodation Range**. *Vision (Basel, Switzerland)* 2019, **3**(3).
116. Charman WN: **Keeping the world in focus: How might this be achieved?** *Optom Vis Sci* 2011, **88**(3):373-376.
117. Berntsen DA, Sinnott LT, Mutti DO, Zadnik K: **Accommodative lag and juvenile-onset myopia progression in children wearing refractive correction**. *Vision Res* 2011, **51**(9):1039-1046.
118. Mutti DO, Mitchell GL, Hayes JR, Jones LA, Moeschberger ML, Cotter SA, Kleinstein RN, Manny RE, Twelker JD, Zadnik K: **Accommodative lag before and after the onset of myopia**. *Invest Ophthalmol Vis Sci* 2006, **47**(3):837-846.
119. Kang P, Wildsoet CF: **Acute and short-term changes in visual function with multifocal soft contact lens wear in young adults**. *Cont Lens Anterior Eye* 2016, **39**(2):133-140.
120. Weizhong L, Zhikuan Y, Wen L, Xiang C, Jian G: **A longitudinal study on the relationship between myopia development and near accommodation lag in myopic children**. *Ophthalmic Physiol Opt* 2008, **28**(1):57-61.
121. Gwiazda J, Thorn F, Held R: **Accommodation, accommodative convergence, and response AC/A ratios before and at the onset of myopia in children**. *Optom Vis Sci* 2005, **82**(4):273-278.
122. Ciuffreda KJ, Wallis DM: **Myopes show increased susceptibility to nearwork aftereffects**. *Invest Ophthalmol Vis Sci* 1998, **39**(10):1797-1803.
123. Li L, Wen L, Lan W, Zhu H, Yang Z: **A novel approach to quantify environmental risk factors of myopia: Combination of wearable devices and big data science**. *Transl Vis Sci Technol* 2020, **9**(13):17.
124. Wen L, Cheng Q, Lan W, Cao Y, Li X, Lu Y, Lin Z, Pan L, Zhu H, Yang Z: **An objective comparison of light intensity and near-visual tasks between rural and urban school children in China by a wearable device Clouclip**. *Transl Vis Sci Technol* 2019, **8**(6):15.
125. Wen L, Cao Y, Cheng Q, Li X, Pan L, Li L, Zhu H, Lan W, Yang Z: **Objectively measured**

**near work, outdoor exposure and myopia in children**. *Br J Ophthalmol* 2020, **104**(11):1542-1547.

126. Dutheil F, Oueslati T, Delamarre L, Castanon J, Maurin C, Chiambaretta F, Baker JS, Ugbolue UC, Zak M, Lakbar I *et al*: **Myopia and near work: A systematic review and meta-analysis**. *Int J Environ Res Public Health* 2023, **20**(1).
127. Mutti DO, Mitchell GL, Moeschberger ML, Jones LA, Zadnik K: **Parental myopia, near work, school achievement, and children's refractive error**. *Invest Ophthalmol Vis Sci* 2002, **43**(12):3633-3640.
128. Lu B, Congdon N, Liu X, Choi K, Lam DS, Zhang M, Zheng M, Zhou Z, Li L, Liu X *et al*: **Associations between near work, outdoor activity, and myopia among adolescent students in rural China: The Xichang Pediatric Refractive Error Study report no. 2**. *Archives of ophthalmology (Chicago, Ill : 1960)* 2009, **127**(6):769-775.
129. Saw SM, Shankar A, Tan SB, Taylor H, Tan DT, Stone RA, Wong TY: **A cohort study of incident myopia in Singaporean children**. *Invest Ophthalmol Vis Sci* 2006, **47**(5):1839-1844.
130. Saw SM, Chan B, Seenyen L, Yap M, Tan D, Chew SJ: **Myopia in Singapore kindergarten children**. *Optometry (St Louis, Mo)* 2001, **72**(5):286-291.
131. Jones-Jordan LA, Mitchell GL, Cotter SA, Kleinstein RN, Manny RE, Mutti DO, Twelker JD, Sims JR, Zadnik K: **Visual activity before and after the onset of juvenile myopia**. *Invest Ophthalmol Vis Sci* 2011, **52**(3):1841-1850.
132. Woodman-Pieterse EC, Read SA, Collins MJ, Alonso-Caneiro D: **Regional changes in choroidal thickness associated with accommodation**. *Invest Ophthalmol Vis Sci* 2015, **56**(11):6414-6422.
133. Williams R, Bakshi S, Ostrin EJ, Ostrin LA: **Continuous objective assessment of near work**. *Sci Rep* 2019, **9**(1):6901.
134. Ribeiro F, Ferreira TB, Silva D, Matos AC, Gaspar S, Piñero DP: **Analysis of daily visual habits in a presbyopic population**. *J Ophthalmol* 2023, **2023**:6440954.
135. Leung TW, Flitcroft DI, Wallman J, Lee TH, Zheng Y, Lam CS, Kee CS: **A novel instrument for logging nearwork distance**. *Ophthalmic Physiol Opt* 2011, **31**(2):137-144.
136. Hung GK, Semmlow JL, Ciuffreda KJ: **The near response: Modeling, instrumentation, and clinical applications**. *IEEE Trans Biomed Eng* 1984, **31**(12):910-919.
137. Mompeán J, Aragón J, Artal P: **Energy-efficient design of a presbyopia correction wearable powered by mobile GPUs and FPGAs**. *The Journal of Supercomputing* 2022, **78**.
138. Mompeán J, Aragón JL, Artal P: **Portable device for presbyopia correction with optoelectronic lenses driven by pupil response**. *Sci Rep* 2020, **10**(1):20293.
139. Atchison DA: **Recent advances in representation of monochromatic aberrations of human eyes**. *Clin Exp Optom* 2004, **87**(3):138-148.
140. Christaras D, Tsoukalas S, Papadogiannis P, Börjeson C, Volny M, Lundström L, Artal P, Ginis H: **Central and peripheral refraction measured by a novel double-pass instrument**. *Biomed Opt Express* 2023, **14**(6):2608-2617.
141. Santamaría J, Artal P, Bescós J: **Determination of the point-spread function of human eyes using a hybrid optical-digital method**. *J Opt Soc Am A* 1987, **4**(6):1109-1114.
142. Swiatczak B, Schaeffel F: **Emmetropic, but not myopic human eyes distinguish positive defocus from calculated blur**. *Invest Ophthalmol Vis Sci* 2021, **62**(3):14.

143. Smith EL, 3rd, Huang J, Hung LF, Blasdel TL, Humbird TL, Bockhorst KH: **Hemiretinal form deprivation: Eevidence for local control of eye growth and refractive development in infant monkeys**. *Invest Ophthalmol Vis Sci* 2009, **50**(11):5057-5069.
144. Wallman J, Gottlieb MD, Rajaram V, Fugate-Wentzek LA: **Local retinal regions control local eye growth and myopia**. *Science (New York, NY)* 1987, **237**(4810):73-77.
145. Langaas T, Riddell PM, Svarverud E, Ystenaes AE, Langeggen I, Bruenech JR: **Variability of the accommodation response in early onset myopia**. *Optom Vis Sci* 2008, **85**(1):37-48.
146. Atchison DA, Jones CE, Schmid KL, Pritchard N, Pope JM, Strugnell WE, Riley RA: **Eye shape in emmetropia and myopia**. *Invest Ophthalmol Vis Sci* 2004, **45**(10):3380-3386.
147. Felipe-Marquez G, Nombela-Palomo M, Cacho I, Nieto-Bona A: **Accommodative changes produced in response to overnight orthokeratology**. *Graefes Arch Clin Exp Ophthalmol* 2015, **253**(4):619-626.
148. Gong CR, Troilo D, Richdale K: **Accommodation and phoria in children wearing multifocal contact lenses**. *Optom Vis Sci* 2017, **94**(3):353-360.
149. Papadogiannis P, Romashchenko D, Vedhakrishnan S, Persson B, Lindskoog Pettersson A, Marcos S, Lundström L: **Foveal and peripheral visual quality and accommodation with multifocal contact lenses**. *J Opt Soc Am A* 2022, **39**(6):B39-B49.
150. Arias A, Ohlendorf A, Artal P, Wahl S: **In-depth optical characterization of spectacle lenses for myopia progression management**. *Optica* 2023, **10**(5):594-603.
151. Rahimi-Nasrabadi H, Jin J, Mazade R, Pons C, Najafian S, Alonso JM: **Image luminance changes contrast sensitivity in visual cortex**. *Cell reports* 2021, **34**(5):108692.
152. Lam CSY, Tang WC, Tse DY, Lee RPK, Chun RKM, Hasegawa K, Qi H, Hatanaka T, To CH: **Defocus Incorporated Multiple Segments (DIMS) spectacle lenses slow myopia progression: A 2-year randomised clinical trial**. *Br J Ophthalmol* 2020, **104**(3):363-368.
153. Liu X, Wang P, Xie Z, Sun M, Chen M, Wang J, Huang J, Chen S, Chen Z, Wang Y *et al*: **One-year myopia control efficacy of cylindrical annular refractive element spectacle lenses**. *Acta Ophthalmol* 2023, **101**(6):651-657.
154. Nguyen D, Vedamurthy I, Schor C: **Cross-coupling between accommodation and convergence is optimized for a broad range of directions and distances of gaze**. *Vision Res* 2008, **48**(7):893-903.
155. Ren Q, Yue H, Zhou Q: **Effects of orthokeratology lenses on the magnitude of accommodative lag and accommodativeconvergence/accommodation**. *J Cent South Univ* 2016, **41**(2):169-173.

# List of figures

# List of tables

# Supplementary tables

| **Table S1. Peripheral refraction comparison in various progression groups (1-year study)** | | | | | |
|---|---|---|---|---|---|
| ***Hyperopes*** | | | | | |
| Region | Slow progression | Moderate progression | Fast progression | *Corrected p*-ANOVA | *Corrected p*-Student |
| S1 | 0.13±0.39 | 0.32±0.42 | 0.12±0.51 | 0.782 | 0.961 |
| S2 | 0.47±0.29 | 0.43±0.6 | 0.4±0.17 | 0.95 | 0.918 |
| S3 | 0.95±1.47 | 0.53±0.58 | 0.43±0.22 | 0.782 | 0.918 |
| M1 | 0.24±0.45 | 0.42±0.34 | 0.37±0.32 | 0.782 | 0.918 |
| M2 | 0.78±0.27 | 0.63±0.18 | 0.71±0.2 | 0.782 | 0.918 |
| M3 | 0.94±1.05 | 0.53±0.3 | 0.72±0.33 | 0.782 | 0.918 |
| L1 | 0.29±0.43 | 0.42±0.54 | 0.52±0.49 | 0.782 | 0.918 |
| L2 | 0.53±0.33 | 0.33±0.34 | 0.55±0.24 | 0.782 | 0.961 |
| L3 | 0.52±0.49 | 0.14±0.41 | 0.47±0.34 | 0.782 | 0.961 |
| ***Emmetropes*** | | | | | |
| Region | Refraction-slow | Refraction-Moderate | Refraction-Fast | *Corrected p*-ANOVA | *Corrected p*-Student |
| S1 | -0.14±0.5 | -0.26±0.43 | -0.3±0.51 | 0.487 | 0.273 |
| S2 | -0.14±0.41 | -0.27±0.35 | -0.44±0.38 | 0.041 | 0.017 |
| S3 | -0.02±0.45 | -0.12±0.4 | -0.16±0.48 | 0.487 | 0.302 |
| M1 | -0.02±0.38 | -0.04±0.28 | -0.1±0.39 | 0.64 | 0.401 |
| M2 | 0.13±0.23 | 0.1±0.27 | -0.04±0.27 | 0.046 | 0.018 |
| M3 | 0.13±0.33 | 0.02±0.34 | 0.04±0.36 | 0.487 | 0.316 |
| L1 | 0.16±0.48 | 0.17±0.33 | 0.13±0.38 | 0.902 | 0.734 |
| L2 | 0.09±0.28 | 0.03±0.27 | -0.08±0.26 | 0.071 | 0.024 |
| L3 | 0±0.38 | -0.15±0.33 | -0.14±0.32 | 0.273 | 0.216 |
| ***Myopes*** | | | | | |
| Region | Refraction-slow | Refraction-Moderate | Refraction-Fast | *Corrected p*-ANOVA | *Corrected p*-Student |
| S1 | -1.27±0.98 | -0.92±0.66 | -2.21±1.56 | 0 | 0.014 |
| S2 | -1.84±1.21 | -1.4±0.77 | -3.17±1.75 | 0 | 0.007 |
| S3 | -1.08±1.03 | -0.98±0.72 | -2.29±1.45 | 0 | 0.007 |
| M1 | -1.24±1 | -0.8±0.67 | -2.09±1.61 | 0.001 | 0.024 |
| M2 | -1.6±1.17 | -1.09±0.78 | -2.86±1.85 | 0 | 0.01 |

| | | | | | |
|---|---|---|---|---|---|
| M3 | -0.97±1.14 | -0.87±0.7 | -2.17±1.48 | 0 | 0.007 |
| L1 | -0.84±1.03 | -0.54±0.69 | -1.73±1.65 | 0.002 | 0.024 |
| L2 | -1.45±1.2 | -1.04±0.79 | -2.69±1.94 | 0 | 0.011 |
| L3 | -1.13±1.22 | -0.97±0.71 | -2.29±1.67 | 0.001 | 0.01 |

S(number), M(number) and L(number) were used to present Mean±Standard Deviation of peripheral refraction in corresponding region. The border of regions S, M and L were based on horizontal meridian y=+5.5° and y=-5.5°. The border of regions 1, 2 and 3 were based on vertical meridian x=-10.5° and x=10.5°. *p*-ANOVA means the statistics between peripheral refraction in the three progressive groups (slow, moderate, and fast groups). P-Student mean the two-simple t-test for the comparison between slow and fast groups. The False Discovery Rate (FDR) method was applied to correct p-values for ANOVA and two-simple student t-test for the expected percent of false predictions less than 0.05 in multiple comparisons.

**Table S2. Correlation analysis for peripheral refraction and myopia progression for 1-year study.**

| ***Hyperopes*** | | | | |
|---|---|---|---|---|
| Region | r-SER | Corrected p-SER | r-AL | Corrected p-AL |
| S1 | 0.178 | 0.85 | -0.341 | 0.776 |
| S2 | 0.167 | 0.85 | -0.301 | 0.776 |
| S3 | 0.353 | 0.85 | -0.251 | 0.776 |
| M1 | -0.048 | 0.85 | -0.098 | 0.776 |
| M2 | 0.216 | 0.85 | -0.099 | 0.776 |
| M3 | 0.224 | 0.85 | -0.095 | 0.776 |
| L1 | -0.065 | 0.85 | -0.16 | 0.776 |
| L2 | 0.045 | 0.85 | -0.116 | 0.776 |
| L3 | 0.116 | 0.85 | -0.066 | 0.782 |
| ***Emmetropes*** | | | | |
| Region | r-SER | Corrected p-SER | r-AL | Corrected p-AL |
| S1 | 0.146 | 0.186 | -0.185 | 0.062 |
| S2 | 0.308 | 0.007 | -0.385 | 0 |
| S3 | 0.141 | 0.186 | -0.21 | 0.04 |
| M1 | 0.078 | 0.459 | -0.152 | 0.119 |
| M2 | 0.256 | 0.026 | -0.379 | 0 |
| M3 | 0.137 | 0.186 | -0.207 | 0.04 |

| | | | | |
|---|---|---|---|---|
| L1 | 0.012 | 0.895 | -0.072 | 0.444 |
| L2 | 0.243 | 0.026 | -0.31 | 0.002 |
| L3 | 0.196 | 0.081 | -0.246 | 0.018 |
| ***Myopes*** | | | | |
| Region | r-SER | Corrected p-SER | r-AL | Corrected p-AL |
| S1 | 0.242 | 0.036 | 0.177 | 0.377 |
| S2 | 0.298 | 0.017 | 0.117 | 0.458 |
| S3 | 0.339 | 0.01 | -0.009 | 0.939 |
| M1 | 0.224 | 0.047 | 0.198 | 0.377 |
| M2 | 0.282 | 0.018 | 0.144 | 0.406 |
| M3 | 0.339 | 0.01 | 0.009 | 0.939 |
| L1 | 0.255 | 0.03 | 0.174 | 0.377 |
| L2 | 0.286 | 0.018 | 0.138 | 0.406 |
| L3 | 0.31 | 0.016 | 0.069 | 0.705 |
| The correlation analysis for peripheral refraction in S1, S2, S3, M1, M2, M3, L1, L2 and L3 and myopia progression. The myopia progression was expressed as the change of refractive error in central retina and the increase of axial length in follow-up. Correlation coefficient r-value for refractive change and AL change were used as terms r-SER and r-AL. All p values were corrected with FDR method. | | | | |

| **Table S3. Peripheral refraction comparison in various progression groups (2-year study)** | | | | | |
|---|---|---|---|---|---|
| ***Hyperopes*** | | | | | |
| Region | Slow progression | Moderate progression | Fast progression | *Corrected p*-ANOVA | *Corrected p*-Student |
| S1 | 0.45±0.49 | 0.31±0.53 | 0.51±0.14 | 1 | 0.988 |
| S2 | 0.44±0.27 | 0.37±0.26 | 0.46±17 | 1 | 0.988 |
| S3 | 0.38±0.25 | 0.41±0.41 | 0.47±0.28 | 1 | 0.988 |
| M1 | 0.55±0.29 | 0.49±0.39 | 0.53±0.08 | 1 | 0.988 |
| M2 | 0.7±0.21 | 0.7±0.18 | 0.7±0.12 | 1 | 0.988 |
| M3 | 0.56±0.23 | 0.56±0.39 | 0.53±0.09 | 1 | 0.988 |
| L1 | 0.7±0.29 | 0.56±0.44 | 0.64±0.3 | 1 | 0.988 |
| L2 | 0.57±0.26 | 0.5±0.19 | 0.55±0.08 | 1 | 0.988 |
| L3 | 0.4±0.27 | 0.34±0.39 | 0.36±0.12 | 1 | 0.988 |
| ***Emmetropes*** | | | | | |

| Region | Refraction-slow | Refraction-Moderate | Refraction-Fast | *Corrected p*-ANOVA | *Corrected p*-Student |
|---|---|---|---|---|---|
| S1 | -0.11±0.52 | -0.21±0.51 | -0.4±0.43 | 0.121 | 0.04 |
| S2 | -0.06±0.36 | -0.2±0.35 | -0.48±0.32 | <0.001 | <0.001 |
| S3 | 0.05±0.45 | -0.02±0.42 | -0.23±0.38 | 0.077 | 0.03 |
| M1 | 0.03±0.39 | -0.05±0.39 | -0.15±0.33 | 0.208 | 0.068 |
| M2 | 0.17±0.2 | 0.13±0.27 | -0.06±0.24 | 0.004 | 0.001 |
| M3 | 0.15±0.33 | 0.11±0.35 | -0.02±0.35 | 0.17 | 0.068 |
| L1 | 0.25±0.5 | 0.11±0.43 | 0.1±36 | 0.327 | 0.189 |
| L2 | 0.14±0.3 | 0.06±0.31 | -0.08±0.28 | 0.067 | 0.018 |
| L3 | 0.04±0.41 | -0.07±0.33 | -0.19±0.35 | 0.111 | 0.04 |
| ***Myopes*** | | | | | |
| Region | Refraction-slow | Refraction-Moderate | Refraction-Fast | *Corrected p*-ANOVA | *Corrected p*-Student |
| S1 | -1.16±1.27 | -1.42±1.46 | -1.2±0.78 | 0.99 | 0.969 |
| S2 | -1.82±1.67 | -1.99±1.44 | -2±0.98 | 0.99 | 0.969 |
| S3 | -1.05±1.24 | -1.26±1.1 | -1.52±0.61 | 0.99 | 0.969 |
| M1 | -1.18±1.27 | -1.23±1.46 | -1.09±0.75 | 0.99 | 0.969 |
| M2 | -1.65±1.6 | -1.58±1.47 | -1.63±1.01 | 0.99 | 0.969 |
| M3 | -1.02±1.42 | -1.11±1.12 | -1.31±0.51 | 0.99 | 0.969 |
| L1 | -0.81±1.27 | -0.94±1.43 | -0.76 | 0.99 | 0.969 |
| L2 | -1.56±1.58 | -1.46±1.5 | -1.48±0.93 | 0.99 | 0.969 |
| L3 | -1.24±1.53 | -1.16±1.22 | -1.29±0.62 | 0.99 | 0.969 |

S(number), M(number) and L(number) were used to present Mean±Standard Deviation of peripheral refraction in corresponding region. The border of regions S, M and L were based on horizontal meridian y=+5.5° and y=-5.5°. The border of regions 1, 2 and 3 were based on vertical meridian x=-10.5° and x=10.5°. *p*-ANOVA means the statistics between peripheral refraction in the three progressive groups (slow, moderate, and fast groups). P-Student mean the two-simple t-test for the comparison between slow and fast groups. The False Discovery Rate (FDR) method was applied to correct p-values for ANOVA and two-simple student t-test for the expected percent of false predictions less than 0.05 in multiple comparisons.

| **Table S4. Correlation analysis for peripheral refraction and myopia progression for 2-year study.** | | | | |
|---|---|---|---|---|
| ***Hyperopes*** | | | | |
| Region | r-SER | Corrected p-SER | r-AL | Corrected p-AL |
| S1 | 0.014 | 0.983 | 0.278 | 0.958 |
| S2 | 0.032 | 0.983 | 0.054 | 0.979 |
| S3 | -0.075 | 0.983 | 0.154 | 0.958 |
| M1 | 0.045 | 0.983 | 0.179 | 0.958 |
| M2 | -0.024 | 0.983 | -0.129 | 0.958 |
| M3 | 0.011 | 0.983 | 0.181 | 0.958 |
| L1 | 0.071 | 0.983 | 0.043 | 0.979 |
| L2 | 0.006 | 0.983 | -0.123 | 0.958 |
| L3 | 0.089 | 0.983 | -0.004 | 0.987 |
| ***Emmetropes*** | | | | |
| Region | r-SER | Corrected p-SER | r-AL | Corrected p-AL |
| S1 | 0.208 | 0.063 | -0.215 | 0.053 |
| S2 | 0.432 | <0.001 | -0.48 | <0.001 |
| S3 | 0.259 | 0.025 | -0.314 | 0.007 |
| M1 | 0.154 | 0.166 | -0.181 | 0.099 |
| M2 | 0.348 | 0.004 | -0.364 | 0.002 |
| M3 | 0.211 | 0.063 | -0.25 | 0.026 |
| L1 | 0.102 | 0.34 | -0.119 | 0.265 |
| L2 | 0.297 | 0.014 | -0.302 | 0.007 |
| L3 | 0.261 | 0.025 | -0.301 | 0.007 |
| ***Myopes*** | | | | |
| Region | r-SER | Corrected p-SER | r-AL | Corrected p-AL |
| S1 | -0.002 | 0.991 | 0.346 | 0.092 |
| S2 | 0.051 | 0.991 | 0.259 | 0.129 |
| S3 | 0.185 | 0.991 | 0.105 | 0.492 |
| M1 | -0.017 | 0.991 | 0.345 | 0.092 |
| M2 | 0.009 | 0.991 | 0.288 | 0.113 |
| M3 | 0.133 | 0.991 | 0.138 | 0.412 |
| L1 | 0.032 | 0.991 | 0.295 | 0.113 |
| L2 | 0.013 | 0.991 | 0.28 | 0.113 |
| L3 | 0.045 | 0.991 | 0.216 | 0.197 |
| The correlation analysis for peripheral refraction in S1, S2, S3, M1, M2, M3, L1, L2 and L3 and | | | | |

myopia progression. The myopia progression was expressed as the change of refractive error in central retina and the increase of axial length in follow-up. Correlation coefficient r-value for refractive change and AL change were used as terms r-SER and r-AL. All p values were corrected with FDR method.

**Table S5. Relative peripheral refraction (RPR) for different categories and visits.**

| Baseline | | | | | |
|---|---|---|---|---|---|
| Region | Category 1 (EM-EM-EM) | Category 2 (EM-EM-MY) | Category 3 (EM-MY-MY) | *Corrected p*-ANOVA | *Corrected p*-Student |
| S1 | -0.26±0.52 | -0.29±0.58 | -0.24±0.34 | 0.935 | 0.002 |
| S2 | -0.25±0.31 | -0.35±0.31 | -0.33±0.28 | 0.777 | 0.314 |
| S3 | -0.16±0.4 | -0.17±0.31 | 0.02±0.51 | 0.671 | <0.001 |
| M1 | -0.07±0.39 | -0.1±0.4 | 0±0.26 | 0.806 | <0.001 |
| M2 | 0.07±0.09 | 0.06±0.06 | 0.06±0.08 | 0.907 | 0.123 |
| M3 | -0.01±0.3 | 0.04±0.2 | 0.21±0.37 | 0.459 | <0.001 |
| L1 | 0.13±0.46 | 0.09±0.45 | 0.29±0.35 | 0.671 | <0.001 |
| L2 | 0±0.22 | 0.01±0.18 | 0.07±0.18 | 0.752 | 0.007 |
| L3 | -0.14±0.3 | -0.13±0.25 | 0±0.3 | 0.671 | <0.001 |
| First follow-up | | | | | |
| Region | Category 1 (EM-EM-EM) | Category 2 (EM-EM-MY) | Category 3 (EM-MY-MY) | *Corrected p*-ANOVA | *Corrected p*-Student |
| S1 | -0.28±0.56 | -0.24±0.6 | 0.06±0.47 | 0.112 | 0.044 |
| S2 | -0.29±0.29 | -0.36±0.3 | -0.21±0.36 | 0.363 | 0.418 |
| S3 | -0.16±0.48 | -0.05±0.3 | 0.39±0.64 | 0.007 | 0.007 |
| M1 | -0.04±0.412 | 0±0.42 | 0.29±0.33 | 0.024 | 0.011 |
| M2 | 0.07±0.08 | 0.04±0.09 | 0.1±0.1 | 0.136 | 0.34 |
| M3 | 0.04±0.36 | 0.13±0.22 | 0.49±0.5 | 0.004 | 0.006 |
| L1 | 0.14±0.43 | 0.17±0.53 | 0.57±0.43 | 0.011 | 0.006 |
| L2 | 0.02±0.16 | 0±0.25 | 0.17±0.25 | 0.058 | 0.042 |
| L3 | -0.13±0.35 | -0.04±0.31 | 0.32±0.41 | 0.004 | 0.003 |
| Second follow-up | | | | | |
| Region | Category 1 (EM-EM-EM) | Category 2 (EM-EM-MY) | Category 3 (EM-MY-MY) | *Corrected p*-ANOVA | *Corrected p*-Student |
| S1 | -0.22±0.59 | 0.11±0.67 | 0.33±0.61 | 0.024 | 0.006 |

| | | | | | |
|---|---|---|---|---|---|
| S2 | -0.32±0.42 | -0.21±0.35 | -0.14±0.4 | 0.322 | 0.151 |
| S3 | -0.16±0.6 | 0.26±0.39 | 0.68±0.72 | <0.001 | <0.001 |
| M1 | 0.02±0.041 | 0.34±0.51 | 0.49±0.46 | 0.009 | 0.002 |
| M2 | 0.04±0.09 | 0.11±0.1 | 0.13±0.11 | 0.024 | 0.012 |
| M3 | -0.03±0.42 | 0.34±0.28 | 0.78±0.62 | <0.001 | <0.001 |
| L1 | 0.2±0.42 | 0.54±0.61 | 0.79±0.55 | 0.004 | 0.001 |
| L2 | -0.01±0.18 | 0.15±0.33 | 0.23±0.31 | 0.024 | 0.005 |
| L3 | -0.16±0.39 | 0.17±0.37 | 0.61±0.63 | <0.001 | <0.001 |

Comparison among 3 categories for average RPR in 9 squared regions in different visits. The rules for dividing the regions were based on two horizontal meridians y=+5.5° and y=-5.5°, and two vertical meridians x=-10.5° and x=10.5°. S, M and L were used to represent superior, middle, and lower side of the regions, with suffix number 1, 2 and 3 to further indicate temporal, middle, and nasal side of the maps. One-way ANOVA test were used to compare the RPR difference in the three categories (*p*-ANOVA) and two-simple t-test were used to compare the RPR difference just in Category 1 and Category 3 (*p*-Student). The False Discovery Rate (FDR) method was applied to correct p-values for the expected percent of false predictions less than 0.05 in multiple comparisons. All quantitative data were present with Mean ± Standard Deviation.

**Table S6. Peripheral refraction (PR) for different categories and visits.**

| Baseline | | | | | |
|---|---|---|---|---|---|
| Region | Category 1 (EM-EM-EM) | Category 2 (EM-EM-MY) | Category 3 (EM-MY-MY) | *Corrected p*-ANOVA | *Corrected p*-Student |
| S1 | -0.07±0.55 | -0.29±0.55 | -0.47±0.37 | 0.043 | <0.001 |
| S2 | -0.06±0.34 | -0.34±0.28 | -0.57±0.27 | <0.001 | <0.001 |
| S3 | 0.02±0.42 | -0.16±0.3 | -0.22±0.47 | 0.15 | <0.001 |
| M1 | 0.11±0.41 | -0.09±0.4 | -0.24±0.29 | 0.022 | <0.001 |
| M2 | 0.26±0.2 | 0.07±0.23 | -0.18±0.17 | <0.001 | <0.001 |
| M3 | 0.18±0.31 | 0.04±0.27 | -0.03±0.37 | 0.14 | <0.001 |
| L1 | 0.31±0.46 | 0.1±0.44 | 0.05±0.35 | 0.12 | <0.001 |
| L2 | 0.18±0.27 | 0.02±0.23 | -0.17±0.2 | <0.001 | <0.001 |
| L3 | 0.05±0.35 | -0.12±0.28 | -0.23±0.3 | 0.033 | <0.001 |
| First follow-up | | | | | |
| Region | Category 1 (EM-EM-EM) | Category 2 (EM-EM-MY) | Category 3 (EM-MY-MY) | *Corrected p*-ANOVA | *Corrected p*-Student |

| | | | | | |
|---|---|---|---|---|---|
| S1 | -0.2±0.6 | -0.52±0.57 | -0.8±0.38 | <0.001 | <0.001 |
| S2 | -0.21±0.35 | -0.64±0.27 | -1.07±0.33 | <0.001 | <0.001 |
| S3 | -0.08±0.5 | -0.34±0.26 | -0.47±0.57 | 0.029 | 0.019 |
| M1 | 0.04±0.44 | -0.29±0.4 | -0.57±0.25 | <0.001 | <0.001 |
| M2 | 0.15±0.2 | -0.25±0.21 | -0.76±0.23 | <0.001 | <0.001 |
| M3 | 0.12±0.39 | -0.16±0.25 | -0.37±0.48 | 0.001 | 0.001 |
| L1 | 0.22±0.44 | -0.12±0.5 | -0.29±0.33 | 0.001 | <0.001 |
| L2 | 0.1±0.25 | -0.28±0.27 | -0.69±0.29 | <0.001 | <0.001 |
| L3 | -0.05±0.41 | -0.32±0.3 | -0.54±0.39 | 0.001 | <0.001 |
| Second follow-up | | | | | |
| Region | Category 1 (EM-EM-EM) | Category 2 (EM-EM-MY) | Category 3 (EM-MY-MY) | *Corrected p*-ANOVA | *Corrected p*-Student |
| S1 | -0.31±0.6 | -0.84±0.55 | -1.15±0.47 | <0.001 | <0.001 |
| S2 | -0.41±0.45 | -1.16±0.41 | -1.61±0.55 | <0.001 | <0.001 |
| S3 | -0.26±0.51 | -0.7±0.41 | -0.8±0.67 | 0.01 | 0.008 |
| M1 | -0.07±0.42 | -0.61±0.39 | -0.99±0.39 | <0.001 | <0.001 |
| M2 | -0.05±0.24 | -0.84±0.3 | -1.35±0.5 | <0.001 | <0.001 |
| M3 | -0.12±0.44 | -0.62±0.32 | -0.7±0.62 | <0.001 | <0.001 |
| L1 | 0.1±0.44 | -0.42±0.46 | -0.68±0.4 | <0.001 | <0.001 |
| L2 | -0.1±0.3 | -0.81±0.33 | -1.24±0.5 | <0.001 | <0.001 |
| L3 | -0.25±0.45 | -0.78±0.3 | -0.87±0.57 | <0.001 | <0.001 |

Comparison among 3 categories for average PR in 9 squared regions in different visits. The rules for dividing the regions were based on two horizontal meridians y=+5.5° and y=-5.5°, and two vertical meridians x=-10.5° and x=10.5°. S, M and L were used to represent superior, middle, and lower side of the regions, with suffix number 1, 2 and 3 to further indicate temporal, middle, and nasal side of the maps. One-way ANOVA test were used to compare the RPR difference in the three categories (*p*-ANOVA) and two-simple t-test were used to compare the RPR difference just in Category 1 and Category 3 (*p*-Student). The False Discovery Rate (FDR) method was applied to correct p-values for the expected percent of false predictions less than 0.05 in multiple comparisons. All quantitative data were present with Mean ± Standard Deviation.

| **Table S7. Longitudinal comparison for RPR for each category.** | | | | |
|---|---|---|---|---|
| Category | Region | F | P | Pairwise comparison |
| Category 1 (EM-EM-EM) | S1 | 1.057 | 0.367 | - |
| | S2 | 0.755 | 0.484 | - |
| | S3 | 0.016 | 0.984 | - |
| | M1 | 2.41 | 0.117 | - |
| | M2 | 1.327 | 0.289 | - |
| | M3 | 0.934 | 0.410 | - |
| | L1 | 0.835 | 0.449 | - |
| | L2 | 0.510 | 0.609 | - |
| | L3 | 0.165 | 0.849 | - |
| | Region | F | P | Pairwise comparison |
| Category 2 (EM-EM-MY) | S1 | 11.115 | 0.002 | 13, 23 |
| | S2 | 8.231 | 0.005 | 13, 23 |
| | S3 | 11.32 | 0.001 | 13, 23 |
| | M1 | 19.534 | <0.001 | 12, 13, 23 |
| | M2 | 7.099 | 0.008 | 23 |
| | M3 | 10.182 | 0.002 | 13, 23 |
| | L1 | 22.383 | <0.001 | 13, 23 |
| | L2 | 8.707 | 0.002 | 23 |
| | L3 | 25.97 | <0.001 | 12 |
| | Region | F | P | Pairwise comparison |
| Category 3 (EM-MY-MY) | S1 | 21.072 | <0.001 | 12, 13, 23 |
| | S2 | 6.713 | 0.006 | 12, 13 |
| | S3 | 20.776 | <0.001 | 12, 13, 23 |
| | M1 | 25.175 | <0.001 | 12, 13, 23 |
| | M2 | 5.238 | 0.014 | 12, 13, 23 |
| | M3 | 18.102 | <0.001 | 12, 13, 23 |
| | L1 | 22.383 | <0.001 | 12, 13, 23 |
| | L2 | 8.707 | 0.002 | 12, 13, 23 |
| | L3 | 25.97 | <0.001 | 12, 13, 23 |
| Repeated measured ANOVA test (RM-ANOVA) was used to evaluate the evolution of relative peripheral refraction for each progression categories. The evaluation was based on 9 squared | | | | |

regions that evenly divided the 2-D maps (S-superior side, M-middle side, L-lower side, 1-temporal side, 2-middle, 3-nasal side). If a significant difference was found in RM-ANOVA ($p$<0.05), the results of pairwise comparison would be presented in the table (all $p$-values were adjusted with Bonferroni correction), with numbers 12, 13 and 23 indicating the difference between [baseline and 1st follow-up], [baseline and 2nd follow-up] and [1st follow-up and 2nd follow-up], separately.

**Table S8. Longitudinal comparison for PR for each category.**

| Category | Region | F | P | Pairwise comparison |
|---|---|---|---|---|
| Category 1 (EM-EM-EM) | S1 | 10.69 | 0.001 | 12, 13 |
| | S2 | 15.381 | <0.001 | 12, 13, 23 |
| | S3 | 5.278 | 0.015 | 13, 23 |
| | M1 | 8.121 | 0.003 | 13, 23 |
| | M2 | 14.604 | <0.001 | 12, 13, 23 |
| | M3 | 10.356 | 0.001 | 13, 23 |
| | L1 | 11.165 | 0.001 | 13, 23 |
| | L2 | 21.774 | <0.001 | 12, 13, 23 |
| | L3 | 15.544 | <0.001 | 12, 13, 23 |
| | Region | F | P | Pairwise comparison |
| Category 2 (EM-EM-MY) | S1 | 46.991 | <0.001 | 12, 13, 23 |
| | S2 | 31.565 | <0.001 | 12, 13, 23 |
| | S3 | 8.445 | 0.004 | 12, 13, 23 |
| | M1 | 42.685 | <0.001 | 12, 13, 23 |
| | M2 | 54.091 | <0.001 | 12, 13, 23 |
| | M3 | 16.377 | <0.001 | 12, 13, 23 |
| | L1 | 58.642 | <0.001 | 12, 13, 23 |
| | L2 | 59.581 | <0.001 | 12, 13, 23 |
| | L3 | 25.35 | <0.001 | 12, 13, 23 |
| | Region | F | P | Pairwise comparison |
| Category 3 (EM-MY-MY) | S1 | 41.027 | <0.001 | 12, 13, 23 |
| | S2 | 52.742 | <0.001 | 12, 13, 23 |

| | | | | |
|---|---|---|---|---|
| | S3 | 22.633 | <0.001 | 12, 13, 23 |
| | M1 | 39.484 | <0.001 | 12, 13, 23 |
| | M2 | 55.229 | <0.001 | 12, 13, 23 |
| | M3 | 23.114 | <0.001 | 12, 13, 23 |
| | L1 | 36.657 | <0.001 | 12, 13, 23 |
| | L2 | 44.043 | <0.001 | 12, 13, 23 |
| | L3 | 24.407 | <0.001 | 12, 13, 23 |
| Repeated measured ANOVA test (RM-ANOVA) was used to evaluate the evolution of peripheral refraction for each progression categories. The evaluation was based on 9 squared regions that evenly divided the 2-D maps (S-superior side, M-middle side, L-lower side, 1-temporal side, 2-middle, 3-nasal side). If a significant difference was found in RM-ANOVA ($p<0.05$), the results of pairwise comparison would be presented in the table (all p-values were adjusted with Bonferroni correction), with numbers 12, 13 and 23 indicating the difference between [baseline and 1st follow-up], [baseline and 2nd follow-up] and [1st follow-up and 2nd follow-up], separately. | | | | |

**Table S9. The analysis of confounding factors for each progressive group.**

| Group | Factors | Slightly | Moderate | Fast | Test | P |
|---|---|---|---|---|---|---|
| HY | Range of SER progression (D) | >0 | [-0.4, 0] | <-0.4 | - | - |
| | Age (years) | 12.33±1.51 | 11.88±1.36 | 11.17±1.72 | F=0.905 | 0.423a |
| | Gender (male, female) | 3, 3 | 3, 4 | 3, 4 | $\chi2$=3.725 d | 0.155 b |
| | Baseline SER (D) | 0.77±0.28 | 0.65±0.18 | 0.77±0.2 | F=0.698 | 0.511 a |
| | Baseline AL (mm) | 23.03±0.76 | 22.83±0.75 | 22.73±0.52 | F=0.304 | 0.742 a |
| | Baseline Height | 152.5±10.57 | 148.25±14.63 | 145.33±10.45 | F=0.51 | 0.609 |
| | Parental myopia | 5, 0, 0, 0, 1 | 3, 0, 0, 0, 4 | 6, 0, 0, 0, 1 | $\chi2$=3.725 d | 0.155 b |
| | Mean distance (cm) | 61.94±20.38 | 65.76±18.48 | 56.67±34.72 | F=0.218 | 0.806 |
| | Light intensity (lux) | 219.62±162.23 | 189.82±58.28 | 111.28±76.01 | $\chi2$=5.335 | 0.069 |

| | | | | | | |
|---|---|---|---|---|---|---|
| | Mean of Near distance | 15.71±6.12 | 17.92±7 | 13.61±8.67 | F=0.607 | 0.557 |
| | Time of Near distance | 6.9±1.49 | 8.08±1.03 | 6.62±1.73 | F=1.983 | 0.168 |
| | Time over 1000 lux | 0.52±0.68 | 0.44±0.23 | 0.13±0.13 | $\chi 2$=5.082 | 0.079 |
| | AL change | 0.05±0.1 | 0.08±0.06 | 0.26±0.26 | $\chi 2$=5.923 | 0.052 c |
| EM | Range of SER progression | >0 | [-0.37, 0] | <-0.37 | - | - |
| | Age | 12.28±1.39 | 12.5±1.48 | 11.53±1.56 | F=4.546 | 0.013 |
| | Gender (male, female) | 21, 18 | 20, 18 | 17, 21 | $\chi 2$=0.748 | 0.688 |
| | Baseline SER (D) | 0.05±0.25 | 0.03±0.26 | -0.09±0.28 | F=0.323 | 0.043<br>1 VS 3<br>2 VS 3 |
| | Baseline AL (mm) | 23.14±0.66 | 23.28±0.67 | 23.13±0.64 | F=0.675 | 0.511 |
| | Baseline Height | 152.12±21.08 | 150.72±19.03 | 150.11±9.32 | F=0.137 | 0.872 |
| | Parental myopia | 32, 2, 0, 0, 5 | 33, 0, 1, 1, 3 | 27, 1, 3, 0, 7 | $\chi 2$=9.772 | 0.281 |
| | Mean distance | 59.62±32.74 | 58.27±30.96 | 77.21±25.5 | F=4.753 | 0.01<br>1 VS 3<br>2 VS 3 |
| | Light intensity (lux) | 199.01±108.86 | 166.79±129.63 | 168.26±111.45 | F=0.936 | 0.395 |
| | Mean of Near distance | 16.19±8.86 | 15.02±8.91 | 19.94±6.66 | F=3.723 | 0.027 |
| | Time of Near distance | 6.93±2.11 | 6.83±2.14 | 6.79±1.93 | F=0.238 | 0.789 |
| | Time over 1000 lux | 0.4±0.37 | 0.34±0.9 | 0.32±0.36 | F=0.469 | 0.627 |
| | AL change | 0.05±0.07 | 0.12±0.08 | 0.33±0.15 | F=73.793 | <0.001 |
| MYO | Range of SER progression | >-0.4 | [-0.75, -0.4] | <-0.75 | - | - |

| | | | | | | |
|---|---|---|---|---|---|---|
| | Age | 12.78±1.01 | 12.35±1.16 | 12.5±1.07 | F=1.085 | 0.343 |
| | Gender (male, female) | 11, 16 | 11, 15 | 9, 17 | $\chi 2$=0.361 | 0.835 |
| | Baseline SER | -1.76±1.21 | -1.18±0.8 | -3±1.87 | $\chi 2$=14.996 | <0.001 * |
| | Baseline AL (mm) | 23.72±0.81 | 23.49±0.7 | 24.62±0.93 | F=13.712 | <0.001 * 1 vs 3 2 vs 3 |
| | Baseline height (cm) | 157.57±7.77 | 148.15±23.43 | 154.62±7.18 | F=2.803 | 0.067 a |
| | Parental myopia | 19, 1, 3, 1, 3 | 19, 0, 2, 2, 3 | 17, 4, 3, 1, 1 | $\chi 2$=8.159 | 0.418 b |
| | Mean distance | 63.3±27.45 | 64.41±26.14 | 67.75±22.72 | F=0.21 | 0.811 |
| | Light intensity (lux) | 184.43±79.23 | 182.48±89.86 | 158.89±65.23 | F=0.828 | 0.441 |
| | Mean of Near distance | 18.14±6.86 | 17.99±7.85 | 18.57±5.7 | F=0.048 | 0.953 |
| | Time of Near distance | 6.87±1.91 | 7.07±2.04 | 7.64±1.51 | F=1.225 | 0.3 |
| | Time over 1000 lux | 0.33±0.3 | 0.36±0.32 | 0.26±0.19 | $\chi 2$=0.621 | 0.733 |
| | AL change | 0.14±0.1 | 0.34±0.2 | 0.41±0.18 | F=19.602 | <0.001 * 1 vs 2 1 vs 3 |

HY: hyperopes; EM: emmetropes; MYO: myopes.
The results are presented as mean and 1 standard deviation. The number of parental myopia was described with five consecutive numbers, each number corresponding to one situation: no myopia for both parents, father myopia, mother myopia, both parents have myopia, unclear.
The visual behavior was recorded by clou-clip and presented as: (1) the mean of viewing distance in a week (Mean distance), (2) the mean of ambient light intensity in a week (Mean lux), (3) the mean of viewing distance for the near work in a week (viewing distance less than 60 cm, Mean of near distance), (4) the mean of duration of near work activity (Time of near distance), (5) the average of the duration exposing to more than 1000 lux (that's equal to outdoor activities, Time over 1000 lux).
a One-way ANOVA tests
c Chi-Square test
c Kruskal-Wallis H test

d The expected count less than 5 and greater than 1 in Chi-square test.

**Table S10A. Tests of Between-Subjects Effects**

Measure: Bias

Transformed Variable: Average

| Source | Type III Sum of Squares | df | Mean Square | F | Sig. |
|---|---|---|---|---|---|
| Intercept | 145.809 | 1 | 145.809 | 28.869 | .000 |
| Angle | 90.798 | 2 | 45.399 | 8.989 | .001 |
| Error | 227.284 | 45 | 5.051 | | |

**Table S10B. Mauchly's Test of Sphericity[a]**

Measure: Bias

| Within Subjects Effect | Mauchly's W | Approx. Chi-Square | df | Sig. | Epsilon[b] | | |
|---|---|---|---|---|---|---|---|
| | | | | | Greenhouse-Geisser | Huynh-Feldt | Lower-bound |
| Distance | .000 | 390.041 | 20 | .000 | .255 | .274 | .167 |

Tests the null hypothesis that the error covariance matrix of the orthonormalized transformed dependent variables is proportional to an identity matrix.

a. Design: Intercept + Angle

Within Subjects Design: Distance

b. May be used to adjust the degrees of freedom for the averaged tests of significance. Corrected tests are displayed in the Tests of Within-Subjects Effects table.

**Table S10C. Tests of Within-Subjects Effects**

Measure: Bias

| Source | | Type III Sum of Squares | df | Mean Square | F | Sig. |
|---|---|---|---|---|---|---|
| Distance | Sphericity Assumed | 305.737 | 6 | 50.956 | 479.573 | .000 |
| | Greenhouse-Geisser | 305.737 | 1.528 | 200.028 | 479.573 | .000 |
| | Huynh-Feldt | 305.737 | 1.642 | 186.233 | 479.573 | .000 |
| | Lower-bound | 305.737 | 1.000 | 305.737 | 479.573 | .000 |
| Distance * Angle | Sphericity Assumed | 120.137 | 12 | 10.011 | 94.222 | .000 |
| | Greenhouse-Geisser | 120.137 | 3.057 | 39.300 | 94.222 | .000 |
| | Huynh-Feldt | 120.137 | 3.283 | 36.589 | 94.222 | .000 |
| | Lower-bound | 120.137 | 2.000 | 60.069 | 94.222 | .000 |
| Error(Distance) | Sphericity Assumed | 28.688 | 270 | .106 | | |
| | Greenhouse-Geisser | 28.688 | 68.781 | .417 | | |
| | Huynh-Feldt | 28.688 | 73.876 | .388 | | |
| | Lower-bound | 28.688 | 45.000 | .638 | | |

**Table S10D. Tests of Within-Subjects Contrasts**

Measure: Bias

| Source | Distance | Type III Sum of Squares | df | Mean Square | F | Sig. |
|---|---|---|---|---|---|---|
| Distance | Linear | 302.705 | 1 | 302.705 | 616.603 | .000 |
| | Quadratic | 1.155 | 1 | 1.155 | 14.431 | .000 |
| | Cubic | .801 | 1 | .801 | 18.768 | .000 |
| | Order 4 | .970 | 1 | .970 | 81.317 | .000 |
| | Order 5 | .005 | 1 | .005 | .649 | .425 |
| | Order 6 | .100 | 1 | .100 | 23.451 | .000 |
| Distance * Angle | Linear | 116.656 | 2 | 58.328 | 118.813 | .000 |
| | Quadratic | 2.840 | 2 | 1.420 | 17.742 | .000 |
| | Cubic | .145 | 2 | .072 | 1.692 | .196 |
| | Order 4 | .446 | 2 | .223 | 18.709 | .000 |
| | Order 5 | .031 | 2 | .016 | 2.031 | .143 |
| | Order 6 | .018 | 2 | .009 | 2.159 | .127 |
| Error(Distance) | Linear | 22.092 | 45 | .491 | | |
| | Quadratic | 3.602 | 45 | .080 | | |
| | Cubic | 1.921 | 45 | .043 | | |
| | Order 4 | .537 | 45 | .012 | | |
| | Order 5 | .344 | 45 | .008 | | |
| | Order 6 | .193 | 45 | .004 | | |